The mechanistic pathways of transcranial direct current stimulation (tDCS) in cerebellar adaptation

Suman Das

Colophon

The mechanistic pathways of transcranial direct current stimulation (tDCS) in cerebellar adaptation

The work presented in this PhD thesis was performed in the Department of Neuroscience at the Erasmus MC in Rotterdam, The Netherlands. Supported by the C7: Marie Curie FP7 ITN Initiative of the European Commission (C7 - Cerebellar-Cortical Control: Cells, Circuits, Computation, and Clinic) and the TC2N (Trans Channel Neuroscience Network).

Cover design: Kanad Baneerjee

Layout: Suman Das

Printed by: RIDDERPRINT - The Netherlands
ISBN/EAN: **ISBN 978-94-6299-765-3**

The mechanistic pathways of transcranial direct current stimulation (tDCS) in cerebellar adaptation

De mechanistische grondslagen van transcraniële gelijkstroom stimulatie (tDCS) in cerebellaire adaptatie

Proefschrift

ter verkrijging van de graad van doctor aan de
Erasmus Universiteit Rotterdam
op gezag van de
rector magnificus

Prof.dr. H.A.P. Pols

en volgens besluit van het College voor Promoties

De openbare verdediging zal plaatsvinden op
woensdag 22 November 2017 om 13:30 uur

door

Suman Das

geboren te Kolkata, India

ERASMUS UNIVERSITEIT ROTTERDAM

Promotiecommissie

Promotor:	Prof.dr. M.A. Frens
Commissie:	Prof.dr. Dagmar Timmann
	Dr. M. Schonewille
	Dr. R.W. Selles
Co-promotor:	Dr. P.J. Holland

Dedicated

To

My Mother

whose loving spirit sustains me still

My Father

who's been a rock of stability throughout my life

My Brother

to bring out the best artistic soul in me in solving scientific riddles

My amazing Wife

whose sacrifice and care made it possible to accomplish this work

And to my beautiful daughters Dhriti and Malini who are indeed a treasure from the Lord

Table of Contents

The mechanistic pathway of transcranial direct current stimulation (tDCS) in cerebellar adaptation

Abstract

The thesis explores the mechanistic pathways of transcranial direct current stimulation (tDCS) in modulating a cerebellar dependent adaptation task. tDCS is a noninvasive brain stimulation technique that modulates neuronal excitability and shows promise in the treatment of several neurological and psychiatric disorders. The modulatory role of tDCS opens a new door for its therapeutic usage in cerebellar patients. In order to optimize tDCS as an intervention to alleviate symptoms of cerebellar disorders, we need to understand the pathways through which tDCS modulates cerebellar learning. Hence, this thesis uses behavioral paradigms in various experimental models (such as mice with different genetic backgrounds and healthy human subjects), electrophysiological and computational techniques to dissect out the pathways involved in tDCS dependent modulation of cerebellar adaptation.

We have developed an animal model of cerebellar tDCS, i.e. termed as DCS, as a primary step towards unraveling the mechanistic pathways of tDCS in cerebellar adaptation. In **Chapter 2**, we used a simple gain down vestibulo-ocular reflex (VOR) adaptation task to probe the effects of DCS in wildtype and L7PP2B mice that lack synaptic and intrinsic potentiation of the Purkinje cell (PC). Our findings suggest that the facilitation of gain down following anodal stimulation has a robust link to this potentiation mechanism. One of the reasons to use these mutant mice is that they fail to learn almost every cerebellar dependent learning task. If DCS can augment learning in these mice, the potential use of DCS in motor rehabilitation therapy can be increased.

The role of tDCS in rehabilitation therapy can be further optimized if we study its efficacy in human brain. Therefore, we have done a similar VOR adaptation study in humans in **Chapter 3**. Surprisingly, we found no effects of tDCS on VOR adaptation in humans. The reasons for the differences in the results of the mouse and human studies are hard to determine. Perhaps, they are the result of difference in the effects of tDCS on the flocculus in the two paradigms. Perhaps it is the result of differences in the visual processing circuitry between species. We tend to believe that our results are in the line with evidence showing that tDCS is likely to affect superficial brain regions and not deeper structures. This adds valuable information towards optimizing tDCS in various cerebellar diseases.

We have demonstrated a stark difference between our animal and human experiments. Interestingly, researchers demonstrate that anodal stimulation of human cerebellum facilitates learning in locomotor, force field adaptation and eye-blink conditioning tasks while cathodal stimulation hinders leaning in all these tasks. The literature shows that tDCS has more complicated, polarity dependent effects on the

neuronal network than was originally imagined. In **Chapter 4**, we present recording of neuronal multi-unit activity (MUA) from a population of neurons from epochs before (pre-DCS) and after (post-DCS, 30 mins after the cessation of stimuli) DCS sessions. MUA was recorded from neurons in the cerebellar cortex while DCS was applied at the cortical surface directly above the recording. Our study demonstrates three major effects of DCS on cerebellar neuronal activity. First, DCS has polarity independent effects on neuronal activity in the control mice. Second, despite genetic deletion of long-term depression (LTD) at PF-PC synapses, both anodal and cathodal effects on neuronal activity tends to be alike to the effects in the wild type mice. Third, our preliminary data suggests when PC long-term potentiation (LTP) is genetically ablated, anodal induced early vs late phase neuronal activity shows negative correlation, whereas the cathodal effects on the early vs late phase post-stimulation neuronal activity remains positively correlated. Further, research is required to confirm these findings. Hence, these results demonstrate that the effect of anodal stimulation may depend on the robustness of the potentiation mechanism of PC. It is important to replicate our findings in humans with cerebellar disorders so that a clear linkage can be made between cerebellar disorder and disrupted synaptic mechanisms. Meanwhile, other available mutant mice models may help unravel the mechanistic pathways of tDCS in the cerebellar network. At the least, we will be able to gather knowledge about how mouse and human brains respond differentially to the stimulation.

Finally, we have implemented a detailed computational model (based on previous theoritical work in our lab) which can, with a single set of parameters, mimic the behavior of a wide range of compensatory eye movement (CEM) behaviors, including adaptation of the VOR in **Chapter 5**. In that model, it was proposed that CEM are generated by a state-predicting feedback control (SPFC) framework where specific functional roles can be ascribed to specific nuclei in the CEM circuitry. The model shows that floccular damage leads to mal-adaptation of VOR. Hence, this supports the findings from animal study that the gain down adaptation of VOR can be altered when floccular activity is modulated by applying tDCS.

Ultimately, the experiments presented in this thesis have gathered multilevel information of tDCS on cerebellar network and helped to integrate cross species knowledge in order to utilize this technique optimally in the field of motor rehabilitation.

General Introduction

Impact of transcranial direct current stimulation on neuronal functions

Suman Das, Peter Holland, Maarten A. Frens, Opher Donchin

Transcranial direct current stimulation (tDCS), a noteworthy noninvasive brain stimulation technique, has demonstrated beneficial effects in a wide range of neurological disorders, such as stroke (Boggio *et al.*, 2007; Kim *et al.*, 2014), Alzheimer's disease (Boggio *et al.*, 2009) and various movement disorders (Benninger *et al.*, 2010), or psychiatric conditions such as depression (Murphy *et al.*, 2009), schizophrenia (Brunelin *et al.*, 2012) and addiction (Dunlop *et al.*, 2016). Exponential growth of its use in various clinical conditions creates a pressing demand to understand the mechanism for its optimal applications (Dubljevic *et al.*, 2014). To date, numerous animal and human studies have permitted researchers to delineate the role of tDCS in modulating neuronal processes underlying specific behaviors. In parallel, reproducibility of tDCS effects has been weak in some behaviors (Gladwin *et al.*, 2012; Lally *et al.*, 2013; Wiethoff *et al.*, 2014). Some have suggested that too few tDCS studies test effects at the individual level, reproducible within an individual, in a double-blind design (Horvath *et al.*, 2014). In a meta-analysis, the same group claimed than combining data across studies eliminates the statistical significance of the effect of tDCS on almost all measures of brain activity except on the motor evoked potential (Horvath *et al.*, 2015a; Horvath *et al.*, 2015b). Moreover, the effects of tDCS is sensitive to the types of tasks, such as active and passive property of a task (Thirugnanasambandam *et al.*, 2011a; Miyaguchi *et al.*, 2013), cognitive to motor aspects of a task (Quartarone *et al.*, 2004; Antal *et al.*, 2007; Madhavan *et al.*, 2016). A clear understanding of the mechanisms through which tDCS may have its effects is conspicuously necessary.

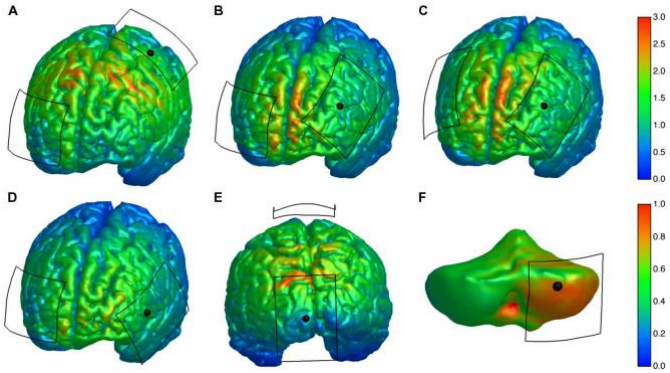

Figure 1: Prediction of global vs focal spread of current field

The maximum result of stimulation was found in between the two electrodes. The electric field (mV/cm) had spread over multiple gyri on both hemispheres, roughly centered on the midline, with the highest values closer to the anode. The peak electric field locations (mV/cm) on the surface of the GM for (A) M1, (B) left DLPFC, (C) dual DLPFC, (D) IFG, and (E) Oz and (F) cerebellum stimulation shifted away from the electrodes.

Field strength Scales were adjusted (same scale for Figures A–E, shown at top right). The black dot in each panel indicated the target of stimulation and the electrode–skin interface was outlined in black. GM – Cerebral gray matter, M1- Motor cortex, DLPFC- Dorsolateral prefrontal cortices, IFG- Inferior frontal gyrus, SO- Supraorbital, Oz- occipital cortex as determined in the standardized 10–20 system for electrode placement (Rampersad *et al.*, 2014).

Behavioral modulation depends on changes in the neuronal firing rate and pattern – essentially changes in the biophysical properties – or changes in the synaptic efficacy – modulations in release probability, uptake and post-synaptic sensitivity (Thorpe *et al.*, 2001; Takemura *et al.*, 2002). Moreover, changes in individual neurons ultimately express themselves as network effects that can be focal or spread across multiple brain regions. Hence, we have explicitly emphasized polarity specific effects of tDCS from sub-cellular processing to circuit level communication which may be related to variation in behavioral responses.

Here, the aim is to give a comprehensive and state-of-the-art overview of how these issues are currently addressed with a focus on the polarity specific effects of the tDCS from neuron to network. We will start in Section 1 with an overview of the firing rate modulation. This section will discuss the factors which regulate the polarity specific effects of tDCS on rate modulation, with an excursion to distance dependent modulation, orientation and structure of the neuron. Section 2 will portray active channels as a system that supports tDCS dependent intrinsic plasticity of neurons. Section 3 and 4 will depict how tDCS leads to alteration in neurotransmitter and neuromodulator function and vice versa. Section 5 will cover the effects of tDCS on network oscillation and coupling. Section 6 will on to the recent developments that address the question of whether tDCS effects are global or focal using advanced and precise behavioral methods. We will end in Section 7 with a discussion of online vs offline effects of tDCS on neuronal functions. Thereafter, we conclude by giving an outlook on possible future developments for the elucidation of tDCS function.

1.1 Effects of electrode polarity and placement on neuronal response

tDCS modulates neural activity by applying a weak constant electrical current (amplitude <2mA) through scalp electrodes (Stagg and Nitsche, 2011). The effects depend on the polarity of stimulation: anodal stimulation applies positive current whereas cathodal stimulation applies negative current at the target. The effects also depend on the distance of neuronal structures from the current and their orientation relative to the current.

Distance from the stimulating electrode can affect the polarity of effect in the target region. For instance, in cerebral cortex of anesthetized rodents, anodal stimulation increased the spontaneous firing and the number of active units close to the electrode (depth < 500µm) while cathodal tDCS reduced the spontaneous firing (Bindman *et al.*, 1964). These effects lasted more than an hour after stimulation. In contrast, neurons in deep cortical layers were often deactivated by anodal and activated by cathodal stimulation (Purpura *et al.*, 1965). This difference may be because intensity varies with distance from the electrode (Figure 1, 2). This possibility was explored *in vitro* by varying the intensity of a homogenous electrical field – applied to an isolated turtle cerebellum. Surprisingly, at all intensities there were always a few neurons that responding the opposite way: excited by cathodal and inhibited by anodal stimulation (Chan and Nicholson, 1986). We propose that polarity-reversal after a specific depth may be due to difference in the neuronal lateral connections and morphology, rather dropping in intensity. In support of this idea, studies in isolated turtle cerebellum (Chan *et al.*, 1988), rodent hippocampal slice (Bikson *et al.*, 2004) and ferret visual cortex slice (Frohlich *et al.*, 2010) demonstrated no polarity-revers al with different intensity. Rather, the field strength altered the membrane voltage linearly up until the point that stimulation led to generation of action potentials (Figure 3). However, we must be careful in

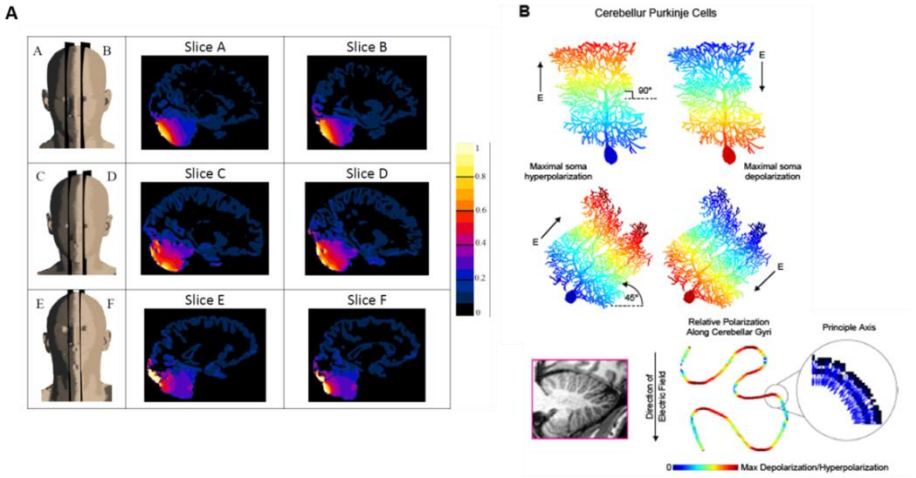

Figure 2: Various modelling studies to predict the effects of tDCS on cerebellum at the macro and the micro scale

(A) The higher amplitudes of current field generated by cerebellar tDCS were below the active electrode in the cerebellum at cortical level within the posterior lobe in "Ella" (top row), "Billie" (middle row) and "Duke" model. There was a minor spread of electric field toward the occipital region of the cortex. The current spread to other structures was negligible (Parazzini *et al.*, 2013). **(B)** The Polarization of cerebellum was heterogeneous along the gyri. The linear polarization of the Purkinje cells along the somato–dendritic axis depended on the orientation of the cell to the current flow (Rahman *et al.*, 2014).

connecting diverse animal studies because *in vitro* preparations are different in many ways than the intact brain.

Now, we consider the effects of orientation. Pyramidal neurons (dendro-axonic orientation) parallel to the current field were activated by anodal and inhibited by cathodal stimulation (Bindman *et al.*, 1964). Similarly, Purkinje cells (PC) and stellate inter-neurons with a dendro-axonic orientation parallel to the current vector were maximally modulated (Chan and Nicholson, 1986); apical dendrites of the PC were depolarized while the rest of the dendrites and soma were hyperpolarized during anodal stimulation (Chan *et al.*, 1988). Conversely, cathodal stimulation depolarized the soma and hyperpolarized apical dendrites (Figure 2B). Furthermore, Kabokov *et al*., (2012) revealed that field-excitatory post-synaptic potential (fEPSP) on hippocampal slices was maximally suppressed when the action potential traveled toward the cathode and was either facilitated or remained unchanged when propagated toward the anode (Figure 4). Overall it appears that axonal orientation determines whether the electric field is excitatory or inhibitory and dendritic orientation affects the magnitude of the stimulation effect.

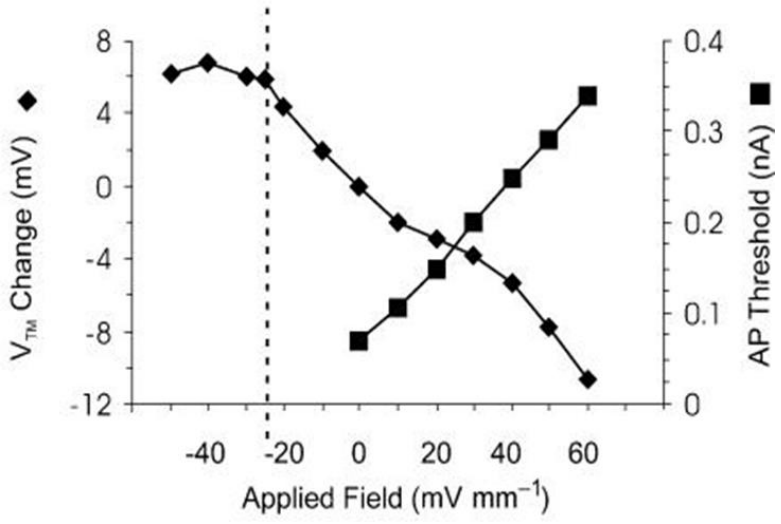

Figure 3: The effects of applied fields on the AP threshold of CA1 stratum oriens neurons

Positive and negative extracellular applied fields increased and decreased the threshold intracellular current needed for AP generation, respectively. The spike initiation zone for oriens was near soma which was depolarized by negative fields and hyperpolarized by positive fields paralled to the somato-dendritic axis.

Effect of applied fields on transmembrane potentials (♦) and threshold for triggering a single AP with an intracellular current pulse (200 ms) during field application (▪). Vertical dashed line indicates the threshold for generation of spontaneous AP by uniform field application; average transmembrane potential was measured during the inter-spike interval (Bikson *et al.*, 2004).

Third, the morphology (size and structure) of neurons determines the extent of polarity specific effects. The polarity specific modulation was significantly higher in pyramidal neurons (EPSP size

and firing rate) than non-pyramidal neurons in feline encephale isole preparation (Purpura *et al.*, 1965). Moreover, the soma of layer-V pyramidal neurons in rodent slice preparation was depolarized the most by anodal stimulation (Ranman *et al.*, 2009). Therefore, it could be argued that the volume of the soma determines the degree of tDCS dependent modul ation because layer-V pyramidal neuron has bigger soma than other neighboring neurons. While it is plausible that higher cell volume leads to more modulation, it may also be that the dendritic microstructure gates stimulation effects by influencing the shape of the spatial field. One experiment demonstrated that the peak amplitude and time constant of membrane polarization varied along the axis of neurons with the maximal polarization observed at the tips of basal and apical dendrites of CA1 neurons (Bikson *et al.*, 2009). Hence, we can postulate that interference of dendro-somatic passive cable properties could modulate the effects of tDCS on neurons.

In summary, these data suggest that polarity specific effects of tDCS depend on distance from the stimulation electrode, current gradient, pre-synaptic axonal orientation, post-synaptic dendritic orientation and neuronal morphology. To unravel tDCS effects on neurons, future experiments must be conducted in the awake behaving animal as most of the neurophysiological data, till now, have come from *in vitro* experiments or anesthetized preparations.

1.2 Effects on intracellular plasticity mechanisms

Both anodal and cathodal tDCS primarily affect the trans-membrane potential which appears to have its major effect by either driving or inhibiting calcium (Ca^{2+}) influx. Alteration of intracellular Ca^{2+} concentration is critical for plasticity (Soderling and Derkach, 2000; Lamont and Weber, 2012) which, may, ultimately induce the long-lasting effects of tDCS on the neuronal network (Figure 5).

tDCS initiates plasticity by altering intracellular Ca^{2+} concentration. Anodal stimulation of cerebral cortex and hippocampus increased intracellular Ca^{2+} concentration (Islam *et al.*, 1995a; Bikson *et al.*, 2004) (Figure 5). A rise in intracellular Ca^{2+} concentration drives early gene expressions which, in turn, regulate short and long-term plasticity (Greer *et al.*, 2008). Interestingly, cerebellar anodal stimulation led to Ca^{2+} spikes. Moreover, cerebellar dual-responsive neurons (activated by both anodal and cathodal stimulation (Chan and Nicholson, 1986) generated Na^{+}-spikes during anodal and produced Ca^{2+}-spikes during cathodal stimulation (Chan

et al., 1988). In cortex, cathodal stimulation does not cause Ca^{2+} spikes, but in cerebellum, it does. This region specific Ca^{2+}-spiking is characteristic of the complexity of the effects of tDCS stimulation and the difficulties involved in interpreting results.

Voltage dependent channels are influenced by tDCS. Anodal stimulation of the sensorimotor cortex led to greater Ca^{2+} accumulation on the stimulation side compared to the contralateral side (Islam *et al.*, 1995a). In the presence of N-methyl-D-aspartate (NMDA) blockers, Ca^{2+} dependent expression of early gene (c-fos) on the anodal stimulation side was absent, except around the polarized point itself (Islam *et al.*, 1995b). Hippocampal slice studies also showed residual changes in Ca^{2+} levels, even in the presence of NMDA blockade (Bikson *et al.*, 2004), supporting the latter idea that NMDA is not the only method by which Ca^{2+} influx can occur. This has fed speculation of an alternative mechanism that is dependent on voltage-sensitive Ca^{2+} channels (VGCC). Recently, Christie *et al.*, 2011 (Christie *et al.*, 2011) showed that sub-threshold somatic depolarization was sufficient to activate axonal VGCCs that elicited Ca^{2+} influx. Hence, it can be concluded from these animal studies that anodal tDCS opens Ca^{2+} channels by increasing the transmembrane potential. Furthermore, higher intensity and longer duration anodal stimulation has greater effects on Ca^{2+} accumulation (Islam *et al.*, 1995a).

As in animal studies, application of NMDA channel antagonists and agonists in human subjects led to abolished (Liebetanz *et al.*, 2002; Nitsche *et al.*, 2003) and enhanced (Nitsche *et al.*, 2004b) anodal effects respectively. Additionally, application of Ca^{2+} channel blockers selectively eliminated the excitability enhancement by anodal stimulation on cerebral cortex (Nitsche *et al.*, 2003) suggesting that VGCC may play a role in manipulating Ca^{2+} accumulation in tDCS in humans. Understanding how studies of Ca^{2+} regulation at the cellular level in humans and animals relate to each other is non-trivial as the distribution of channel subtypes is species specific (McKay *et al.*, 2006).

1.3 Effects on neurotransmission

The excitability of a neuronal network can be modified either by modulating the release-probability or the receptor-affinity of neurotransmitters. tDCS may modulate the rate of neurotransmitter release by affecting either action potential propagation success or vesicle release

probability (Figure 5). Affinity modulation could be achieved by engaging various neuromodulators.

In fact, tDCS does affect neurotransmitter concentration. Anodal stimulation reduced local gamma-aminobutyric acid (GABA) concentration while cathodal stimulation reduced both glutamate (Glu) and GABA concentrations in human cortex (Stagg *et al.*, 2009; Kim *et al.*, 2014). A significant decrease in GABA levels in response to anodal tDCS with effects developing during stimulation and persisting for at least 30 min following stimulation (Bachtiar *et al.*, 2015).

Anodal stimulation may facilitate learning by reduction in GABAergic inhibitory tone as happens in the amygdala (Wolff *et al.*, 2014). Similar evidence that a combined reduction of both Glu and GABA might reduce network excitability does not exist. However, anodal stimulation does enhance the MEP amplitude and cathodal stimulation does reduce it (Nitsche *et al.*, 2003). The expected increases in cortical excitability following anodal tDCS is multifactorial, and certainly are driven by modulation of both GABAergic and glutamatergic signaling. Consequently, it would be predicted that the anodal effect, at least, should be abolished by a GABA agonist. Convincingly, the administration of activity dependent $GABA_A$ agonist blocker eliminated the faciliatory effects of anodal stimulation on MEP (Nitsche *et al.*, 2004c). However, in a more recent study atDCS over primary-motor cortex had no effects on GABA concentration and receptor activity in either healthy or with mild Traumatic Brain Injury patients (Wilke *et al.*, 2017).

So far, no direct measurements of neurotransmitter concentration following tDCS have been performed in animals. Contrasting with the human findings, the available evidence seems to suggest that the anodal stimulation might increase Glu and GABA levels. The mechanism could be through (i) sub-threshold depolarization and (ii) network oscillation. For instance, Christie *et al*., (2011) demonstrated that sub-threshold depolarization of the cerebellar molecular layer inter-neurons (MLIs) enhanced GABA release. Subthreshold oscillations in the dendrites of mitral cells in the accessory olfactory bulb are coupled to dendritic Glu release (Castro *et al.*, 2009). Since subthreshold depolarization (Stagg and Nitsche, 2011) and enhancement of oscillations (Reato *et al.*, 2015) are presumably the main mechanisms through which anodal tDCS effects are mediated, suggests that anodal tDCS actually increases both Glu and GABA release. If so, learning would need to be facilitated when both Glu and GABA synaptic release are strengthened, like in an acetylcholine-mediated learning mechanism (Mitsushima *et al.*, 2013). These ideas are merely

suggestive: we are presenting evidence taken from different experiments performed in different brain regions with different methodologies; however, they raise interesting research possibilities.

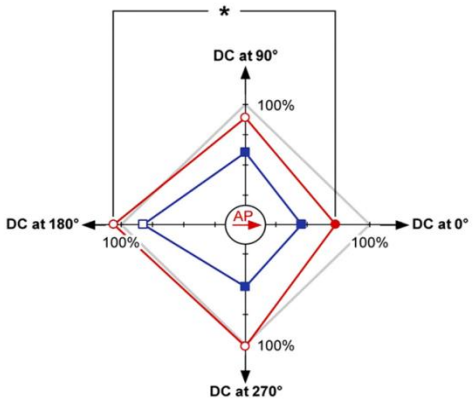

Figure 4: Effects of DCS on axonal AP transmission depended on the relative orientation of the DC current vector and the vector of the AP propagation

The parallel or antiparallel DC field had nonsymmetrical effect on the AP vector. Interestingly, DCS had symmetrical effects when the DC vector was perpendicular to the AP vector.

The diagram showed amplitudes of normalized amplitudes before DCS in gray (100%) and during 100- and 200-µA DCS as red circles and blue squares, respectively. The direction of the AP vector was shown as the red arrow in the origin, and the directions of the DC current correspond to the back arrows at the ends of the axes. Filled circles and squares correspond to statistically significant effects on the amplitude. Open symbols correspond to non-significant variations. *P<0.05 (Kabakov *et al.*, 2012)

1.4 Neuromodulators and tDCS

Neuromodulators, a special class of neurotransmitters, have slow reuptake and breakdown in the synapse (Murphy *et al.*, 2004; Daws *et al.*, 2009) and modify the dynamics of channels, instead of directly opening them (Do *et al.*, 2012; Dembrow *et al.*, 2014; Lu *et al.*, 2014). tDCS interacts with neuromodulators in two ways. First, by affecting neuromodulator release, tDCS can affect neuromodulator concentration at the synapse. Second, conversely, the concentration of a neuromodulator, by affecting synaptic dynamics, can change the effect that tDCS has on that synapse.

tDCS and serotonin enhance each other's function. Anodal tDCS reduced the symptoms of major depressive disorders (Murphy *et al.*, 2009) having compromised serotonergic system (Morrissette and Stahl, 2014). Thus, tDCS magnifies the activity of serotonergic system. However, effects of tDCS on the serotonergic system seem to be mediated by specific variants of the serotonin transporter (5-HTTLPR) (Brunoni *et al.*, 2013). We, therefore, speculate that genetic polymorphism regulates the individual sensitivity towards tDCS. Plausibly, this is the reason for inter-subject variability in tDCS dependent MEP modulation (Wiethoff *et al.*, 2014). Incremental increases in extracellular serotonin levels, using selective serotonin reuptake inhibitor (SSRI), boost anodal facilitation and caused cathodal stimulation to have an excitatory effect (Nitsche *et al.*, 2009). No existing models explain how serotonin might reverse the cathodal and enhance the anodal effects of tDCS.

Nevertheless, the evidence does support a bidirectional relationship: anodal tDCS promotes the function of the serotonergic system and serotonin facilitates anodal effects.

Anodal tDCS drives brain-derived neurotrophic factor (BDNF) mediated long-term plasticity (LTP). Mutation of BDNF, an important neuromodulator of plasticity (Pezet *et al.*, 2002) impairs motor memory (Morin-Moncet *et al.*, 2014). Possibly, tDCS modulates skill learning by altering BDNF dependent cortical plasticity. This notion was validated by an *in vitro* M1 study in which the anodal stimulation promoted BDNF-dependent LTP (Fritsch *et al.*, 2010). It is plausible that tDCS: (i) enhances secretion of BDNF which influences the spike-time dependent plasticity (Tanaka *et al.*, 2008) and, (ii) modulates the BDNF mediated late-phase of plasticity (Pang *et al.*, 2004). We must understand how and when tDCS drives different pathways of plasticity.

Other neuromodulators have complex effects. A dopamine (DA) agonist turned the anodal facilitation into inhibition on cortical excitability and prolonged the cathodal inhibition (Kuo *et al.*, 2007). Thus, DA effects on tDCS are precisely opposite to those of serotonin. Nicotine (Thirugnanasambandam *et al.*, 2011b) and cholinesterase-blockers (Kuo *et al.*, 2008) both had the effect of abolishing both anodal and cathodal effects. Amphetamine enhanced and prolonged the anodal effects (Nitsche *et al.*, 2004a), but has not been tested in cathodal stimulation. Significant reduction in anodal after-effect could be observed by administration of a β-receptor antagonist. All in all, clinical application of tDCS will require awareness of the potential interactions and also the influences of specific genetic backgrounds.

1.5 Modulation of brain oscillations

Brain oscillations may be a sensitive target for tDCS. Oscillation driven synchronization of neuronal activity within and across different cortical regions may provide a means for the binding of information processed in separate cortical assemblies (Engel *et al.*, 2001). Empirically, alterations in neural oscillations have been found in all major psychiatric diseases (Buzsaki *et al.*, 2012). The hope is that tDCS could provide clinical relief by strengthening or weakening oscillatory activities within brain regions (Figure 5). In the next couple of paragraphs, we discuss how tDCS modulates oscillatory activity of the brain.

tDCS induces transient and reversible effects on high-frequency beta and gamma oscillations. Cathodal stimulation significantly decreased visually evoked oscillations at these frequencies

while anodal stimulation led to a slight increase (Antal *et al.*, 2004). Simultaneous oppositely polarized stimulation of both agonist and antagonist cortical hand movement regions (with the agonist stimulated anodally) lead to increase in gamma activity in functionally connected regions during movement (Polania *et al.*, 2011). Both of these studies showed an enhancement in high frequency oscillations followed by anodal stimulation.

Cathodal stimulation also suppressed (and anodal stimulation enhanced) gamma oscillations in *in vitro* rodent hippocampus (Reato *et al.*, 2010) and ferret visual cortex (Frohlich *et al.*, 2010). Anodal stimulation increased oscillatory frequency by shortening the duration of the Down state but not the Up state of multi-unit activity. Longer anodal stimulation could also induce lasting effects in gamma oscillations (Reato *et al.*, 2015). In summary, (i) tDCS can modulate synchronization and topological functional organization of the brain by altering specific frequency bands and (ii) in active neuronal networks, anodal tDCS induces long-lasting facilitatory effects on high frequency oscillations. tDCS induced gamma modulation may be a suitable method to promote higher order cognitive processes in certain neurological diseases.

1.6 Global vs focal influence

As we've discussed, anodal stimulation is usually excitatory and cathodal stimulation is usually inhibitory. A separate question is how focal the action is. Some modelling studies reported that the effect of tDCS on neuronal activity is global (throughout the brain), whereas the nature of current spread depends on electrode montage (position and size) (Datta *et al.*, 2011, Dougherty *et al.*, 2014) (Figure 1, 2). Nevertheless, behavioral studies show specificity – tDCS modulates a particular behavior when applied to a preferred brain region with a specific montage (Vallar and Bolognini, 2011). This specificity suggests that effects are more local than might be expected from some of the modeling studies. In the following paragraphs, we will first review arguments that tDCS effects are global, and then review arguments that the effects are focal.

Application of tDCS over a specific brain region induces neuronal modulation in that region and its downstream regions (Li *et al.*, 2015) (Figure 1, 2A). Anodal stimulation of the rodent frontal cortex enhanced its neuronal activity as well as in the nucleus-accumbens (Takano *et al.*, 2011). Ipsilateral anodal stimulation of rodent cortex led to increased intracellular Ca^{2+} accumulation (Islam *et al.*, 1995a) and early gene expressions (Moriwaki *et al.*, 1995) in the ipsilateral connected

cortical and sub-cortical regions. Strikingly, ipsilateral anodal stimulation on the ischemic cortex in a rodent stroke model led to dendro-axonal growth in both hemispheres (Yoon *et al.*, 2012). The combined intervention of anodal and cathodal stimulation on contralateral sides changed the intra-hemispheric and the inter-hemispheric topological functional organization as well as the intra-cortical synchronization in human (Polania *et al.*, 2011). These studies all argue that tDCS effects are not completely focal.

Behavioral studies justify focal specificity of tDCS. For instance, psychomotor performance improves with anodal stimulation of the facilitatory loop (the circuit whose activity promotes a behavior) and/-or with cathodal stimulation of the competitive loop (the circuit whose activity hinders a behavior) (Vines *et al.*, 2008). One measure of focal specificity is the minimum distance between stimulating electrodes that produce the same behavioral effect. Anodal stimulation of the cerebellum but not M1 increased the ability to learn visuomotor (Galea *et al.*, 2011) and force field (Herzfeld *et al.*, 2014) adaptation tasks. Thus, tDCS can distinguish anatomically well separated targets. Left M1 anodal stimulation induced relatively greater improvement in right handed motor skill than right M1 stimulation (Schambra *et al.*, 2011). At a much finer scale, anodal stimulation of the left supplementary motor area (SMA) and M1 both led to improvement in a visuomotor skill task but left pre-SMA stimulation did not (Vollmann *et al.*, 2013). High-definition tDCS promises to allow stimulation of subparts of cortical sub-regions (Villamar *et al.*, 2013). Hence, tDCS has potential as a focal non-invasive brain stimulation technique in neuro-rehabilitation.

1.7 Online vs offline effects

Long lasting offline (post-stimulation) effects are crucial for effective intervention. Thus, the effectiveness of tDCS is questioned not only in terms of its specificity but also in terms of the extent of offline effects.

The offline effects of tDCS are evident in some circumstances. More than an hour long offline effects in firing rate (Bindman *et al.*, 1964), fEPSP (Fritsch *et al.*, 2010) and gamma oscillations (Reato *et al.*, 2015) was induced after 10 min stimulation of rodent cortex. Similarly, anodal stimulation on humans showed a lasting effect on the MEP amplitude (Horvath *et al.*, 2014) and in GABA and Glu concentration (Stagg *et al.*, 2009). Similar findings for neuromodulators are limited as the interactions between neuromodulators and tDCS were measured through drug administration that had acute receptor saturation and washout effects (Nitsche *et al.*, 2009; Kuo *et*

al., 2008; Thirugnanasambandam *et al.*, 2011b). Recently, a meta-review claimed that tDCS on human has an offline neurophysiological effect only on MEP amplitude modulation (Horvath *et al.*, 2014). One key complicating issue, highlighted in this section, is the multiplicity of mechanisms through which tDCS may work across brain regions. Focusing in on how tDCS might have an offline effect, there a few cellular mechanisms might mediate it - intracellular Ca^{2+} concentration (Bikson *et al.*, 2004; Islam *et al.*, 1995a) and early gene expressions (Moriwaki *et al.*, 1995). Unfortunately, available studies do not provide temporal data on offline effects. We think there is a need to take specific cellular mechanism which can be divided into finer time scales and then look for online vs offline effects of tDCS.

Few behavioral experiments explored offline effects of tDCS. Anodal stimulation paired to learning facilitated locomotor (Jayaram *et al.*, 2012), force field (Herzfeld *et al.*, 2014) adaptation and eye-blink conditioning (Zuchowski *et al.*, 2014) tasks while cathodal stimulation retarded all. Surprisingly, post-stimulation deadaptation curves (Schambra *et al.*, 2011; Jayaram *et al.*, 2012) or extinction rate (Zuchowski *et al.*, 2014) showed no polarity specific differences. In summary, we can say that it is just too early to say anything clear about online and offline effects of tDCS on either a cellular or a behavioral level. Moreover, offline effects of tDCS are not very consistent across various tests. Thus, we need careful observation to clarify online vs offline effects of tDCS.

1.8 Conclusion

In conclusion, future experiments studying polarity specific effects of tDCS on the brain need to accomplish a detailed monitoring and manipulation of cellular and sub-cellular processes in animals while performing tasks that optimally engage (and differentiate) brain states and regional associations. These will likely include sensorimotor / cognitive tasks under the influence of tDCS, together with massive parallel monitoring of distributed neuronal activities and/or manipulating pathways and transmitter systems. Such an experiment has not been performed so far, but the recent achievements in this direction reviewed here, give cause for hope that the next couple of years will see significant progress in this endeavor. This paper has suggested ways of improving such analyses by emphasizing the complementarity between the different methods of brain function investigation and the overriding need to use them in combination with one another.

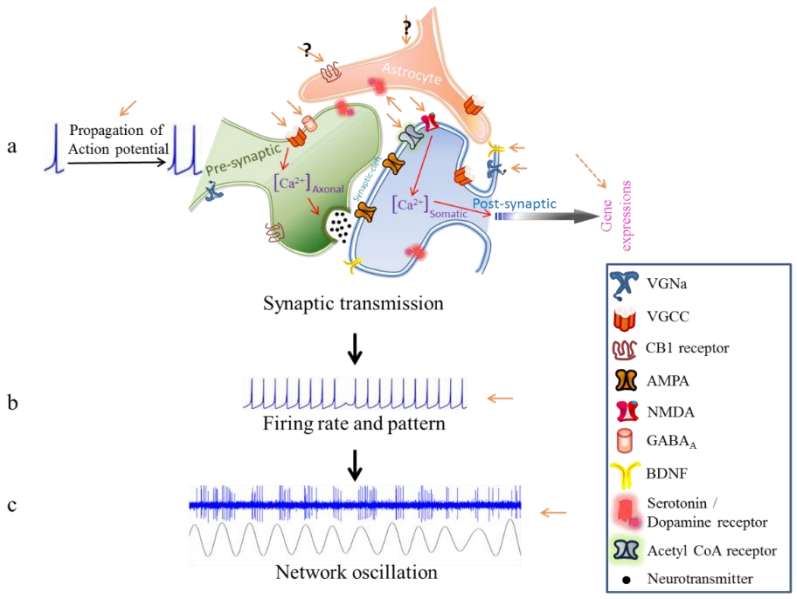

Figure 5: Simplistic diagram showing the neurophysiological effects of tDCS

(a) tDCS can modulate generation and propagation of action potential (AP) as well as neuronal plasticity. Anodal tDCS dependent sub-threshold depolarization of neurons augments action potential generation and propagation. Increment of pre-synaptic intracellular calcium ions via activation of voltage-gated calcium channels (VGCC), anodal tDCS enhances neurotransmitter (glutamate and gamma-aminobutyric acid GABA) release probability at the synaptic cleft. At the post-synaptic side, anodal stimulation enhances intracellular calcium concentration by facilitating N-methyl-D-aspartate (NMDA) channel. Moreover, accumulation of intracellular calcium ion promotes synaptic plasticity by regulating gene transcription. Overall, anodal tDCS enhances excitability of neuronal network. In contrast, cathodal tDCS inhibits neuronal excitability by hindering activation of voltage-gated ion channels. Interestingly, voltage-gates ion channels are also present in Glia cells which regulate neuronal plasticity. Currently, no result describes how tDCS modulates homeostasis of neuro-glial plasticity. Neuromodulators (for example - serotonin, brain-derived neurotrophic factor (BDNF), dopamine etc.) alter polarity specific effects of tDCS. These neuromodulators, furthermore, affect tDCS dependent neuronal plasticity mechanisms. We have no clear idea how other neuromodulators (like endocannabinoids) regulate polarity specific effects of tDCS.

(b) tDCS can modulate neuronal firing rate and pattern locally. Faciliatory effects of anodal tDCS and inhibitory effects of cathodal tDCS on neuronal excitability depend not only on the distance from active electrode but also on the orientation of neurons. Neurons closest to the electrode having dendro-axonic orientation parallel to the electric are influenced the most.

(c) At the network level tDCS induces changes in brain oscillation. tDCS induces transient and reversible effects on high-frequency beta and gamma oscillations. Oscillation driven synchronization of neuronal activity within and across different cortical regions is crucial for binding of information. Therefore, tDCS dependent modulations of brain oscillations may influence behavioral responses.

Direct modulatory effects of tDCS, Indirect modulatory effects of tDCS,

Excitatory signalling cascade

References

Antal, A. *et al.* (2004) Oscillatory brain activity and transcranial direct current stimulation in humans. *Neuroreport* 15, 1307–1310

Antal, A., *et al.* (2007) Towards unravelling task-related modulations of neuroplastic changes induced in the human motor cortex. *Eur J Neurosci* 26, 2687–2691.

Bachtiar, V., *et al.* (2015) Modulation of GABA and resting state functional connectivity by transcranial direct current stimulation. *eLife* 4, e08789.

Bikson, M. *et al.* (2004) Effects of uniform extracellular DC electric fields on excitability in rat hippocampal slices in vitro. *J. Physiol. (Lond.)* 557, 175–190

Benninger, D.H. *et al.* (2010) Transcranial direct current stimulation for the treatment of Parkinson's disease. *J. Neurol. Neurosurg. Psychiatr.* 81, 1105–1111

Bindman, L.J. *et al.* (1964) THE ACTION OF BRIEF POLARIZING CURRENTS ON THE CEREBRAL CORTEX OF THE RAT (1) DURING CURRENT FLOW AND (2) IN THE PRODUCTION OF LONG-LASTING AFTER-EFFECTS. *J. Physiol. (Lond.)* 172, 369–382

Boggio, P.S. *et al.* (2007) Repeated sessions of noninvasive brain DC stimulation is associated with motor function improvement in stroke patients. *Restor. Neurol. Neurosci.* 25, 123–129

Boggio, P.S. *et al.* (2009) Temporal cortex direct current stimulation enhances performance on a visual recognition memory task in Alzheimer disease. *J Neurol Neurosurg Psychiatry* 80, 444–447

Brunelin, J. *et al.* (2012) Efficacy and safety of bifocal tDCS as an interventional treatment for refractory schizophrenia. *Brain Stimul* 5, 431–432

Brunoni, A.R. *et al.* (2013) Impact of 5-HTTLPR and BDNF polymorphisms on response to sertraline versus transcranial direct current stimulation: implications for the serotonergic system. *Eur Neuropsychopharmacol* 23, 1530–1540

Buzsáki, G. and Watson, B.O. (2012) Brain rhythms and neural syntax: implications for efficient coding of cognitive content and neuropsychiatric disease. *Dialogues Clin Neurosci* 14, 345–367

Castro, J.B. and Urban, N.N. (2009) Subthreshold glutamate release from mitral cell dendrites. *J. Neurosci.* 29, 7023–7030

Chan, C.Y. and Nicholson, C. (1986) Modulation by applied electric fields of Purkinje and stellate cell activity in the isolated turtle cerebellum. *J. Physiol. (Lond.)* 371, 89–114

Chan, C.Y. *et al.* (1988) Effects of electric fields on transmembrane potential and excitability of turtle cerebellar Purkinje cells in vitro. *J. Physiol. (Lond.)* 402, 751–771

Christie, J.M. *et al.* (2011) Ca(2+)-dependent enhancement of release by subthreshold somatic depolarization. *Nat. Neurosci.* 14, 62–68

Datta, A. *et al.* (2011) Individualized model predicts brain current flow during transcranial direct-current stimulation treatment in responsive stroke patient. *Brain Stimul* 4, 169–174

Daws, L.C. (2009) Unfaithful neurotransmitter transporters: focus on serotonin uptake and implications for antidepressant efficacy. *Pharmacol. Ther.* 121, 89–99

Dembrow, N. and Johnston, D. (2014) Subcircuit-specific neuromodulation in the prefrontal cortex. *Front Neural Circuits* 8, 54

Do, J. *et al.* (2012) Functional roles of neurotransmitters and neuromodulators in the dorsal striatum. *Learn. Mem.* 20, 21–28

Dougherty, E.T. *et al.* (2014) Multiscale coupling of transcranial direct current stimulation to neuron electrodynamics: modeling the influence of the transcranial electric field on neuronal depolarization. *Comput Math Methods Med* 2014, 360179

Dubljević, V. *et al.* (2014) The Rising Tide of tDCS in the Media and Academic Literature. *Neuron* 82, 731–736

Dunlop, K., *et al* (2016). Noninvasive brain stimulation treatments for addiction and major depression. *Ann. N.Y. Acad. Sci.*, n/a-n/a. doi:10.1111/nyas.12985.

Engel, A.K. and Singer, W. (2001) Temporal binding and the neural correlates of sensory awareness. *Trends Cogn. Sci. (Regul. Ed.)* 5, 16–25

Fritsch, B. *et al.* (2010) Direct current stimulation promotes BDNF-dependent synaptic plasticity: potential implications for motor learning. *Neuron* 66, 198–204
Fröhlich, F. and McCormick, D.A. (2010) Endogenous electric fields may guide neocortical network activity. *Neuron* 67, 129–143
Galea, J.M. *et al.* (2011) Dissociating the roles of the cerebellum and motor cortex during adaptive learning: the motor cortex retains what the cerebellum learns. *Cereb. Cortex* 21, 1761–1770
Gladwin, T. E., *et al.* (2012) Anodal tDCS of dorsolateral prefontal cortex during an Implicit Association Test. *Neurosc Lett* 517, 82–86.
Greer, P.L. and Greenberg, M.E. (2008) From synapse to nucleus: calcium-dependent gene transcription in the control of synapse development and function. *Neuron* 59, 846–860
Herzfeld, D.J. *et al.* (2014) Contributions of the cerebellum and the motor cortex to acquisition and retention of motor memories. *Neuroimage* 98, 147–158
Horvath, J.C. *et al.* (2014) Transcranial direct current stimulation: five important issues we aren't discussing (but probably should be). *Front Syst Neurosci* 8, 2
Horvath, J.C. *et al.* (2015a) Evidence that transcranial direct current stimulation (tDCS) generates little-to-no reliable neurophysiologic effect beyond MEP amplitude modulation in healthy human subjects: A systematic review. *Neuropsychologia* 66, 213–236
Horvath, J.C. *et al.* (2015b) Quantitative Review Finds No Evidence of Cognitive Effects in Healthy Populations From Single-session Transcranial Direct Current Stimulation (tDCS). *Brain Stimul* 8, 535–550
Islam, N. *et al.* (1995a) Increase in the calcium level following anodal polarization in the rat brain. *Brain Res.* 684, 206–208
Islam, N. *et al.* (1995b) c-Fos expression mediated by N-methyl-D-aspartate receptors following anodal polarization in the rat brain. *Exp. Neurol.* 133, 25–31
Jayaram, G. *et al.* (2012) Modulating locomotor adaptation with cerebellar stimulation. *J Neurophysiol* 107, 2950–2957
Kabakov, A.Y. *et al.* (2012) Contribution of axonal orientation to pathway-dependent modulation of excitatory transmission by direct current stimulation in isolated rat hippocampus. *J. Neurophysiol.* 107, 1881–1889
Kim, S. *et al.* (2014) tDCS-induced alterations in GABA concentration within primary motor cortex predict motor learning and motor memory: a 7 T magnetic resonance spectroscopy study. *Neuroimage* 99, 237–243
Kim, Y.J. *et al.* (2014) Facilitation of corticospinal excitability by virtual reality exercise following anodal transcranial direct current stimulation in healthy volunteers and subacute stroke subjects. *J Neuroeng Rehabil* 11, 124
Kuo, M.F. *et al.* (2007) Focusing effect of acetylcholine on neuroplasticity in the human motor cortex. *J. Neurosci.* 27, 14442–14447
Kuo, M.F. *et al.* (2008) Boosting focally-induced brain plasticity by dopamine. *Cereb. Cortex* 18, 648–651
Lally, N. *et al.* (2013) Does excitatory fronto-extracerebral tDCS lead to improved working memory performance? *F1000Res* 2. doi:10.12688/f1000research.2-219.v2.
Lamont, M.G. and Weber, J.T. (2012) The role of calcium in synaptic plasticity and motor learning in the cerebellar cortex. *Neurosci Biobehav Rev* 36, 1153–1162
Li, H. *et al.* (2015) The temporary and accumulated effects of transcranial direct current stimulation for the treatment of advanced Parkinson's disease monkeys. *Sci Rep* 5, 12178
Liebetanz, D. *et al.* (2002) Pharmacological approach to the mechanisms of transcranial DC-stimulation-induced after-effects of human motor cortex excitability. *Brain* 125, 2238–2247
Lu, B. *et al.* (2014) BDNF and synaptic plasticity, cognitive function, and dysfunction. *Handb Exp Pharmacol* 220, 223–250
Madhavan, S. *et al.* (2016) Reliability and Variability of tDCS Induced Changes in the Lower Limb Motor Cortex. *Brain Sci* 6.
McKay, B.E. *et al.* (2006) Ca(V)3 T-type calcium channel isoforms differentiallydistribute to somatic and dendritic compartments in rat central neurons. *Eur. J. Neurosci.* 24, 2581–2594

Mitsushima, D. *et al.* (2013) A cholinergic trigger drives learning-induced plasticity at hippocampal synapses. *Nat Commun* 4, 2760

Miyaguchi, S. *et al.* (2013) Corticomotor excitability induced by anodal transcranial direct current stimulation with and without non-exhaustive movement. *Brain Res* 1529, 83–91.

Morin-Moncet, O. *et al.* (2014) BDNF Val66Met polymorphism is associated with abnormal interhemispheric transfer of a newly acquired motor skill. *J. Neurophysiol.* 111, 2094–2102

Morrissette, D.A. and Stahl, S.M. (2014) Modulating the serotonin system in the treatment of major depressive disorder. *CNS Spectr* 19 Suppl 1, 57–67; quiz 54–57, 68

Moriwaki, A. *et al.* (1995) Induction of Fos expression following anodal polarization in rat brain. *Psychiatry Clin. Neurosci.* 49, 295–298

Murphy, D.L. *et al.* (2004) Serotonin transporter: gene, genetic disorders, and pharmacogenetics. *Mol. Interv.* 4, 109–123

Murphy, D.N. *et al.* (2009) Transcranial direct current stimulation as a therapeutic tool for the treatment of major depression: insights from past and recent clinical studies. *Curr Opin Psychiatry* 22, 306–311

Nitsche, M.A. *et al.* (2003) Pharmacological modulation of cortical excitability shifts induced by transcranial direct current stimulation in humans. *J. Physiol. (Lond.)* 553, 293–301

Nitsche, M.A. *et al.* (2004a) Catecholaminergic consolidation of motor cortical neuroplasticity in humans. *Cereb. Cortex* 14, 1240–1245

Nitsche, M.A. *et al.* (2004b) Consolidation of human motor cortical neuroplasticity by D-cycloserine. *Neuropsychopharmacology* 29, 1573–1578

Nitsche, M.A. *et al.* (2004c) GABAergic modulation of DC stimulation-induced motor cortex excitability shifts in humans. *Eur. J. Neurosci.* 19, 2720–2726

Nitsche, M.A. *et al.* (2009) Serotonin affects transcranial direct current-induced neuroplasticity in humans. *Biol. Psychiatry* 66, 503–508

Pang, P.T. *et al.* (2004) Cleavage of proBDNF by tPA/plasmin is essential for long-term hippocampal plasticity. *Science* 306, 487–491

Parazzini, M. *et al.* (2013) Computational model of cerebellar transcranial direct current stimulation. , in *2013 35th Annual International Conference of the IEEE Engineering in Medicine and Biology Society (EMBC)*, pp. 237–240

Pezet, S. *et al.* (2002) BDNF: a neuromodulator in nociceptive pathways? *Brain Res. Brain Res. Rev.* 40, 240–249

Polanía, R. *et al.* (2011) Modulating functional connectivity patterns and topological functional organization of the human brain with transcranial direct current stimulation. *Hum Brain Mapp* 32, 1236–1249

Purpura, D.P. and Mcmurtry, J.G. (1965) INTRACELLULAR ACTIVITIES AND EVOKED POTENTIAL CHANGES DURING POLARIZATION OF MOTOR CORTEX. *J. Neurophysiol.* 28, 166–185

Quartarone, A., *et al.* (2004) Long lasting effects of transcranial direct current stimulation on motor imagery. *Neuroreport* 15, 1287–1291.

Radman, T. *et al.* (2009) Role of cortical cell type and morphology in subthreshold and suprathreshold uniform electric field stimulation in vitro. *Brain Stimul* 2, 215–228, 228.e1–3

Rahman, A. *et al.* (2014) Polarizing cerebellar neurons with transcranial Direct Current Stimulation. *Clin Neurophysiol* 125, 435–438

Rampersad, S.M. *et al.* (2014) Simulating transcranial direct current stimulation with a detailed anisotropic human head model. *IEEE Trans Neural Syst Rehabil Eng* 22, 441–452

Reato, D. *et al.* (2010) Low-intensity electrical stimulation affects network dynamics by modulating population rate and spike timing. *J. Neurosci.* 30, 15067–15079

Reato, D. *et al.* (2015) Lasting modulation of in vitro oscillatory activity with weak direct current stimulation. *J. Neurophysiol.* 113, 1334–1341

Schambra, H.M. *et al.* (2011) Probing for hemispheric specialization for motor skill learning: a transcranial direct current stimulation study. *J. Neurophysiol.* 106, 652–661

Soderling, T.R. and Derkach, V.A. (2000) Postsynaptic protein phosphorylation and LTP. *Trends Neurosci.* 23, 75–80

Stagg, C.J. *et al.* (2009) Polarity-sensitive modulation of cortical neurotransmitters by transcranial stimulation. *J. Neurosci.* 29, 5202–5206

Stagg, C.J. and Nitsche, M.A. (2011) Physiological basis of transcranial direct current stimulation. *Neuroscientist* 17, 37–53

Takano, Y. *et al.* (2011) A rat model for measuring the effectiveness of transcranial direct current stimulation using fMRI. *Neurosci. Lett.* 491, 40–43

Takemura, A. and Kawano, K. (2002) Sensory-to-motor processing of the ocular-following response. *Neurosci. Res.* 43, 201–206

Tanaka, J.-I. *et al.* (2008) Protein synthesis and neurotrophin-dependent structural plasticity of single dendritic spines. *Science* 319, 1683–1687

Thirugnanasambandam, N., *et al.* (2011a) Isometric contraction interferes with transcranial direct current stimulation (tDCS) induced plasticity: evidence of state-dependent neuromodulation in human motor cortex. *Restor Neurol Neurosci* 29, 311–320.

Thirugnanasambandam, N. *et al.* (2011b) Nicotinergic impact on focal and non-focal neuroplasticity induced by non-invasive brain stimulation in non-smoking humans. *Neuropsychopharmacology* 36, 879–886

Thorpe, S. *et al.* (2001) Spike-based strategies for rapid processing. *Neural Netw* 14, 715–725

Vallar, G. and Bolognini, N. (2011) Behavioural facilitation following brain stimulation: implications for neurorehabilitation. *Neuropsychol Rehabil* 21, 618–649

Villamar, M.F. *et al.* (2013) Focal modulation of the primary motor cortex in fibromyalgia using 4×1-ring high-definition transcranial direct current stimulation (HD-tDCS): immediate and delayed analgesic effects of cathodal and anodal stimulation. *J Pain* 14, 371–383

Vines, B.W. *et al.* (2008) Modulating activity in the motor cortex affects performance for the two hands differently depending upon which hemisphere is stimulated. *Eur. J. Neurosci.* 28, 1667–1673

Vollmann, H. *et al.* (2013) Anodal transcranial direct current stimulation (tDCS) over supplementary motor area (SMA) but not pre-SMA promotes short-term visuomotor learning. *Brain Stimul* 6, 101–107

Wiethoff, S. *et al.* (2014) Variability in response to transcranial direct current stimulation of the motor cortex. *Brain Stimul* 7, 468–475

Wilke, S., *et al.* (2017) No Effect of Anodal Transcranial Direct Current Stimulation on Gamma-Aminobutyric Acid Levels in Patients with Recurrent Mild Traumatic Brain Injury. *J Neurotrauma* 34, 281–290.

Wolff, S.B.E. *et al.* (2014) Amygdala interneuron subtypes control fear learning through disinhibition. *Nature* 509, 453–458

Yoon, K.J. *et al.* (2012) Functional improvement and neuroplastic effects of anodal transcranial direct current stimulation (tDCS) delivered 1 day vs. 1 week after cerebral ischemia in rats. *Brain Res.* 1452, 61–72

Zuchowski, M.L. *et al.* (2014) Acquisition of conditioned eyeblink responses is modulated by cerebellar tDCS. *Brain Stimul* 7, 525–531

Chapter Two

Deletion of long-term potentiation of cerebellar Purkinje cell ablates effects of anodal direct current stimulation on vestibulo-ocular reflex habituation

Suman Das, Marcella Spoor, Tafadzwa M. Sibindi, Peter Holland, Martijn Schonewille, Chris I De Zeeuw, Maarten A. Frens, Opher Donchin

Deletion of long-term potentiation of cerebellar Purkinje cell ablates effects of anodal direct current stimulation on vestibulo-ocular reflex habituation

Abstract

Anodal direct current stimulation (DCS) of the cerebellum facilitates adaptation tasks, but the mechanism underlying this effect is poorly understood. We have evaluated whether the effects of DCS effects depend on plasticity of cerebellar Purkinje cells (PCs). Here, we have successfully developed a mouse model of cerebellar DCS, allowing us to present the first demonstration of cerebellar DCS driven behavioral changes in rodents. We have utilized a simple gain down vestibulo-ocular reflex (VOR) adaptation paradigm, that stabilizes a visual image on the retina during brief head movements, as behavioral tool. Our results provide evidence that anodal stimulation has an acute post-stimulation effect on baseline gain reduction of VOR (VOR gain in sham, anodal and cathodal group are 0.75 ± 0.12, 0.68 ± 0.1 and 0.78 ± 0.05 respectively). Moreover, this anodal induced decrease in VOR gain is directly dependent on the PP2B medicated synaptic long-term potentiation and intrinsic plasticity pathways of PCs.

2.1 Introduction

Transcranial direct current stimulation (tDCS) modulates cerebellar dependent motor learning tasks (Avila *et al*., 2015; Hardwick *et al*., 2014; Herzfeld *et al*., 2014; Jayaram *et al*., 2012) by applying a weak constant electrical current (amplitude <2 mA) through scalp electrodes. This technique allows us to stimulate the target region by the positive (anodal) or negative (cathodal) current (Das *et al*., 2016). Data collected in humans suggests that polarity specific effects of tDCS may be obtained by changing cerebellar cortical excitability (Galea *et al*., 2009). However, the mechanism behind tDCS dependent modulation of motor learning is unclear (Das *et al*., 2016). To optimally use tDCS in various cerebellar dependent motor learning disorders, a better understanding of mechanisms is vital (Bastian *et al*., 2011; Benussi *et al*., 2015; Hardwick *et al*., 2014; Ivry *et al*., 2004; Xu-Wilson *et al*., 2009).

Various animal models of DCS (direct current stimulation that is not transcranial) serve in exploration of the mechanism of tDCS (Bindman *et al*., 1964; Creutzfeldt *et al*., 1962; Purpura *et al*., 1965). In these models, a small part of the skull is removed at the site of stimulation in order to reduce the inter-subject variability of transcranial-conductance.

Our current study aims to explore the mechanism of action of DCS on cerebellar learning. To probe polarity specific effects of DCS on cerebellar learning, we employed a gain-down vestibulo-ocular reflex (VOR) adaptation task. The VOR aims to compensate for head movement by making an eye movement in the opposite direction, in order to stabilize the image on the retina (Probst *et al*., 1986). This compensatory eye movement can be adapted based on mismatched visual input, a process that requires the cerebellum (Kawato *et al*., 1992). Here we presented a sinusoidal optokinetic by using a 360º virtual environment and vestibular stimulus by using a turn-table in phase, resulting in a decrease of the response to the same vestibular stimulus in the dark (Tempia *et al*., 1992). The turn-table mimics the head movement while the movement direction of the virtual environment demands orientation specific compensation of the eye movement (similar to the natural environment).

The gain-down adaptation of the VOR (Tiliket *et al.*, 1993) may depend partly on both the cerebellar flocculus and the downstream vestibular nuclei (VN) (Ito *et al*., 1982; Lisberger *et al*., 1974). To test the importance of PC plasticity in polarity-specific DCS modulation, we

investigated L7-PP2B mice, lacking postsynaptic and intrinsic plasticity of PC (Schonewille *et al*., 2010). Our prediction is that at least some DCS effects (caused either by anodal or cathodal stimulation) would be compromised in this mutant because DCS has an extensive modulatory role on PC dendrites (Chan *et al*., 1986; Chan *et al*., 1988).

A rodent model of DCS has been validated in cortical spreading depression (Liebetanz *et al*., 2005) and epilepsy (Liebetanz *et al*., 2006a). Anodal stimulation of frontal cortex enhances the Blood-oxygen-level dependent (BOLD) signal, an indication of higher neuronal activity (Takano *et al*., 2011). Furthermore, DCS alters neocortical plasticity not only by altering pre-synaptic sensitivity (Márquez-Ruiz *et al*., 2012) but also by promoting brain-derived neurotrophic factor (BDNF) dependent long-term potentiation (LTP) (Fritsch *et al*., 2010). As the plasticity mechanisms of the cerebellar cortex are different from those in neocortex (Hansel *et al*., 2005; Lamont and Weber, 2012) there is ample justification for an animal model of cerebellar DCS. Moreover, the cerebellum is ideal to identify the mechanism(s) of DCS because – (i) the structure of rodent cerebellum is clear and accessible, (ii) the plasticity mechanisms are well studied and (iii) there is a wide range of mutant mouse models available to test which pathways are functionally relevant (De Zeeuw *et al*., 2011). Therefore, the present study focuses not only on developing an animal model of cerebellar DCS but also utilizes one of the most important mutant mouse models to unravel the role of PC plasticity in mediating DCS effects on VOR adaptation.

2.2 Methods

2.2.1 Summary of methodology

C57BL/6 (wild type, N=24) and L7-PP2B (LTP deficient mutants, N=22) mice were implanted with a DCS-implant for administration of direct current stimulation (DCS) over the cerebellum. DCS was applied to separate groups of mice as anodal, cathodal or sham-stimulation. Eye movements were recorded using an infrared-sensitive CCD camera during horizontal VOR gain-down adaptation learning. In testing sessions, the eye response to vestibular stimulation, i.e. the motion of the table, (amplitude of 5° at 1 Hz frequency) in the dark was recorded. In training sessions, vestibular and visual stimulation (amplitude of 5° at 1 Hz frequency) were coupled so as to cause reduction of the VOR gain. Two baseline test sessions were followed by 10 min of DC stimulation and then by an additional baseline test session. There were then 5 training sessions of

5 min each, each followed by a test session. We subsequently compared the reduction of VOR gain in the different stimulation groups and across strains.

2.2.2 Experimental paradigm

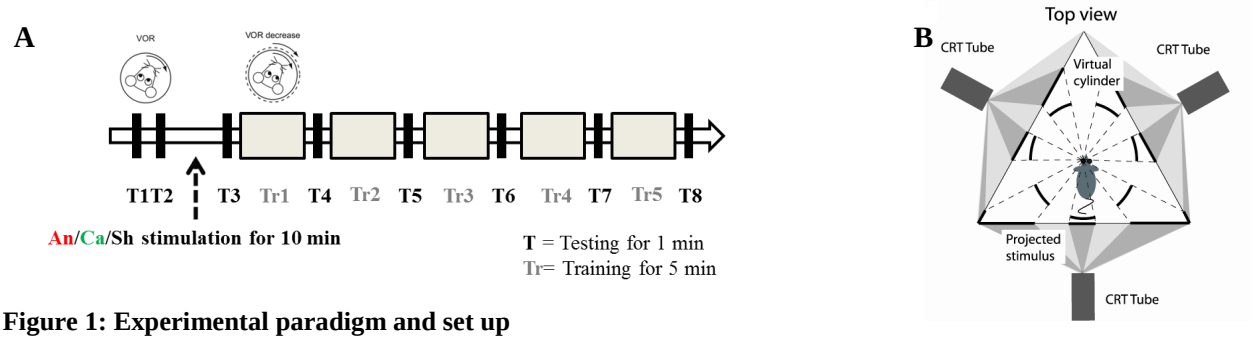

Figure 1: Experimental paradigm and set up

A) Schematic diagram of the experimental paradigm. *T* represents a testing session where the animal is exposed to VOR in dark by moving the turn table in a sinusoidal manner (5º amplitude at 1 Hz). *Tr* represents the training session where the animal is presented with a sinusoidal visual cue which is in phase with the table movement. After two testing session (*T1* and *T2*) the animals are randomly assigned to the anodal (*An*), cathodal (*Ca*) or sham (*Sh*) stimulation. **B) Schematic diagram of the experimental apparatus.** Top down view describes the position of the mouse in relation to the virtual environment created by three projectors.

Mice were habituated to the experimental apparatus for a minimum of 2 days to reduce the novelty-induced anxiety and restrain-stress after they recovered from the surgery.

Each experiment consisted of 8 test (T) and 5 training (Tr) sessions. The duration of each test session was 1 min, and the duration of each training session was 5 min. In test sessions, a sinusoidal vestibular stimulation which was generated by moving the table with a 5° amplitude at 1 Hz frequency, was applied in the dark. Eye movements were recorded simultaneously. In training sessions, in phase vestibular and optokinetic sinusoidal stimuli (5° amplitude at 1 Hz frequency) were given (Figure 1A), in order to reduce the VOR gain. Eye movements were continuously recorded.

Every experiment was initiated by two baseline measurements of VOR (T1 and T2). Then the mice were randomly divided into 3 groups, and received anodal, cathodal or sham DC stimulation. The current amplitude was ramped up over 30 s to 113.2 µA and kept constant for 10 min (positive polarity for the anodal group, negative polarity for the cathodal group). For the sham group, amplitude was then immediately ramped down (over 30 s) while for the anodal and cathodal groups current was maintained for 10 min of stimulation. After the stimulation, another session of testing

(T3) was conducted and then gain-down adaptation learning training was initiated. A testing session was conducted to calculate the learning rate after every training session (Figure 1A).

2.2.3 Experimental procedure

2.2.3.1 Animals

C57BL/6 (N=24) mice were acquired from Charles River laboratories, Inc. (Wilmington, MA, USA). L7-PP2B mutants (N=22) were bred in Erasmus MC, Rotterdam. Mouse lines used in this study have been described previously (Schonewille *et al.*, 2010). Three to four mice were caged together in temperature-regulated (22 ± 1° C) housing with a 12:12 light-day cycle. Behavioral experiments were performed in the light cycle. Food and water was provided *ad libitum*. All experiments were reviewed and approved by the Erasmus animal ethics committee and conducted in accordance with Animal Welfare Committee of the Erasmus University and the European Communities Council Directive (86/609/EEC).

2.2.3.2 Surgery

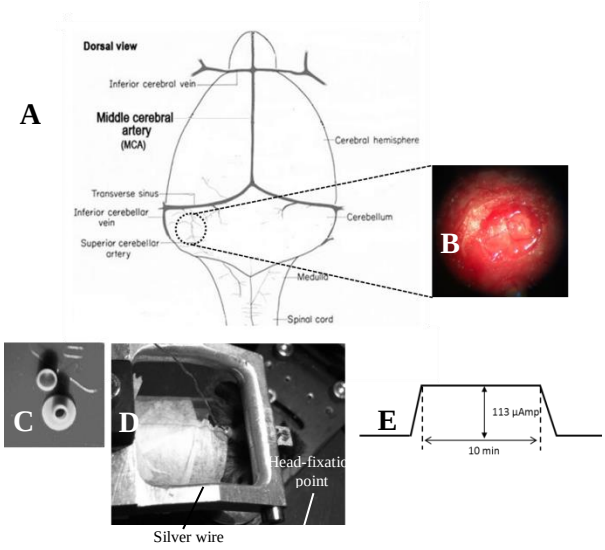

Figure 2: DCS location and procedure

A) Schematic representation of craniotomy for placement of implant over the cerebellum of a mouse brain. B) Craniotomy. Anatomical location for the DCS-implant placement. **C) DCS implant.** The DCS chamber serves as a bridge between the stimulating electrode and the brain. Above the chamber is the cap that serves to protect the brain from infection. **D) Stimulating the mice cerebellum.** The DCS chamber is filled with saline (0.9% NaCl) solution. A silver wire that touches the saline solution but not the dura directly is connected to the current generator (SUI-91, Isolated current source). During stimulation of the mouse is awake but head restrained. **E) Stimulation paradigm.** DCS is ramped up to 113 µAmp. The current is maintained at its peak value for 10 min. After the stimulation, the current is ramped down.

Mice, aged 10-12 weeks, were handled for 2 days before the surgery to reduce the effect of handling-induced stress. The surgical procedure was performed under sterile conditions. Isoflurane (5% induction, 1.5% in 0.5 L/min O_2 and 0.2 L/min air) was administered as an anesthetic drug while body temperature was regulated around 36.5 ± 0.5° via a feedback-controlled heating pad.

Breathing profile was continuously monitored. After shaving the head, a 1 cm long mid-sagittal incision was given. The bone was etched (37.5% phosphoric acid, Kerr, CA, USA) and a primer (Optibond, Kerr, CA, USA) was applied. To immobilize the animal during eye tracking, a pedestal containing two M1.4 nuts was glued to the skull using dental acrylic (Charisma, Flowline, Hereaus Kulzer GmBH, Germany).

In order to place a DCS implant, a circular craniectomy (approx. 2 mm in diameter) on the left occipital bone was performed after careful removal of the neck-muscles (vertical and horizontal) (Figure 2 A,B). The placement was on the center of the left parietal bone (by keeping the superior cerebellar artery at the center of the implant). A lubricating ointment (Duratears, Alcon Nederland BV, NL) was applied epidurally to protect the exposed area of brain from drying. The DCS implant (Figure 2C) was placed identically in all animals using an anatomical marker (Figure 2A, B) and then glued to the skull using cyanoacrylate gel (Plastic One Inc., VA, USA).

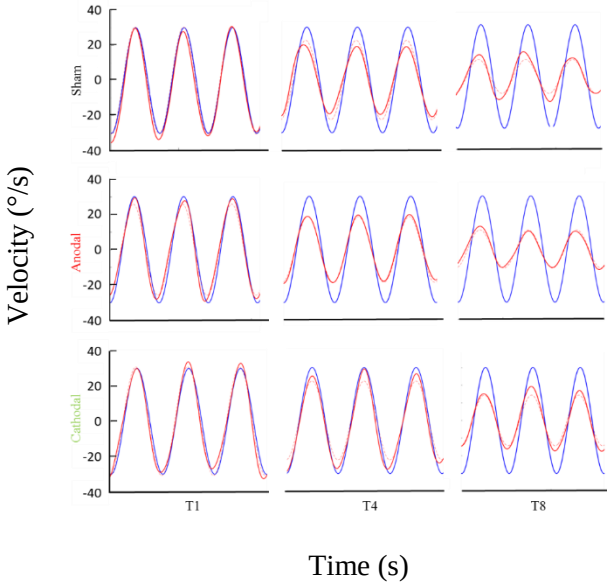

Figure 3: Examples of eye movement in different stimulation conditions.

Examples of filtered eye velocity illustrate results from mice that exhibited a decrease in the VOR after training with sham (top panels), anodal (middle panels) and cathodal (bottom panels) stimulation. Blue is vestibular stimulus and red is eye amplitude (solid red line is filtered eye-velocity, dotted red line fitted sine wave). Eye-trace of each stimulus condition has been presented during pre-training (T1), after first-training (T4) and after final-training (T8) in the left, middle and right panels, respectively.

The mice were given an analgesic (0.1ml/mg of body weight Buprenorphine/Temgesic) and placed under an infrared heating lamp until the animals started to move. Mice were allowed at least 4-5 days to recover before recordings were performed.

2.2.4 Apparatus

2.2.4.1 Visual and vestibular stimulation

Mice were head-fixed in a restrainer, which was fixed onto the center of a turntable, placed at the center of an isolateral triangle made by three projector-screens. A panoramic virtual reality display with 360° field of view was created by projecting

monochrome green dots on to those screens (Figure 1B). Horizontal rotation of the turntable was driven by a servomotor (Mavilor-DC motor 80, Infranor, Spain). Visual stimuli and movement of the turntable were under control of in-house software written in C++. Training and testing sessions were evoked by rotating the dots and/or the turntable sinusoidally. During each session, stimuli were ramped up to their peak velocity in 5 s for a smooth transition from static to dynamic state. They were also ramped down at the end.

2.2.4.2 Eye Movement Recordings

Eye movements were recorded with an infrared video system (ETL-200 with marker tracking modifications; ISCAN, Burlington, MA). The camera and lens were mounted under the table surface to reduce hindrance of the mouse vision. A hot mirror which was transparent to visible light and reflective to infrared light was used. The eye was illuminated with three infrared LEDs. The camera, mirror and LEDs were all mounted on an arm that could rotate about the vertical axis over a range of 26.12° (peak to peak). Eye movement recordings and calibration procedures were similar to those described by Stahl *et al.*, 2000. Images of the eye were captured at 120 Hz with an infrared-sensitive CCD camera. The eye image contained a bright corneal reflection and a dark pupil reflection. The image was focused by manipulating the offset and the gain of the detectors through the ISCAN software. From this image, x and y positions of each of the three markers were recorded in real time giving their location on a 512 X 256-pixel grid, with a resolution of one-third pixel horizontally and one-tenth pixel vertically (van Alphen *et al.*, 2010). These x and y translational positions of eye on the grid were converted into the angular rotation of the eyeball by the ISCAN system (resolution of 0.2° over a ±25° horizontal and ±20° vertical range using the pupil/corneal reflection difference). The horizontal and vertical pupil position data from the ISCAN were output as ±5 VDC signals. A delay of 30ms in the eye movement signal was introduced by the video system. Furthermore, this output signal was low-pass filtered with a cutoff frequency of 300 Hz (Cyberamp 380; Axon Instruments, CA, USA), sampled at 1 kHz and stored for offline analysis.

2.2.4.3 Direct current stimulation

A low amplitude (113 μA) of continuous DCS was applied using a constant current stimulator (SUI-91, Isolated current source, Cygnus Technology Inc., NC, USA; range = 0.1 μA - 10 mA).

This intensity corresponded to a current density of 3.6 mA/cm^2 (Liebetanz *et al.*, 2009). Currents were applied to the epidural surface of the cerebellar cortex through a circular DCS implant with a defined contact area (2 mm inner diameter). Prior to stimulation, the electrode was filled with saline solution (0.9% NaCl). A silver wire electrode connected to the stimulation device was attached to the DCS implant such that the tip of the silver wire touched the top level of the saline solution but did not touch the brain directly. This circular active electrode (Figure 2C) was chosen to create a symmetric current density without any edge effects (Ambrus *et al.*, 2011). A disposable foam electrode (Kendall Medi-Trace mini resting ECG electrode, Davis medical products Inc., CA, USA), was placed onto the ventral thorax of the animal to complete the circuit. The entire circuit was connected through a multimeter to check online current amplitude. Mice were awake during DCS to prevent possible interactions between DCS effects and anesthetic drugs. In addition, mice were introduced to the adaptation task right after the stimulation to quantify acute effects of stimulation. To avoid stimulation break effects (Liebetanz *et al.*, 2009), the current intensity was ramped up and down gradually over 30 s.

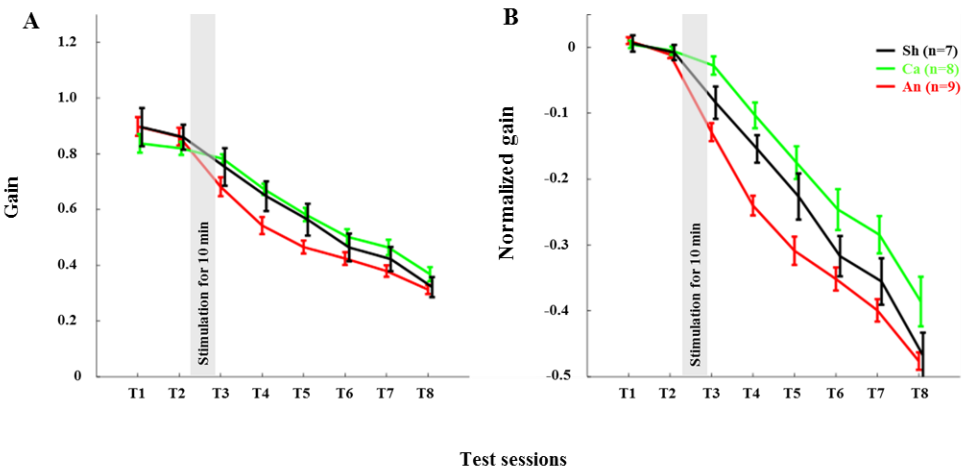

Figure 4: Anodal stimulation reduces VOR gain acutely in wild type C57BL/6 mice.

A) Time course of gain reduction due to adaptation: Trial-to-trial changes in mean VOR gain during VOR-decrease training. The VOR was tested pre- and post-training by measuring the eye movement response to the vestibular stimulus. **B) Time course of normalized gain reduction due to adaptation:** Trial-to-trial changes in mean normalized VOR gain during VOR-decrease training. Black, Green and Red lines are for sham, cathodal and anodal stimulation conditions respectively. The grey bar indicates the stimulation period. Error bars represent SEM.

2.2.5 Data analysis

Custom routines written in MATLAB (The MathWorks Inc., Natick, MA, USA) were designed and employed for automated offline data analysis. The position signal was shifted 30ms back in time to correct for the camera delay. A median filter (width 50ms) with a low-pass cutoff of 10 Hz was applied to smooth the position

data before transforming to velocity domain by a Savitski-Golay differentiating filter (frequency 50 Hz with a 3° polynomial). Rapid eye movements were detected and removed via a velocity threshold (150°/s). Then a 3 Hz FIR Butterworth low pass filter of 50 ms width was applied.

The processed data was divided into non-overlapping epochs of 2s (corresponding to two cycles of the stimulus). Amplitude data was obtained by fitting sine waves to the eye movement data in custom-made Matlab curve fitting routines using the least-squares method. Median amplitude values of the eye movement were calculated from the fitted sine waves. Gain was calculated for each testing session as the ratio between the fit eye velocity amplitude and stimulus velocity amplitude (***S***).

$$G_{Tn} = \frac{E_{Tn}}{S}$$

E= fit eye amplitude of a testing session, *n*=1 through 8,
S = stimulus amplitude

Mice were excluded when the absolute difference between baseline gains ($G_{T1} - G_{T2}$) was greater than 0.2. The baseline gain (***G_B***) was set as the mean of gains in G_{T1} and G_{T2}. Normalized gain (***G_N***) was also calculated for every test session.

$$G_N = \frac{G_B - G}{G_B + G}$$

2.2.6 Statistical analysis

Statistical analysis of the data was performed using SPSS 20.0 (SPSS, Chicago, IL). A three-way mixed-ANOVA with repeated measures was used to compare interaction and group effects, as the data showed a normal distribution. Significance levels were set to 0.05. Later on, a Bonferroni corrected post-hoc analysis was applied to find intra- / inter-group interactions. Values are represented here as mean ± SEM.

2.3 Results:

2.3.1 Degree of adaptation at the end of training session

The VOR gain-down adaptation paradigm caused a gradual reduction in VOR-amplitude in all mice (Figure 3, 4, 5, 6). Initially, the amplitude of the eye movement was similar to the stimulus

amplitude; i.e., the gain at T1 for C57BL/6 and L7-PP2B mice was 0.88 ± 0.03 and 1.03 ± 0.03, respectively (Figure 4, 6). The baseline VOR gain in L7-PP2B of more than 1 indicated that the eye amplitude overshot the head amplitude in these mice. After being subjected for 25 min to the gain-down training, the amplitude of VOR at T8 was reduced for both C57BL/6 (raw T8 gain = 0.33 ± 0.03) and L7-PP2B (raw T8 gain = 0.70 ± 0.03) group. In our multivariate ANOVA on the non-normalized data, the main effect of training over the time course was highly significant, $F(7,34) = 46.20$, $p < 0.001$. However, comparison of the sham stimulation data showed that the degree of adaptation was significantly higher in C57BL/6 than L7-PP2B mice, $F(5,40) = 14.94$, $p < 0.001$.

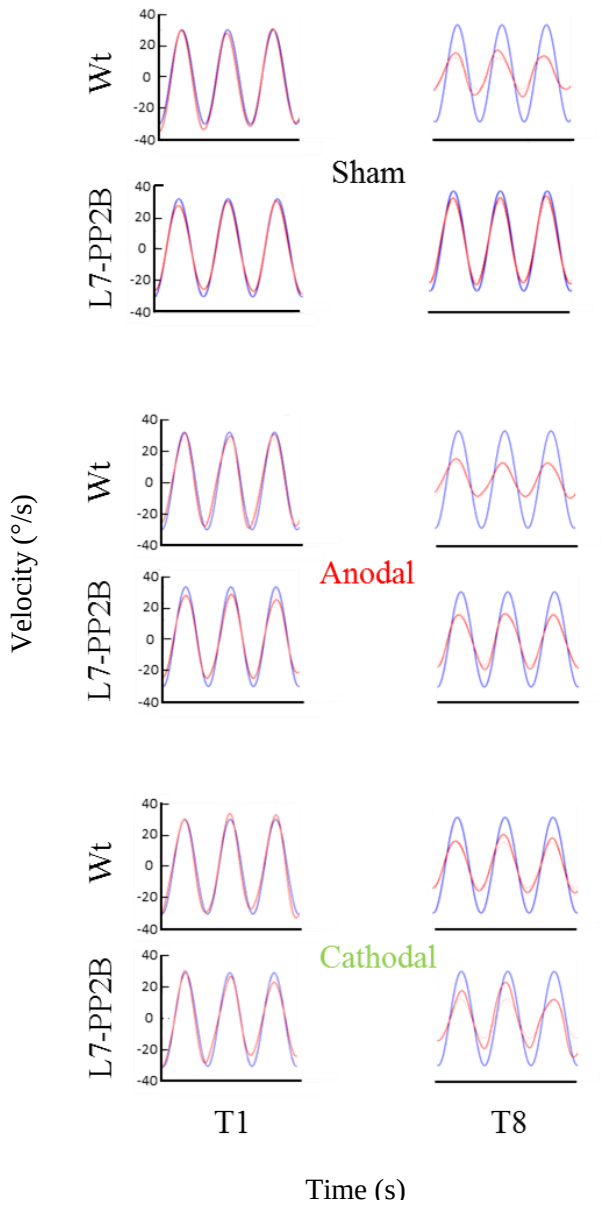

Figure 5: Raw eye plots show clear deficit in learning of L7-PP2B mice in all three stimulus conditions.

Example filtered eye velocity traces illustrate typical results from mice of both genetic backgrounds before (T1) and after (T8) adaptation. Blue is vestibular stimulus and red is eye velocity (solid red line is filtered eye-signal, dotted red line is the fitted sine wave). Eye amplitude decreases from pre- to post-training sessions (T1 and T8 respectively) in wild type mice. In contrast, L7-PP2B (LTP mutant) undergoes little change between T1 and T8 sessions.

2.3.2 Reduction of gain in C57BL/6 and L7-PP2B mice

The reduction in gain made across the eight test sessions was strongly dependent upon the genetic composition of mice, $F(7,38) = 4.98$, $p < 0.001$. We sought to find out at which steps the gain was maximally reduced between C57BL/6 and L7-PP2B mice. To do that, we checked the gain difference between two successive test sessions and then compared that across the mouse types. The tests of within-subjects

contrasts illustrated that the gain reduction from T5 to T6 ($F(5,40) = 2.48$, $p < 0.05$) and from T7 to T8 ($F(5,40) = 2.66$, $p < 0.05$) was significantly greater for C57BL mice compared to the L7-PP2B mice.

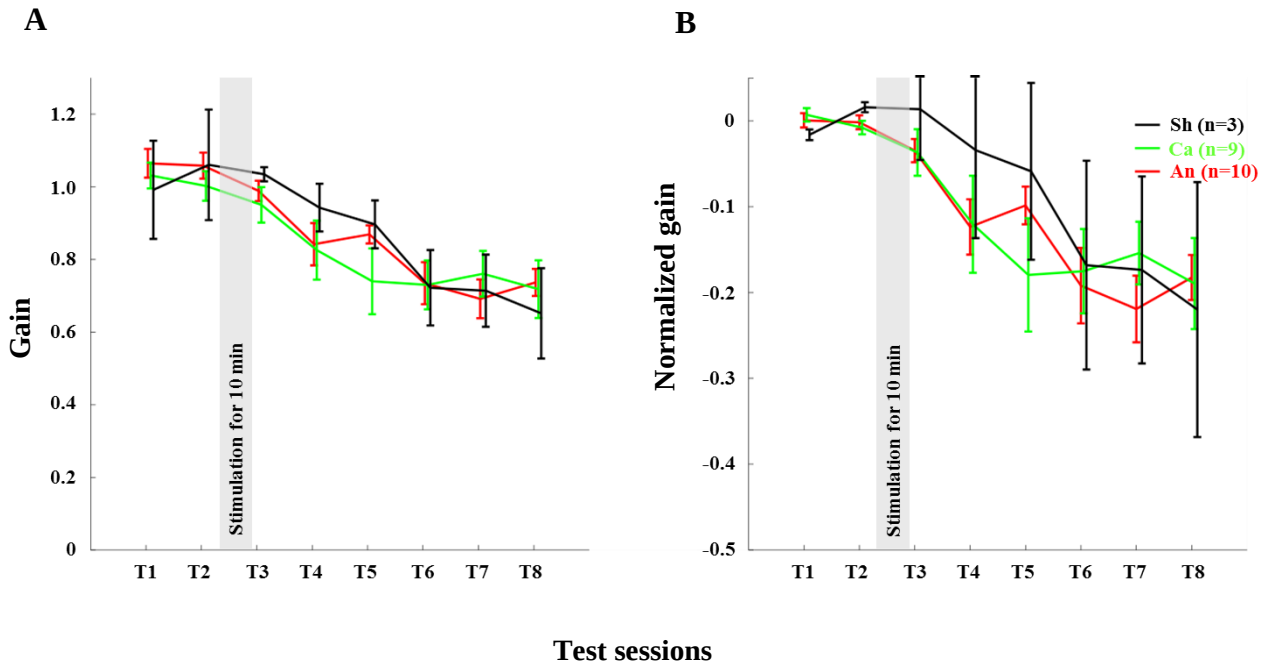

Figure 6: Genetic ablation of PC plasticity in L7-PP2B mice abolishes effects of anodal stimulation on gain-down adaptation. A) Plot of gain during gain-down adaptation:

Trial-to-trial changes in VOR gain during VOR-decrease training in L7-PP2B mice. The VOR was tested pre- and post-training by measuring the eye movement response to the vestibular stimulus. **B) Plot of normalized gain throughout the course of the behavioral paradigm:** Trial-to-trial changes in VOR gain during VOR-decrease training. Black, Green and Red lines are for sham, cathodal and anodal stimulation conditions respectively. The grey bar indicates the stimulation period. Error bars represent SEM, because of large SEM we do not find any significant difference between the groups.

2.3.3 Effects of DCS on VOR adaptation

ANOVA further indicated that DCS polarity had a significant modulatory role on the gain reduction, $F(14,70) = 2.07$, $p < 0.05$, suggesting that the amplitude of gain decrease across the eight tests (from T1 to T8) was dependent upon stimulus polarity. Moreover, the gain decrease across eight test sessions yielded a significant interaction between stimulus polarity and genetic background of the mice (C57BL/6 and L7-PP2B mice, ($F(7, 35) = 2.52$, $p < 0.05$). In the following sections, we discuss how the modulatory role of DCS was altered depending on the mouse type.

2.3.4 Anodal stimulation reduced VOR gain in C57BL/6 acutely

The anodal stimulation triggered faster initial VOR gain reduction compared to the cathodal stimulation ($F(2, 21) = 9.56$, $p < 0.001$, Figure 4A) in wild type mice. There was a significant post-stimulation reduction of gain at T3 (pre-training reduction of gain) in the anodal group compared to the cathodal group. The contrast analysis, T2 vs T3, comparing the raw gain at T2 with that made in T3, was statistically significant ($F(2, 21) = 6.01$, $p < 0.01$). Interestingly, the anodal, sham and cathodal groups finished at the same degree of adaptation (T8), although the anodal group showed significant initial reduction in VOR gain.

Next, we normalized the gain of every mouse to its own baseline to provide a comparable measure of gain for all animals. Normalized gain (Figure 4B) depicted a clear polarity-dependent divergence in the gain. The initial post-stimulation period showed that the cathodal stimulation significantly decelerated gain reduction compared to the anodal stimulation. The reduction of gain in the sham condition – as expected - remained between the rate in the anodal and the cathodal conditions (Figure 4B).

2.3.5 Deletion of PP2B in PC abolished anodal effect

Anodal stimulation lost its modulatory role when potentiation was eliminated from PCs (Figure 6A, B). Anodal stimulation failed to improve learning in L7-PP2B mice (T8 gain = 0.74 ± 0.04), compared to the sham group (T8 gain = 0.65 ± 0.08; Figure 5). Moreover, anodal stimulation could not reduce the baseline gain in these mutants (T2 gain = 1.06 ± 0.04 , T3 gain = 0.99 ± 0.04). The large error bars in the sham condition is due to low sampling numbers (N = 3). Moreover, we think that chronic mutation (deletion of LTP in PCs) leads to the adoption of various adaptation mechanisms in the network. Therefore, when an external current stimulus was applied the network showed varied responses to cope up with the situation. This could be the case in finding a large variability in the stimulus groups.

An hour long sinusoidal oscillatory stimulus led to decrease in VOR gain (approximately to 28 %) across various species (Clément *et al.*, 2002; Dow *et al*., 1998; Tempia *et al*., 1992). The cause of this VOR gain reduction in rodents has been pointed out as habituation rather than learning

(Tempia *et al*., 1992). Therefore, we think that the gain reduction (27 + 2 %) in L7-PP2B mice (similar to Schonewille *et al.*, 2010) across all three stimulus-conditions is due to the habituation.

2.4 Discussion

Our study demonstrates three major findings of the polarity specific effects of DCS on VOR gain-down adaptation. First, anodal stimulation of cerebellar cortex decreases VOR gain acutely compared to the cathodal stimulation condition in C57BL/6 control mice. Second, despite differences in initial post-stimulation reduction in gain amplitude, the final gain reduction is similar in the anodal and the cathodal stimulation groups of C57BL/6 control mice. Third, our data, remarkably, shows when potentiation of the PCs is genetically ablated in L7-PP2B mice, anodal stimulation no longer led to VOR gain reduction. Hence, our interpretation is that anodal stimulation driven VOR gain reduction depends on a PP2B-dependent PC potentiation pathway, either at the upstream dendritic level or at the downstream axonal level where PCs innervate vestibular nuclei (VN) neurons (Schonewille *et al.*, 2010).

We found that anodal stimulation of the cerebellum decreases VOR gain acutely (Figure 4A, B), though we don't see an effect on adaptation-rate like in other studies (Avila *et al.*, 2015; Herzfeld *et al.*, 2014; Jayaram *et al*., 2012; Zuchowski *et al*., 2014). We see that VOR gain is reduced prior to the training. Perhaps anodal stimulation induced an acute increase in inhibition by enhancing PC activity. Indeed, others have also reported that artificial activation of PCs may contribute to the induction of VOR gain-down adaptation (Nguyen-Vu *et al*., 2013). Moreover, a low amplitude external electric field (EEF) is sufficient to modulate PC activity (Chan and Nicholson, 1986; Chan *et al*., 1988). Together these results suggest that anodal DCS may induce higher PC activity, which in turn could lead to inhibition of its downstream structures.

The possibility that the effects of DCS on plasticity are in part secondary effects on downstream structures comports with there being at least two sites of VOR plasticity (Hansel *et al*., 2005): one in the floccular region of cerebellar cortex and one in the VN (Gao *et al*., 2012). Physiological studies would be necessary to elucidate the relative effects, and these studies would need to include direct measurements from both regions.

We also found that the total gain reduction was similar in the anodal and the cathodal stimulation conditions although the gain reduction at the early phase is clearly different (Figure 4A). In our study, training and testing are assessed post DCS, whereas most of the reports available today are based on stimulation applied during learning. For instance, anodal stimulation facilitates learning in locomotor (Jayaram *et al*., 2012), force field (Herzfeld *et al*., 2014), and saccade (Avila *et al*., 2015) adaptation as well as eye-blink conditioning tasks (Zuchowski *et al*., 2014), while cathodal stimulation hinders leaning in all these tasks. Surprisingly, the post-stimulation deadaptation curve (Jayaram *et al*., 2012; Herzfeld *et al*., 2014) or extinction rate (Zuchowski *et al*., 2014) shows no difference across various stimulation groups. The later finding is notable because irrespective of altered rate and total amount of learning, polarity has no effect on post-stimulation de-adaptation/ learning processes. In our study, we find that DCS has no post-stimulation effect on the learning phase. Therefore, our study clearly depicts both anodal and cathodal stimulation have short-lasting effects on the habituation phase of the gain-down VOR adaptation task. The de-adaptation experiment (like other studies) is redundant, as we have done all the adaptation training sessions in the post-stimulation period. To discover the actual cause, similar experiments should be performed with a gain increase VOR adaptation paradigm (Gao *et al*., 2012).

L7-PP2B mice often showed more than one gain during baseline measurements (Figure 6A). Possibly, the eye overshoots the head-position as we have used higher sinusoidal velocity (amplitude of 5° at 1 Hz frequency). We think that sensory signals coming from the parallel fibers fail to excite PC sharply, as there is no LTP in L7-PP2B mice. Therefore, when the high velocity head-movement stops, PCs could not generate sharp inhibition on the vestibular nuclei to stop the eye-movement. A sub-optimal PC inhibition may have caused facilitation of the eye movement in the absence of the head-movement.

We propose three, non-exclusive, possibilities that may explain reduced sensitivity to anodal stimulation in the L7-PP2B mutants: (i) PCs in the mutants may receive more background inhibition; (ii) plasticity at the PC-VN synapses may be essential for VOR gain-down adaptation (De Zeeuw *et al*., 2015; See CSHP book by Kandel); and /or (iii) plasticity of synapses on PCs in mutants may be saturated, preventing adaptation. The first point reflects the possibility that anodal stimulation may cause inhibition rather than excitation of PCs when there is no LTP or intrinsic plasticity at PCs. Anodal stimulation driven subthreshold depolarization may augment GABA

release from molecular layer interneurons (MLI) (Christie *et al*., 2011; Stagg and Nitsche, 2011) and thereby increase inhibition onto PCs. The second possibility is that anodal DCS has a direct impact on PC-VN plasticity and thereby directly regulates the adaptation process. Loss of PC LTP may retard the effects of anodal stimulation on these synapses. The third reason could be that loss of LTP makes the circuit unresponsive to the pairing of the sensory stimulus with the motor response, as intrinsic plasticity of PCs is also erratic in these mutants (Schonewille *et al.*, 2010). The PP2B transgene may disrupt normal signaling through the PCs or the homeostasis of the network (Lamont and Weber, 2012). This can corrupt the instructive signals sent by Purkinje cells to downstream sites like the VN.

Cathodal stimulation induced inhibition of adaptation in L7-PP2B mutants is significantly stronger compared to C57BL/6 mice but similar to the sham group of L7-PP2B mice (Figure 5; 6B). It is evident that this cathodal suppression is a by-product of the mutation of potentiation at the PCs, as these mice fail to learn cerebellar tasks (Schonewille *et al.*, 2010). In addition, we need to examine to what extent long-term depression (LTD) at PF-PC pathway plays a role following cathodal stimulation.

In conclusion, we have successfully developed a mouse model of cerebellar DCS, allowing us to present the first demonstration of cerebellar DCS driven behavioral changes in rodents. We used this model in combination with the popular paradigm of VOR adaptation to test the effect of current stimulation on motor adaptation. The results presented here provide evidence that anodal DCS reduces VOR gain acutely, an effect that is disrupted by ablation of PP2B in PCs. This study, also finds support for recent claims that anodal and cathodal stimulation modulate cerebellar dependent adaptation acutely through distinct pathways. Future research must address the neuronal activity following cerebellar stimulation to understand the spatiotemporal aspects of DCS effects.

References:

Alphen, B. van, Winkelman, B. H. J., and Frens, M. A. (2010). Three-Dimensional Optokinetic Eye Movements in the C57BL/6J Mouse. *IOVS* 51, 623–630. doi:10.1167/iovs.09-4072.

Ambrus, G. G., Antal, A., and Paulus, W. (2011). Comparing cutaneous perception induced by electrical stimulation using rectangular and round shaped electrodes. *Clinical Neurophysiology* 122, 803–807. doi:10.1016/j.clinph.2010.08.023.

Avila, E., van der Geest, J. N., Kengne Kamga, S., Verhage, M. C., Donchin, O., and Frens, M. A. (2015). Cerebellar transcranial direct current stimulation effects on saccade adaptation. *Neural Plast.* 2015, 968970. doi:10.1155/2015/968970.

Bastian, A. J. (2011). Moving, sensing and learning with cerebellar damage. *Curr. Opin. Neurobiol.* 21, 596–601. doi:10.1016/j.conb.2011.06.007.

Benussi, A., Koch, G., Cotelli, M., Padovani, A., and Borroni, B. (2015). Cerebellar transcranial direct current stimulation in patients with ataxia: A double-blind, randomized, sham-controlled study. *Mov Disord.* 30, 1701–1705. doi:10.1002/mds.26356.

Bindman, L. J., Lippold, O. C. J., and Redfearn, J. W. T. (1964). The action of brief polarizing currents on the cerebral cortex of the rat (1) during current flow and (2) in the production of long-lasting after-effects. *J Physiol* 172, 369–382.

Chan, C. Y., Hounsgaard, J., and Nicholson, C. (1988). Effects of electric fields on transmembrane potential and excitability of turtle cerebellar Purkinje cells in vitro. *J. Physiol. (Lond.)* 402, 751–771.

Chan, C. Y., and Nicholson, C. (1986). Modulation by applied electric fields of Purkinje and stellate cell activity in the isolated turtle cerebellum. *J. Physiol. (Lond.)* 371, 89–114.

Christie, J. M., Chiu, D. N., and Jahr, C. E. (2011). Ca(2+)-dependent enhancement of release by subthreshold somatic depolarization. *Nat. Neurosci.* 14, 62–68. doi:10.1038/nn.2718.

Clément, G., Flandrin, J.-M., and Courjon, J.-H. (2002). Comparison between habituation of the cat vestibulo-ocular reflex by velocity steps and sinusoidal vestibular stimulation in the dark. *Exp Brain Res* 142, 259–267. doi:10.1007/s00221-001-0930-7.

Creutzfeldt, O. D., Fromm, G. H., and Kapp, H. (1962). Influence of transcortical d-c currents on cortical neuronal activity. *Exp. Neurol.* 5, 436–452.

Das, S., Holland, P., Frens, M. A., and Donchin, O. (2016). Impact of Transcranial Direct Current Stimulation (tDCS) on Neuronal Functions. *Front Neurosci* 10, 550. doi:10.3389/fnins.2016.00550.

De Zeeuw, C. I., Hoebeek, F. E., Bosman, L. W. J., Schonewille, M., Witter, L., and Koekkoek, S. K. (2011). Spatiotemporal firing patterns in the cerebellum. *Nat. Rev. Neurosci.* 12, 327–344. doi:10.1038/nrn3011.

De Zeeuw, C. I., and Ten Brinke, M. M. (2015). Motor Learning and the Cerebellum. *Cold Spring Harb Perspect Biol* 7, a021683. doi:10.1101/cshperspect.a021683.

Dow, E. R., and Anastasio, T. J. (1998). Analysis and neural network modeling of the nonlinear correlates of habituation in the vestibulo-ocular reflex. *J Comput Neurosci* 5, 171–190.

Fritsch, B., Reis, J., Martinowich, K., Schambra, H. M., Ji, Y., Cohen, L. G., *et al*. (2010). Direct current stimulation promotes BDNF-dependent synaptic plasticity: potential implications for motor learning. *Neuron* 66, 198–204. doi:10.1016/j.neuron.2010.03.035.

Galea, J. M., Jayaram, G., Ajagbe, L., and Celnik, P. (2009). Modulation of cerebellar excitability by polarity-specific noninvasive direct current stimulation. *J. Neurosci.* 29, 9115–9122. doi:10.1523/JNEUROSCI.2184-09.2009.

Gao, Z., van Beugen, B. J., and De Zeeuw, C. I. (2012). Distributed synergistic plasticity and cerebellar learning. *Nat. Rev. Neurosci.* 13, 619–635. doi:10.1038/nrn3312.

Händel, B., Thier, P., and Haarmeier, T. (2009). Visual motion perception deficits due to cerebellar lesions are paralleled by specific changes in cerebro-cortical activity. *J. Neurosci.* 29, 15126–15133. doi:10.1523/JNEUROSCI.3972-09.2009.

Hansel, C. (2005). When the B-team runs plasticity: GluR2 receptor trafficking in cerebellar long-term potentiation. *Proc Natl Acad Sci U S A* 102, 18245–18246. doi:10.1073/pnas.0509686102.

Hardwick, R. M., and Celnik, P. A. (2014). Cerebellar direct current stimulation enhances motor learning in older adults. *Neurobiol. Aging* 35, 2217–2221. doi:10.1016/j.neurobiolaging.2014.03.030.

Herzfeld, D. J., Pastor, D., Haith, A. M., Rossetti, Y., Shadmehr, R., and O'Shea, J. (2014). Contributions of the cerebellum and the motor cortex to acquisition and retention of motor memories. *Neuroimage* 98, 147–158. doi:10.1016/j.neuroimage.2014.04.076.

Islam, N., Aftabuddin, M., Moriwaki, A., Hattori, Y., and Hori, Y. (1995). Increase in the calcium level following anodal polarization in the rat brain. *Brain Res.* 684, 206–208.

Ito, M. (1982). Cerebellar control of the vestibulo-ocular reflex--around the flocculus hypothesis. *Annu. Rev. Neurosci.* 5, 275–296. doi:10.1146/annurev.ne.05.030182.001423.

Ivry, R. B., and Spencer, R. M. C. (2004). The neural representation of time. *Curr. Opin. Neurobiol.* 14, 225–232. doi:10.1016/j.conb.2004.03.013.

Jayaram, G., Tang, B., Pallegadda, R., Vasudevan, E. V. L., Celnik, P., and Bastian, A. (2012). Modulating locomotor adaptation with cerebellar stimulation. *Journal of Neurophysiology* 107, 2950–2957. doi:10.1152/jn.00645.2011.

Kawato, M., and Gomi, H. (1992). The cerebellum and VOR/OKR learning models. *Trends Neurosci.* 15, 445–453.

Lamont, M. G., and Weber, J. T. (2012). The role of calcium in synaptic plasticity and motor learning in the cerebellar cortex. *Neurosci Biobehav Rev* 36, 1153–1162. doi:10.1016/j.neubiorev.2012.01.005.

Learning and Memory Available at: http://www.cshlpress.com/default.tpl?action=full&--eqskudatarq=1077 [Accessed August 16, 2016].

Liebetanz, D., Fregni, F., Monte-Silva, K. K., Oliveira, M. B., Amâncio-dos-Santos, A., Nitsche, M. A., *et al*. (2006a). After-effects of transcranial direct current stimulation (tDCS) on cortical spreading depression. *Neurosci. Lett.* 398, 85–90. doi:10.1016/j.neulet.2005.12.058.

Liebetanz, D., Klinker, F., Hering, D., Koch, R., Nitsche, M. A., Potschka, H., *et al*. (2006b). Anticonvulsant effects of transcranial direct-current stimulation (tDCS) in the rat cortical ramp model of focal epilepsy. *Epilepsia* 47, 1216–1224. doi:10.1111/j.1528-1167.2006.00539.x.

Liebetanz, D., Koch, R., Mayenfels, S., König, F., Paulus, W., and Nitsche, M. A. (2009). Safety limits of cathodal transcranial direct current stimulation in rats. *Clin Neurophysiol* 120, 1161–1167. doi:10.1016/j.clinph.2009.01.022.

Lisberger, S. G., and Fuchs, A. F. (1974). Response of flocculus Purkinje cells to adequate vestibular stimulation in the alert monkey: fixation vs. compensatory eye movements. *Brain Res.* 69, 347–353.

Márquez-Ruiz, J., Leal-Campanario, R., Sánchez-Campusano, R., Molaee-Ardekani, B., Wendling, F., Miranda, P. C., *et al*. (2012). Transcranial direct-current stimulation modulates synaptic mechanisms involved in associative learning in behaving rabbits. *Proc Natl Acad Sci U S A* 109, 6710–6715. doi:10.1073/pnas.1121147109.

Nguyen-Vu, T. D. B., Kimpo, R. R., Rinaldi, J. M., Kohli, A., Zeng, H., Deisseroth, K., *et al*. (2013). Cerebellar Purkinje cell activity drives motor learning. *Nat. Neurosci.* 16, 1734–1736. doi:10.1038/nn.3576.

Probst, T., Brandt, T., and Degner, D. (1986). Object-motion detection affected by concurrent self-motion perception: psychophysics of a new phenomenon. *Behav. Brain Res.* 22, 1–11.

Purpura, D. P., and Mcmurtry, J. G. (1965). INTRACELLULAR ACTIVITIES AND EVOKED POTENTIAL CHANGES DURING POLARIZATION OF MOTOR CORTEX. *J. Neurophysiol.* 28, 166–185.

Schonewille, M., Belmeguenai, A., Koekkoek, S. K., Houtman, S. H., Boele, H. J., van Beugen, B. J., *et al*. (2010). Purkinje cell-specific knockout of the protein phosphatase PP2B impairs potentiation and cerebellar motor learning. *Neuron* 67, 618–628. doi:10.1016/j.neuron.2010.07.009.

Stagg, C. J., and Nitsche, M. A. (2011). Physiological basis of transcranial direct current stimulation. *Neuroscientist* 17, 37–53. doi:10.1177/1073858410386614.

Stahl, J. S., van Alphen, A. M., and De Zeeuw, C. I. (2000). A comparison of video and magnetic search coil recordings of mouse eye movements. *J. Neurosci. Methods* 99, 101–110.

Takano, Y., Yokawa, T., Masuda, A., Niimi, J., Tanaka, S., and Hironaka, N. (2011). A rat model for measuring the effectiveness of transcranial direct current stimulation using fMRI. *Neurosci. Lett.* 491, 40–43. doi:10.1016/j.neulet.2011.01.004.

Tempia, F., Dieringer, N., and Strata, P. (1991). Adaptation and habituation of the vestibulo-ocular reflex in intact and inferior olive-lesioned rats. *Exp Brain Res* 86, 568–578.

Tiliket, C., Shelhamer, M., Tan, H. S., and Zee, D. S. (1993). Adaptation of the vestibulo-ocular reflex with the head in different orientations and positions relative to the axis of body rotation. *J Vestib Res* 3, 181–195.

Xu-Wilson, M., Chen-Harris, H., Zee, D. S., and Shadmehr, R. (2009). Cerebellar contributions to adaptive control of saccades in humans. *J. Neurosci.* 29, 12930–12939. doi:10.1523/JNEUROSCI.3115-09.2009.

Zuchowski, M. L., Timmann, D., and Gerwig, M. (2014). Acquisition of conditioned eyeblink responses is modulated by cerebellar tDCS. *Brain Stimul* 7, 525–531. doi:10.1016/j.brs.2014.03.010.

Chapter Three

Cerebellar transcranial Direct Current stimulation does not modulate the adaptation of the vestibulo-ocular reflex in humans

Rick van der Vliet, Suzanne Louwen, Opher Donchin, Suman Das, Maarten A. Frens, Peter Holland, Ruud Selles, Jos N. van der Geest

Cerebellar transcranial Direct Current stimulation does not modulate the adaptation of the vestibulo-ocular reflex in humans

Abstract

The vestibulo-ocular reflex (VOR) serves to keep objects stable on the retina during head rotation. Recently, a study in mice showed a modulatory effect of Direct Current Stimulation on the plasticity of this eye movement reflex. We investigated the behavioral effect of cerebellar transcranial Direct Current Stimulation (tDCS) on human VOR plasticity in humans. Based on recent animal and human studies, we expected anodal cerebellar tDCS to enhance and cathodal stimulation to impair VOR plasticity.

We developed and validated a VOR adaptation paradigm with interspersed eye measurements to quantify monitor learning. Using this recording protocol, we directly compared offline anodal and cathodal stimulation to sham mirroring VOR- tDCS experiments reported in mice. Furthermore, we studied the effects of online anodal stimulation on VOR adaptation as tDCS might have different effects when applied just before or during learning. However, in contrast to our expectations, no effect of offline anodal or cathodal stimulation or online anodal stimulation on VOR learning was found.

We suggest that the likely reason for not finding a modulatory effect of tDCS on human VOR adaptation is that the electric field strength in the flocculus was insufficient to affect neuronal firing. Future research is necessary to establish the relation between electric field strength, neuronal firing and behavior before tDCS can be used as a scientific tool in VOR research.

3.1 Introduction

The oculomotor system functions to optimize vision. In foveated animals such as humans, moving the eyes is tantamount to keeping objects of interest on the center of the retina (fovea), which is the area with the highest visual acuity. To this purpose, the oculomotor system produces various gaze-directing and gaze-holding eye movements that prevent slipping of images across the fovea during self-motion. As part of these corrective movements, the short-latency Vestibulo-Ocular Reflex (VOR) generates eye movements in the opposite direction to the head in response to head rotation. Velocity of the head and the reflexive eye movements are identical even when tested in total darkness, culminating in unity VOR gain (eye velocity/ head velocity). However, external perturbations can make this relation inappropriate and result in retinal slip. In this case, adaptive mechanisms increase or decrease eye velocity to improve foveal stabilization (Leigh *et al.*, 2006). This adaptation process has been studied in humans by either coupling head to visual display rotation over the course of hours (Montfoort *et al.*, 2008; Shelhamer *et al.*, 1994; Suzuki *et al.*, 2006; Tiliket *et al.*, 1994) or altering movement of the external world across the retina with magnifying and minifying glasses for several days (Gonshor and Jones, 1976).

The cerebellum is believed to play a crucial role in adapting the VOR through the modification of parallel fiber-Purkinje cell (PF-PC) synapses in the flocculus (Blazquez *et al.*, 2003; Hirata and Highstein, 2001; Lisberger *et al.*, 1994; Schonewille *et al.*, 2011; Watanabe *et al.*, 1985). Supporting the role of Purkinje cells in VOR adaptation, neuropharmacological studies have shown that excitability-modifying agents alter use-dependent plasticity and behavior (Carter and McElligott, 2005; van Neerven *et al.*, 1991). Recently, a study applying cerebellar Direct Current Stimulation (DCS) before VOR training in mice suggested an increase in Purkinje cell firing and VOR adaptation with anodal stimulation and a decrease in firing rate and VOR adaptation with cathodal DCS (Das *et al.*, 2014). This last finding is particularly interesting because transcranial Direct Current Stimulation (tDCS) over the cerebellum in humans has been shown to alter cerebellar excitability (Galea *et al.*, 2009; Oulad Ben Taib and Manto 2013) and influence the rate of adaptive hand movement learning (Block and Celnik, 2013; Galea *et al.*, 2011), locomotor adaptation (Jayaram *et al.*, 2012; Villamer *et al.*, 2013) and saccade adaptation (Avila *et al.*, 2015; Panouilleres *et al.*, 2015). Therefore, human VOR tDCS experiments could open up an opportunity to bridge the gap between human and animal cerebellar research with respect to Direct Current

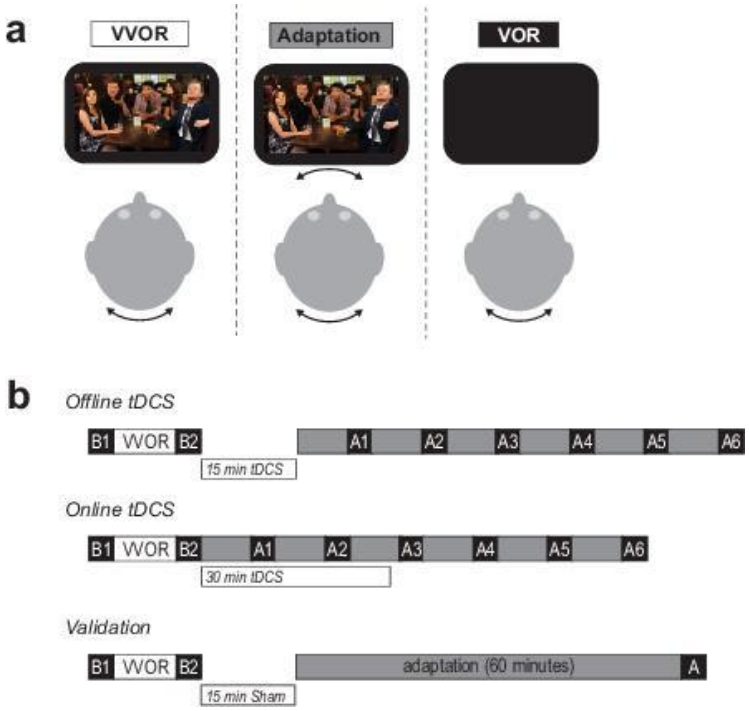

Figure 1 Experimental Setup:

Panel a. The three phases in the experiment. Visually-enhanced Vestibulo-Ocular Reflex (VVOR) was induced by rotating the chair while showing participants a movie that was projected stationary on the screen. VOR adaptation was evoked by simultaneously rotating the chair and the projection with an amplitude of 12° around the vertical axis. VOR eye movements were recorded in total darkness. ***Panel b***. Experimental procedures. All experiments started with two baseline measurements (B1 and B2) separated by 5 minutes of VVOR. In the main experiment (Offline tDCS), stimulation was applied for 15 minutes before training. The adaptation phase consisted of six 10-minute training and 1-minute VOR recording blocks (A1 through A6). In the online tDCS experiment, stimulation was applied for the first 30 minutes during the adaptation phase. In the validation experiment, training consisted of 60 minutes continuous adaptation and 1 VOR recording (A). (Sham) tDCS was applied for 15 minutes prior to adaptation.

Stimulation techniques. Translating tDCS results from animals to humans helps in gaining a more profound understanding of Direct Current Stimulation effects on neuronal excitability and behavior. In turn, this knowledge would aid the design of stimulation protocols for rehabilitation in different patient groups (Brunoni *et al.*, 2012). However, the cerebellar area primarily responsible for VOR adaptation (flocculus) is localized at considerable distance from the skull surface compared to cerebellar areas involved in forcefield (Herzfeld *et al.*, 2014), visuomotor (Galea *et al.*, 2011) or saccadic (Panouilleres *et al.*, 2015) adaptation, which were shown to be modulated by tDCS. Localization of the flocculus deep within the cerebellum might therefore diminish local electric field and decrease stimulation effects. Counter to this line of reasoning, motor cortex stimulation has been shown to modulate cortical excitability (Nitsche and Paulus, 2000; Nitsche and Paulus, 2001; Sriraman *et al.*, 2014) and behavior (Galea *et al.*, 2011; Reis et al., 2009; Reis et al., 2015) at half the current strength used for cerebellar stimulation, and we therefore believe electric field at the flocculus should still be in an effective range.

The present study evaluates the effects of tDCS on VOR adaptation in humans as a follow-up to an experiment in mice (Das *et al.*, 2014) with the ideal to develop a motor learning paradigm that

works in mice and men and helps addressing mechanistic questions on tDCS through physiological and behavioral experiments. For this purpose, a VOR adaptation paradigm with interspersed eye measurements was designed and validated. Using this protocol, we directly compared offline anodal and cathodal stimulation to sham to mirror the VOR-tDCS experiments in mice (Das *et al.*, 2014). In addition, we compared online with offline anodal stimulation because the physiological and behavioral (Datta *et al.*, 2012; Sriraman *et al.*, 2014) effects of tDCS might differ when stimulation is applied just before or during learning. We hypothesized that anodal stimulation over the cerebellum would increase and cathodal offline stimulation would decrease VOR adaptation in humans, similar to the results obtained in mice.

3.2 Material and Methods

3.2.1 Participants

In total, 54 healthy, right-handed participants (37 female; mean age 22 ± 3 years, range 18-29 years) without neurological or vestibular problems were recruited. 25 Participants were included in the main experiment (18 females, mean age 21 ± 2 years, range 18-28 years) and 29 participated in one of the two additional experiments. All participants had normal or corrected-to-normal vision and abstained from drinking coffee, energy drinks or alcohol two hours prior to the experiment. Participants were naïve to the purpose of the study and gave their written informed consent before participation. The Erasmus MC medical ethics committee approved the study.

3.2.2 Offline tDCS Experiment

For the main experiment of this study, VOR adaptation data was obtained in participants receiving either sham, anodal, or cathodal cerebellar transcranial Direct Current Stimulation (tDCS).

3.2.2.1 Experimental Procedure

Participants were seated in a rotational chair placed 224 cm in front of a wide translucent screen (235 cm x 170 cm; see figure 1A) and secured using seat belts. Head position was fixed relative to the chair by means of a custom-made bite-board (Dental Techno Benelux), ensuring concurrent rotation of the head and trunk. Chair rotation frequency was fixed at 0.3 Hz with an amplitude of

12° around the vertical axis, resulting in a peak angular velocity of 22.6 deg/s (see Watanabe et al., 2003).

Visually-enhanced VOR (VVOR) was evoked by back-projecting (Infocus LP 335, Portland, Oregon, United States) a movie (104 cm x 74 cm; "How I Met Your Mother", Twentieth Century Fox Film Cooperation, 2005, no subtitles with audio) onto the translucent screen while the participant was being rotated. A movie was chosen to ensure participants stayed alert and focused throughout the experiment. To induce VOR adaptation, the projection was rotated with identical phase and amplitude as the chair using rotatable mirrors (model number 6900, Cambridge Technology, Cambridge, United Kingdom). This means the projection is always at the same location relative to the participant during rotation. Participants therefore have to suppress their VOR in order to keep the movie stable on their retina which results in a gradual decline of VOR gain when measured in total darkness (Montfoort *et al.*, 2008; Shelhamer *et al.*, 1994; Suzuki *et al.*, 2006; Tiliket *et al.*, 1994). During VOR measurements, the projector was turned off and the room was completely darkened.

3.2.2.2 Eye movement recordings

Two-dimensional binocular eye movements were recorded using infrared video-oculography (Eyelink II, SMI, Germany; 500 Hz sample frequency, resolution of 20 sec of arc, see van der Geest and Frens, 2002). For VOR measurements, participants were asked to keep their eyes fixated at the middle of the screen even though it was completely dark. This location was briefly indicated by a red laser dot. The location of the eyes relative to the cameras was continuously monitored during the experiment to ensure the head remained well stabilized by the bite-board.

3.2.2.3 Transcranial Direct-Current Stimulation (tDCS)

tDCS was delivered through two saline-soaked sponge electrodes (5x5 cm) using a DC stimulator (DC stimulator, NeuroConn GmbH, Ilmenau, Germany). The target electrode was located on the right side of the scalp, 3 cm lateral to the inion. The reference electrode was positioned on the ipsilateral buccinator muscle (see Galea et al., 2009). Current was delivered during 15 minutes at 2 mA for both anodal and cathodal stimulation, resulting in a current density well below the threshold for tissue damage (0.08 vs. 14.3 mA/cm^2, (Liebetanz *et al.*, 2009). In all stimulation

conditions, current amplitude was increased or decreased in a ramp-like fashion over 30 seconds according to a well-established protocol (Galea *et al.*, 2011). In the sham condition, anodal or cathodal direct current was delivered for only 30 seconds, which has been shown to effectively blind participants to the stimulation condition (Gandiga *et al.*, 2006). Stimulation codes were used to keep the experimenter blind to the stimulation condition as well.

3.2.2.4 Experimental Protocol

The experimental protocol consisted of a baseline and an adaptation phase during which eight VOR eye movement recordings were made (see figure 1B). First, two VOR baseline recordings (blocks B1 and B2), separated by 5 minutes of VVOR stimulation, were recorded to assess VOR gain stability. After baseline recordings, cerebellar tDCS was applied for 15 minutes with both the chair and the visual display stationary (offline stimulation). Finally, 6 blocks of 10 minute VOR adaptation and 1-minute VOR recordings (blocks A1 through A6) ensued. Each VOR recording was preceded by a 30 second pause during which the rotation of the chair was stopped, to minimize the effect of habituation on eye movements. The duration of the experiment was approximately 90 minutes.

All participants received the same VOR adaptation protocol. Stimulation condition (anodal, cathodal or sham tDCS) was randomized across participants by an independent researcher; the participant and the researchers collecting and analyzing the data were blind to stimulation condition. The quality of the eye movement data was checked immediately after the recording. If the raw eye movement data of both eyes showed too many blinks, saccades or loss of data during VOR measurements, the participant was excluded from further analysis and replaced by a new one who received the same protocol. Inclusion continued until each of the three stimulation groups contained seven participants.

3.2.3 Online tDCS Experiment

21 Additional participants (17 females, mean age 22 ± 2 years, range 18-28 years) were tested on the same protocol used in experiment 1, but with online anodal or sham cerebellar stimulation during the first three adaptation blocks, i.e., the first 30 minutes of VOR training (online tDCS,

see figure 1B). Because the duration of stimulation was lengthened to thirty minutes, the electrodes were applied to the skin with an EEG paste to prevent drying of the contact during tDCS.

3.2.4 Validation Experiment

Previous studies examining VOR learning generally measured gain adaptation after instead of during training. Therefore, we also conducted a validation experiment without interspersed online measurements to exclude the possibilities that the online recordings used in our study either slowed down vestibular learning by disrupting the visual-vestibular mismatch or accelerated VOR gain down by vestibular habituation to rotation in the absence of visual feedback (Cohen *et al.*, 1992). Eight novel participants (2 females, mean age 24±2 years, range 22-29 years) received VOR adaptation stimulation continuously for 60 minutes rather than 6 times 10 minutes (see figure 1D) without any tDCS stimulation. We compared VOR adaptation between this continuous group and the sham group of the offline tDCS experiment.

3.2.5 Data Analysis

Eyelink data from the VOR blocks was processed using MATLAB 8.2 (The MathWorks Inc., Natick, Massachusetts, United States) for Windows. Eye velocity gains were calculated per participant, eye and recording block according to the following procedure. First, eye position data from the left or right eye was discarded if the pupil was lost for at least an entire recording block during the course of the experiment. Second, saccades and eye-blinks were removed from the horizontal eye position trace using an internal Eyelink routine. Subsequently, the horizontal eye position was smoothened and differentiated with a Savitzky-Golay filter (third order polynomial, 10 Hz critical frequency) to obtain an eye velocity signal. The 1-minute recording block was divided in 18 rotation periods of 3.33 s. Periods without eye position data were excluded from the analysis. A least-squares sine fit was calculated for all remaining periods. Fitted amplitudes were used to calculate the median amplitude and the median absolute deviation (MAD) of the amplitudes. Hereafter, amplitudes differing more than two MADs from the median were discarded.

In each block, the VOR gain was calculated by dividing the mean amplitude of the sine fits by the chair velocity (22.6 deg/s). This procedure yielded eight VOR gain values, one for each recording block. These gains were normalized dividing by the gain obtained in the second baseline block

(B2). Thereafter, the two baseline blocks were averaged to calculate a baseline gain. In case both the left and the right eye were available for analysis, the normalized gains were averaged over the two eyes, resulting in seven normalized gains per participant (one baseline gain and six gains

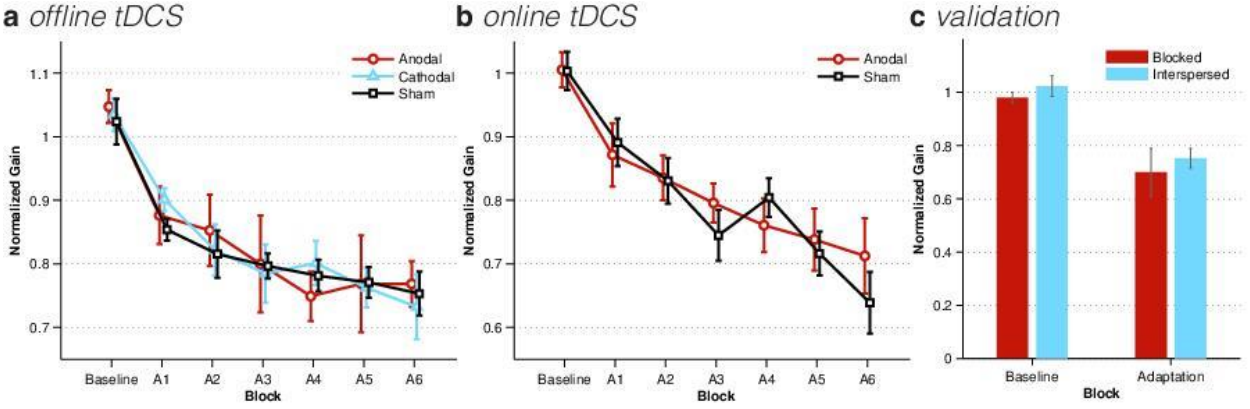

Figure 2 Results:

Panel a. VOR gain evolution for the 3 offline stimulation groups (anodal, cathodal and sham) normalized against block 2. Adaptation blocks are numbered A1 through A6. VOR gain decreased approximately 25% during 6 blocks of adaptation training. Anodal and cathodal tDCS over the cerebellum did not influence adaptation relative to sham stimulation. **Panel b**. VOR gain learning for online and offline (from main experiment 1) stimulation. Time of stimulation with respect to the training does not impact adaptation. ***Panel c***. VOR gain after 1 hour of continuous or interspersed adaptation. Both groups have identical VOR adaptation and the interspersed eye recordings are therefore assumed not to disrupt learning. Error bars represent standard error of the mean.

recorded during the adaptation period). Participants with a gain lower than 0.5 or larger than 1.5 in the first baseline block (B1) were excluded from further analysis.

Statistical analysis was carried out using SPSS 22.0 for Windows. Sample characteristics were compared across groups using chi-square tests for categorical (gender, number of eyes successfully recorded) and t-tests or ANOVAs for continuous parameters (age, number of excluded sinusoids). To examine the effect of offline tDCS on VOR gain adaptation, a mixed ANOVA was carried out with one between-subject factor Group (3 levels: anodal, cathodal, sham) and one within-subject factor Block (7 levels: Baseline and A1 through A6). In addition, to investigate the effect of online tDCS on VOR gain adaptation, a separate analysis was carried out by means of a mixed ANOVA with one between subject factor Group (2 levels: anodal, sham) and one within-subject factor Block (7 levels: Baseline and A1 through A6).

To determine the effect of interspersing the adaptation phase with VOR recordings, we compared the sham group of the offline experiment (interspersed group) with the seven participants receiving

sham in the validation experiment (continuous group). Thereto, we carried out a mixed ANOVA with one between-subject-factor Group (2 levels: interspersed/continuous) and one within-subject factor Block (2 levels: Baseline vs. final Adaptation (A6).

Statistical level of significance was set at 5%. Significant interactions were further analyzed using post-hoc t-tests with Bonferroni correction. Estimates are reported as the mean ± standard deviation (SD).

3.3 Results

3.3.1 Offline tDCS has no Modulatory Effect on VOR Adaptation

Data of four of the 25 included participants in the offline tDCS experiment were discarded due to technical failure (*n=3;* eye link connection stopped working) or too much difference between the baseline blocks (*n*=1). For the analysis, the study sample consisted of 21 young adults (5 male, mean age 21 years, range 18-26 years) yielding seven participants in each of the three groups. Gender ($X^2(2)=0.53$, $p=.80$) and age ($F(2,18)=0.49$, $p=.62$) were distributed equally between stimulation groups. Data quality was also consistent across groups (both eyes recorded successfully in 13 out of 21 participants; $X^2(2)=2.8$, $p=.24$, percentage of excluded sinusoids (20±3.1 %; $F(2,18)=.33$, $p=.72$). The average eye velocity for the second block was similar across stimulation groups ($F(2,18)=0.21$, $p=.81$), justifying the normalization of VOR gains using the recordings of the second block (B2).

Analysis showed a main effect of Block ($F(2.6,46)=21$, $p<.001$, $\eta_p^2=0.53$; Greenhouse-Geisser correction: $\varepsilon=0.43$) indicating a significant decline in VOR gain during the adaptation period (Figure 2A). Post-hoc simple contrasts comparing the consecutive blocks revealed that VOR gain decreased during the first three adaptation blocks (Baseline average: 1.0±0.082, A1: 0.88±0.08, $F(1,18)=27$, $p<.001$; A2: 0.83±0.12, $F(1,18)=6.2$, $p=.023$; A3: 0.79±0.14, $F(1,18)=4.7$, $p=.044$) and stabilized after block 4 (A4: 0.78±0.093, $F(1,18)=0.26$, $p=.61$; A4: 0.77±0.13, $F(1,18)=0.18$, $p=.68$; A6: 0.75±0.11, $F(1,18)=0.28$, $p=.60$). After 60 minutes of VOR adaptation, the average VOR gain in the last adaptation block (A6) was reduced by approximately 28±15% of the baseline gain.

However, we did not observe a main effect of Group ($F(2,18)=0.032$, $p=.97$) nor an interaction between Group and Block ($F(5.1,46)=0.24$, $p=.95$; Greenhouse-Geisser correction: $\varepsilon=0.43$). This suggests that neither offline anodal nor cathodal stimulation have an effect on VOR adaptation (see figure 2A).

3.3.2 Online tDCS has no Modulatory Effect on VOR Adaptation either

Data of seven of the 21 included participants in the offline tDCS experiment were discarded due to technical failure ($n=3$), early termination of the experiment due to nausea ($n=2$) or a high number of saccadic eye movements during VOR measurement ($n=2$). For the analysis, the study sample consisted of 14 young adults (4 male, mean age 22 ±3 years, range 18-28 years).

Statistical analysis did not show a main effect of Group ($F(1,12)=0.081$, $p=.781$) nor an interaction between Block and Group ($F(6,72)=0.803$, $p=.57$). Similar to the online experiment, the main effect of Block ($F(6,72)=23.459$, $p<.001$, $\eta_p^2=0.66$)revealed a decrease in gain during the adaptation blocks (figure 2B).

3.3.3 Eye Measurements during Adaptation Training do not Affect VOR Learning

One participant in the validation experiment was excluded due to too large a difference between the two baseline blocks. The remaining participants ($n=7$, 2 females; ages between 22 and 29 years, mean age 24 years) were compared to the sham group of the online tDCS experiment ($n=7$, 6 females; ages between 19 and 26 years, mean age 22 years).

Statistical analysis comparing the average baseline gain and the gain in the last adaptation block showed no main effect of Group ($F(1,12)=0.63$, $p=.44$), nor an interaction between Group and Block ($F(1,12)=0.010$, $p=.92$). The effect of Block was significant ($F(1,12)=37$, $p<.001$, $\eta_p^2=0.75$, see figure 2C). These results suggest that interspersing the adaptation period with VOR recordings does not hamper or enhance VOR adaptation in any significant way. On average, after 60 minutes of VOR adaptation, the gain was reduced by approximately 28±16% of the baseline gain, which is very similar to the result obtained in the main experiment.

3.4 Discussion

The present study aimed to investigate the effect of cerebellar tDCS on VOR adaptation in humans. Based on recent animal and human studies, it was hypothesized that anodal tDCS over the cerebellum would enhance whereas cathodal stimulation would suppress Vestibulo-Ocular Reflex (VOR) adaptation. However, we found no effect of offline anodal or cathodal or online anodal stimulation on VOR learning.

3.4.1 Effects of VOR Adaptation Training on the VOR

To our knowledge, this study is the first to report the learning rate of acute VOR gain down training in humans. VOR gain rapidly decreases during the first thirty minutes of training and then stabilizes around 75% of the gain before adaptation. This result agrees with observations in monkeys showing fast initial learning during the first 20-40 minutes of training and leveling of VOR gain around 75-80% after 2 hours (Cohen *et al.*, 1992; Partsalis *et al.*, 1995; Yakushin *et al.*, 2000) up until 8 hours (Bello *et al.*, 1991; Cohen *et al.*, 1992; Lisberger *et al.*, 1984; Miles and Eighmy, 1980; Yakushin *et al.*, 2000).

The observed decrease in VOR gain after 30 minutes of training interspersed with VOR measurements is in accordance with previous studies which used a single VOR measurement at the end of the training period (10% - Tiliket *et al.*, 1994; 11% - Shelhamer *et al.*, 1994; 20% - Montfoort *et al.*, 2008; 50% - Suzuki *et al.*, 2006). Indeed, we found no differences in VOR adaptation between our main experiment (with 6 consecutive training periods of 10 minutes) and a control experiment with a single training period of 60 minutes. Therefore, our VOR adaptation protocol, which is similar to many VOR studies in animals (Bello *et al.*, 1991; Boyden *et al.*, 2006; Cohen *et al.*, 1992; Galliano *et al.*, 2013; Partsalis *et al.*, 1995; Schonewille *et al.*, 2011; Wulff *et al.*, 2009; Yakushin *et al.*, 2000) could be used in future research to measure acute VOR learning in humans.

3.4.2 No effects of Cerebellar tDCS on Human VOR Adaptation

Our results indicate that tDCS over the cerebellum does not modulate VOR adaptation in humans, which seems to contrast observations in mice (Das *et al*., 2014). Moreover, our findings in human VOR adaptation do not match the modulatory effect of online anodal cerebellar tDCS in humans

on reaching movement adaptation (Block and Celnik, 2013; Galea *et al*., 2011; Hardwick *et al*., 2014) and locomotion adaptation (Jayaram *et al*., 2012). We chose only to include anodal stimulation in this control experiment as evidence of behavioral modulation is stronger for anodal than cathodal tDCS (Priori *et al*., 2014). Furthermore, we lengthened stimulation duration to 30 minutes to cover as much of the VOR training as possible –similar to the cerebellar studies cited earlier– without compromising participant safety. Coincidentally, this stimulation period overlapped with the fast phase of VOR adaptation.

As suggested in the introduction, we believe the most likely reason for not finding a modulatory effect of tDCS on human VOR adaptation is that the electric field strength in the flocculus was insufficient to modulate neuronal firing when using a standard cerebellar tDCS protocol (Ferrucci *et al*., 2015). In humans, the flocculonodular lobe is located deep within the cerebellum in front of the posterior lobe and near the brainstem (Voogd and Barmack, 2006). The distance from the skull to the flocculus is larger than the distance to cerebellar areas implicated in visuomotor reaching (lobules IV, V and VI of the anterior arm area (Donchin *et al*., 2012, force field reaching (lobules IV and V of the anterior arm area, and saccadic eye movement (lobules VI and VII (Desmurget *et al*., 1998) adaptation. tDCS would therefore induce a weaker local electric field in the flocculus than in any of these other areas. Using a recently developed finite element conduction model, we post-hoc calculated that mean electric field strength normal to the cortex is approximately twice as high in lobules IV, V and VI (0.455 V/m) compared to the nodulus (0.245 V/m) for the standard configuration at 2 mA (Dmochowski *et al*., 2011). Important to note is that in the animal study demonstrating modulatory effects of DCS on VOR adaptation, the cerebellum was stimulated directly after craniotomy without current having to cross the skull (Das *et al*., 2014). The lack of behavioral modulation might thus be explained by an insufficient field strength achieved with the standard stimulation configuration used in our study.

Counter to this argument, motor cortex tDCS at half the current strength gives an electric field similar to the nodulus and has been shown to modulate cortical excitability and physiology. Using the same model as in our calculations, it was shown that the maximal electrical field normal to the cortex averages 0.27 V/m in the motor cortex in three different MRI-derived computational models (Datta *et al*., 2012; Huang *et al*., 2013; Rampersad *et al*., 2014) compared to 0.245 V/m in the nodulus. This voltage difference per distance in the motor cortex has been found to effectively

modulate both cortical excitability in physiological TMS studies (Nitsche and Paulus, 2000; Nitsche and Paulus, 2001; Sriraman *et al*., 2014) and learning in motor skill and adaptation experiments (Galea *et al*., 2011; Reis *et al*., 2009; Reis *et al*., 2015). Therefore, modeled electrical field in the nodulus is comparable to the motor cortex for which convincing results have been reported over recent years.

Unfortunately, the electric field strength range that influences neuronal excitability in the motor cortex and cerebellum and affects behavior is currently unknown. Future research in mice would be necessary to create dose-response curves relating field strength and other stimulation parameters such as electric field direction relative to neuronal orientation, to cellular and behavioral outcomes. Using recently developed targeting models (Datta *et al*., 2012; Dmochowski *et al*., 2011), it would then be possible to design more advanced protocols for the stimulation of a target area at the optimal electric field strength in larger animals such as monkeys or in humans. The added value of first applying these complex configurations in monkeys rather than humans might lie in the possibility to record floccular Purkinje cell excitability during stimulation and to validate the tDCS conduction model.

Within the cerebellum two main regions (the vestibule-cerebellum and the ocular motor vermis) influence eye movements (Colnaghi *et al*., 2010). Lesions of the ocular motor vermis and fastigial nucleus impair accuracy and adaptation of reflexive saccades (while voluntary saccade accuracy may be spared) and affect velocity and adaptation of smooth pursuit (Haarmeier and Kammer, 2010; Ohtsuka and Enoki, 1998). Interestingly, posterior vermis is involved in the adaptation of pursuit initiation. An integration of position and velocity signals on the level of individual cells has also been observed in the flocculus/ paraflocculus and the posterior vermis (Ilg and Their, 2008). The size of the stimulation electrode in our study may have a modulatory role on the vermal function. Therefore, we think what we see is a resultant of the complex effects of stimulation on the cerebellum.

Another reason for the discrepancy between tDCS effects on VOR adaptation in humans and mice might be related to differences in the visual and oculomotor systems between the two species. Humans, as opposed to mice, are foveated animals and therefore use a more extensive repertoire of gaze-holding and gaze-directing eye movements to stabilize images of interest on the retina

(Leigh and Zee, 2006). This might seriously affect VOR adaptation and lead to a different way of learning in humans. For instance, humans can utilize other mechanisms to compensate for retinal slip such as making catch-up saccades which could decrease the retinal error driving VOR adaptation (Melvill *et al*., 1988). In addition, adaptation of the VOR is more gradual in humans and monkeys than in mice, possibly because of the strong significance of vision in foveated animals. Indeed, in humans and other foveated animals, gain changes exceeding 25-30% are only achieved when training is prolonged over multiple days (Gonshor and Jones, 1976; Kuki *et al*., 2004; Lisberger *et al*., 1984; Miles and Eighmy, 1980). This process of chronic adaptation leads to distributed consolidation of the motor memory in the cerebellar cortex and the brainstem and changes in the activation pattern of floccular Purkinje cells (Blazquez *et al*., 2003; Blazquez *et al*., 2006; Hirata and Highstein, 2001; Kahlon and Lisberger, 2000; Kassardjian *et al*., 2005; Lisberger *et al*., 1984; Lisberger *et al*., 1994). This would suggest that chronic adaptation is also functionally distinct from acute adaptation induced by a learning period of about an hour as employed here. In contrast, a single 1-hour VOR training session in mice leads to a 40-50% gain reduction (Boyden *et al*., 2006; Galliano *et al*., 2013; Schonewille *et al*., 2011; Wulff *et al*., 2009). Compared to human, the VOR in mice is therefore relatively easy to modify which makes a distinction between acute and chronic adaptation in mice less obvious. This would suggest that the role of the flocculus during acute VOR adaptation is different between mice and men. Moreover, it is even conceivable that tDCS does not affect acute VOR adaptation in humans.

Addressing this possibility in future experiments, it could be interesting to (1) apply (targeted) tDCS during a different floccular-dependent task such as smooth pursuit adaptation (Kahlon and Lisberger, 2000; Medina and Lisberger, 2008; Yang and Lisberger, 2014), (2) directly target the flocculus with DCS in monkeys, or (3) stimulate the cerebellum on multiple days in humans during chronic adaptation using either head-fixed lenses (Gonshor and Jones, 1976) or coupled visual field rotation while providing unique contextual cues such as head tilt to increase consolidation (Yakushin *et al*., 2003a; Yakushin *et al*., 2003b; Schuber *et al*., 2008). Indeed, recent multiple session skill learning experiments have shown more robust modulatory effects of cerebellar tDCS (Cantarero *et al*., 2015; Wessel *et al*., 2016). Additional experiments in monkeys or humans would be needed to explore the effects of multiple day floccular stimulation on chronic VOR adaptation.

Conclusion

Altogether, we conclude that neither offline (anodal and cathodal) nor online (anodal) tDCS with a standard electrode configuration has an effect on VOR adaptation in humans. However, it is difficult to explain the lack of behavioral modulation to a specific cause, because dose-response data relating local electric field strength to behavior is lacking and VOR adaptation is exceedingly more complex in humans than in mice. Future research is necessary to investigate the relation between electric field strength, learning complexity and behavior results in mice, monkeys and humans before cerebellar tDCS can be used as a scientific tool in VOR research.

References:

Avila, E. *et al.* (2015) Cerebellar transcranial direct current stimulation effects on saccade adaptation. *Neural Plast.* 2015, 968970

Bello, S. *et al.* (1991) The squirrel monkey vestibulo-ocular reflex and adaptive plasticity in yaw, pitch, and roll. *Exp Brain Res* 87, 57–66

Blazquez, P.M. *et al.* (2003) Cerebellar signatures of vestibulo-ocular reflex motor learning. *J. Neurosci.* 23, 9742–9751

Blazquez, P.M. *et al.* (2006) Chronic changes in inputs to dorsal Y neurons accompany VOR motor learning. *J. Neurophysiol.* 95, 1812–1825

Block, H. and Celnik, P. (2013) Stimulating the cerebellum affects visuomotor adaptation but not intermanual transfer of learning. *Cerebellum* 12, 781–793

Boyden, E.S. *et al.* (2006) Selective engagement of plasticity mechanisms for motor memory storage. *Neuron* 51, 823–834

Brunoni, A.R. *et al.* (2012) Clinical research with transcranial direct current stimulation (tDCS): challenges and future directions. *Brain Stimul* 5, 175–195

Cantarero, G. *et al.* (2015) Cerebellar direct current stimulation enhances on-line motor skill acquisition through an effect on accuracy. *J. Neurosci.* 35, 3285–3290

Carter, T.L. and McElligott, J.G. (2005) Cerebellar AMPA/KA receptor antagonism by CNQX inhibits vestibuloocular reflex adaptation. *Exp Brain Res* 166, 157–169

Cohen, H. *et al.* (1992) Habituation and adaptation of the vestibuloocular reflex: a model of differential control by the vestibulocerebellum. *Exp Brain Res* 90, 526–538

Colnaghi, S., *et al.* (2010) Transcranial magnetic stimulation over the cerebellum and eye movements: state of the art. *Funct. Neurol.* 25, 165–171.

Das, S. *et al*. (2014) Polarity-dependent effects of trans-cranial direct current stimulation (tDCS) in cerebellar learning depends on the state of neuronal network. *Brain Stimul.* 7, 3.

Datta, A. *et al.* (2012) Inter-Individual Variation during Transcranial Direct Current Stimulation and Normalization of Dose Using MRI-Derived Computational Models. *Front Psychiatry* 3, 91

Desmurget, M. *et al.* (1998) Functional anatomy of saccadic adaptation in humans. *Nat. Neurosci.* 1, 524–528

Dmochowski, J.P. *et al.* (2011) Optimized multi-electrode stimulation increases focality and intensity at target. *J Neural Eng* 8, 046011

Donchin, O. *et al.* (2012) Cerebellar regions involved in adaptation to force field and visuomotor perturbation. *J. Neurophysiol.* 107, 134–147

Ferrucci, R. *et al.* (2015) Cerebellar tDCS: how to do it. *Cerebellum* 14, 27–30

Galea, J.M. *et al.* (2009) Modulation of cerebellar excitability by polarity-specific noninvasive direct current stimulation. *J. Neurosci.* 29, 9115–9122
Galea, J.M. *et al.* (2011) Dissociating the roles of the cerebellum and motor cortex during adaptive learning: the motor cortex retains what the cerebellum learns. *Cereb. Cortex* 21, 1761–1770
Galliano, E. *et al.* (2013) Silencing the majority of cerebellar granule cells uncovers their essential role in motor learning and consolidation. *Cell Rep* 3, 1239–1251
Gandiga, P.C. *et al.* (2006) Transcranial DC stimulation (tDCS): a tool for double-blind sham-controlled clinical studies in brain stimulation. *Clin Neurophysiol* 117, 845–850
Gonshor, A. and Jones, G.M. (1976) Extreme vestibulo-ocular adaptation induced by prolonged optical reversal of vision. *J. Physiol. (Lond.)* 256, 381–414
Haarmeier, T., and Kammer, T. (2010) Effect of TMS on oculomotor behavior but not perceptual stability during smooth pursuit eye movements. *Cereb. Cortex* 20, 2234–2243.
Hardwick, R.M. and Celnik, P.A. (2014) Cerebellar direct current stimulation enhances motor learning in older adults. *Neurobiol. Aging* 35, 2217–2221
Herzfeld, D.J. *et al.* (2014) Contributions of the cerebellum and the motor cortex to acquisition and retention of motor memories. *Neuroimage* 98, 147–158
Hirata, Y. and Highstein, S.M. (2001) Acute adaptation of the vestibuloocular reflex: signal processing by floccular and ventral parafloccular Purkinje cells. *J. Neurophysiol.* 85, 2267–2288
Huang, Y. *et al.* (2013) Automated MRI segmentation for individualized modeling of current flow in the human head. *J Neural Eng* 10, 066004
Ilg, U. J., and Thier, P. (2008) The neural basis of smooth pursuit eye movements in the rhesus monkey brain. *Brain and Cognition* 68, 229–240.
Jayaram, G. *et al.* (2012) Modulating locomotor adaptation with cerebellar stimulation. *J Neurophysiol* 107, 2950–2957
Kahlon, M. and Lisberger, S.G. (2000) Changes in the responses of Purkinje cells in the floccular complex of monkeys after motor learning in smooth pursuit eye movements. *J. Neurophysiol.* 84, 2945–2960
Kassardjian, C.D. *et al.* (2005) The site of a motor memory shifts with consolidation. *J. Neurosci.* 25, 7979–7985
Kuki, Y. *et al.* (2004) Memory retention of vestibuloocular reflex motor learning in squirrel monkeys. *Neuroreport* 15, 1007–1011
Leigh, RJ. and Zee, DS. (2006) The neurology of eye movements. Oxford: *Oxford University Press*
Liebetanz, D. *et al.* (2009) Safety limits of cathodal transcranial direct current stimulation in rats. *Clin Neurophysiol* 120, 1161–1167
Lisberger, S.G. *et al.* (1984) Signals used to compute errors in monkey vestibuloocular reflex: possible role of flocculus. *J. Neurophysiol.* 52, 1140–1153
Lisberger, S.G. *et al.* (1994) Neural basis for motor learning in the vestibuloocular reflex of primates. II. Changes in the responses of horizontal gaze velocity Purkinje cells in the cerebellar flocculus and ventral paraflocculus. *J. Neurophysiol.* 72, 954–973
Medina, J.F. and Lisberger, S.G. (2008) Links from complex spikes to local plasticity and motor learning in the cerebellum of awake-behaving monkeys. *Nat. Neurosci.* 11, 1185–1192
Melvill Jones, G. *et al.* (1988) Changing patterns of eye-head coordination during 6 h of optically reversed vision. *Exp Brain Res* 69, 531–544
Miles, F.A. and Eighmy, B.B. (1980) Long-term adaptive changes in primate vestibuloocular reflex. I. Behavioral observations. *J. Neurophysiol.* 43, 1406–1425
Montfoort, I. *et al*. (2008) Adaptation of the cervico- and vestibulo-ocular reflex in whiplash injury patients. *J Neurotrauma.* 25(6), 687–93
Nitsche, M.A. and Paulus, W. (2000) Excitability changes induced in the human motor cortex by weak transcranial direct current stimulation. *J. Physiol. (Lond.)* 527 Pt 3, 633–639
Nitsche, M.A. and Paulus, W. (2001) Sustained excitability elevations induced by transcranial DC motor cortex stimulation in humans. *Neurology* 57, 1899–1901

Ohtsuka, K., and Enoki, T. (1998) Transcranial magnetic stimulation over the posterior cerebellum during smooth pursuit eye movements in man. *Brain* 121 (Pt 3), 429–435.
Oulad Ben Taib, N. and Manto, M. (2013) Trains of epidural DC stimulation of the cerebellum tune corticomotor excitability. *Neural Plast.* 2013, 613197
Panouillères, M.T.N. *et al.* (2015) The role of the posterior cerebellum in saccadic adaptation: a transcranial direct current stimulation study. *J. Neurosci.* 35, 5471–5479
Parazzini, M. *et al.* (2013) , Computational model of cerebellar transcranial direct current stimulation. , in *2013 35th Annual International Conference of the IEEE Engineering in Medicine and Biology Society (EMBC)*, pp. 237–240
Partsalis, A.M. *et al.* (1995) Dorsal Y group in the squirrel monkey. I. Neuronal responses during rapid and long-term modifications of the vertical VOR. *J. Neurophysiol.* 73, 615–631
Priori, A. *et al.* (2014) Transcranial cerebellar direct current stimulation and transcutaneous spinal cord direct current stimulation as innovative tools for neuroscientists. *J. Physiol. (Lond.)* 592, 3345–3369
Rahman, A. *et al.* (2014) Polarizing cerebellar neurons with transcranial Direct Current Stimulation. *Clin Neurophysiol* 125, 435–438
Rampersad, S.M. *et al.* (2014) Simulating transcranial direct current stimulation with a detailed anisotropic human head model. *IEEE Trans Neural Syst Rehabil Eng* 22, 441–452
Reis, J. *et al.* (2009) Noninvasive cortical stimulation enhances motor skill acquisition over multiple days through an effect on consolidation. *Proc. Natl. Acad. Sci. U.S.A.* 106, 1590–1595
Reis, J. *et al.* (2015) Time- but not sleep-dependent consolidation of tDCS-enhanced visuomotor skills. *Cereb. Cortex* 25, 109–117
Schonewille, M. *et al.* (2011) Reevaluating the role of LTD in cerebellar motor learning. *Neuron* 70, 43–50
Schubert, M.C. *et al.* (2008) Retention of VOR gain following short-term VOR adaptation. *Exp Brain Res* 187, 117–127
Shelhamer, M. *et al.* (1994) Short-term vestibulo-ocular reflex adaptation in humans. II. Error signals. *Exp Brain Res* 100, 328–336
Sriraman, A. *et al.* (2014) Timing-dependent priming effects of tDCS on ankle motor skill learning. *Brain Res.* 1581, 23–29
Suzuki, K. *et al.* (2006) [Flexibility of adaptation of vestibule-ocular reflex in human beings]. *Nippon Jibiinkoka Gakkai Kaiho* 109, 461–468
Tiliket, C. *et al.* (1994) Short-term vestibulo-ocular reflex adaptation in humans. I. Effect on the ocular motor velocity-to-position neural integrator. *Exp Brain Res* 100, 316–327
van der Geest, J.N. and Frens, M.A. (2002) Recording eye movements with video-oculography and scleral search coils: a direct comparison of two methods. *J. Neurosci. Methods* 114, 185–195
van Neerven, J. *et al.* (1991) Effects of GABAergic and noradrenergic injections into the cerebellar flocculus on vestibulo-ocular reflexes in the rabbit. *Prog. Brain Res.* 88, 485–497
Villamar, M.F. *et al.* (2013) Focal modulation of the primary motor cortex in fibromyalgia using 4×1-ring high-definition transcranial direct current stimulation (HD-tDCS): immediate and delayed analgesic effects of cathodal and anodal stimulation. *J Pain* 14, 371–383
Voogd, J. and Barmack, N.H. (2006) Oculomotor cerebellum. *Prog. Brain Res.* 151, 231–268
Watanabe, E. (1985) Role of the primate flocculus in adaptation of the vestibulo-ocular reflex. *Neurosci. Res.* 3, 20–38
Watanabe, S. *et al.* (2003) Flexibility of vestibulo-ocular reflex adaptation to modified visual input in human. *Auris Nasus Larynx* 30 Suppl, S29–34
Wessel, M.J. *et al.* (2016) Enhancing Consolidation of a New Temporal Motor Skill by Cerebellar Noninvasive Stimulation. *Cereb. Cortex* 26, 1660–1667
Wulff, P. *et al.* (2009) Synaptic inhibition of Purkinje cells mediates consolidation of vestibulo-cerebellar motor learning. *Nat. Neurosci.* 12, 1042–1049
Yakushin, S.B. *et al.* (2000) Functions of the nucleus of the optic tract (NOT). II. Control of ocular pursuit. *Exp Brain Res* 131, 433–447

Yakushin, S.B. *et al.* (2003) Adaptive changes in the angular VOR: duration of gain changes and lack of effect of nodulo-uvulectomy. *Ann. N. Y. Acad. Sci.* 1004, 78–93
Yakushin, S.B. *et al.* (2003) Dependence of adaptation of the human vertical angular vestibulo-ocular reflex on gravity. *Exp Brain Res* 152, 137–142
Yang, Y. and Lisberger, S.G. (2014) Role of plasticity at different sites across the time course of cerebellar motor learning. *J. Neurosci.* 34, 7077–7090

Chapter Four

The modulatory role of anodal direct current stimulation on neuronal population suggests sensitivity towards the long-term potentiation pathway of cerebellar Purkinje cell

Suman Das, Marcella Spoor, Tafadzwa M. Sibindi, Peter Holland, Martijn Schonewille, Chris I De Zeeuw, Maarten A. Frens, Opher Donchin

The modulatory role of anodal direct current stimulation on neuronal population suggests sensitivity towards the long-term potentiation pathway of cerebellar Purkinje cell

Abstract

The polarity specific effects of direct current stimulation (DCS) on the cerebellar network remain poorly understood. We have recorded from cerebellar cortical neurons, the crucial structure for motor learning, in awake mice with targeted deletion of long-term depression (LTD) at parallel-fiber (PF) Purkinje cell synapses (GluR2Δ7) or genetically ablated PC long-term potentiation (LTP) (L7-PP2B mice). Studies in neocortex demonstrate anodal driven facilitation of neocortical activity, plasticity and cellular learning mechanisms. We hypothesized that polarity specific effects of DCS on cerebellar learning may be obtained by changing cerebellar cortical excitability. Therefore, we have utilized acute recordings with glass microelectrodes to monitor multi-unit activity (MUA) during pre- and post-stimulation (30 minutes after the cessation of stimuli) periods. Strikingly, DCS shows no differential effects in the neuronal activity for long time periods (30 minutes post-stimulation) in the wild type and GluR2Δ7 mice. However, preliminary data suggest that the effects of anodal stimulation on the early-phase MUA is reversed in late-phase MUA when the LTP pathway of PC is compromised in L7-PP2B mice. The data also suggest that cathodal stimulation may engage several parallel pathways in order to exert its effects.

4.1 Introduction

Many recent studies indicate polarity specific modulations of direct current stimulation (DCS) on neuronal networks (Stagg and Nitsche, 2011). While there might be different types of polarity specific neuronal modulations, the emphasis in the literature has been that anodal is excitatory and cathodal is inhibitory (AeCi). The AeCi nature of DCS has been utilized in modifying function of the brain under various neurological and neuropsychiatric disorders (Brunelin *et al.*, 2012; Boggio *et al.*, 2007; Buttkus *et al.*, 2011; Murphy *et al.*, 2009). Here, we have explored the polarity specific effects of DCS on the cerebellar neurons which may play a role in cerebellar dependent motor learning tasks (Hardwick and Celnik, 2014; Herzfeld *et al.*, 2014; Jayaram *et al.*, 2012).

Animal models have been extensively utilized to explore the mechanisms of DCS in modulating neocortical activity (Fregni and Pascual-Leone, 2007; Liebetanz *et al.*, 2006a; Liebetanz *et al.*, 2006b). For instance, anodal stimulation has been found to enhance the activity in rat frontal cortex (Takano *et al.*, 2011). This increased activity may affect neocortical plasticity by either accumulating more intracellular calcium ions (Islam *et al.*, 1995a) or altering pre-synaptic sensitivity (Marquez-Ruiz *et al.*, 2012) or promoting brain-derived neurotrophic factor (BDNF) dependent long term potentiation (LTP) formation (Fritsch *et al.*, 2010). In contrast, only a few animal experiments are available which describe the modulatory role of DCS on the cerebellar network.

A low amplitude external electric field (EEF) is sufficient to modulate Purkinje cells (PC) activity. In experiments on the isolated turtle cerebellum, PC and stellate inter-neurons with a dendro-axonic orientation parallel to the current vector (anodal stimulation) are maximally modulated (Chan and Nicholson, 1986). Interestingly, a small number of neurons with orientation parallel to the current vector are excited by both anodal and cathodal stimulation. In general, anodal stimulation increases the excitability of the neurons by depolarizing the apical dendrites of the PC while the rest of the dendrites and soma is hyperpolarized (Chan *et al.*, 1988). Conversely, cathodal stimulation that depolarizes the soma and hyperpolarizes apical dendrites of the PC, reduces neuronal activity.

Various studies in human subjects further support the effects of DCS on the cerebellar network (Galea *et al.*, 2011; Bastian, 2011). The application of anodal and cathodal stimulation lead to an

increase and decrease of the inhibitory tone the cerebellum exerts over the primary motor cortex in humans (Galea *et al.*, 2009). Interestingly, the cathodal effects last longer after the cessation of stimulation. However, until now the knowledge of through which pathway(s) the effects of DCS are mediated is lacking, especially in the case of the cerebellum.

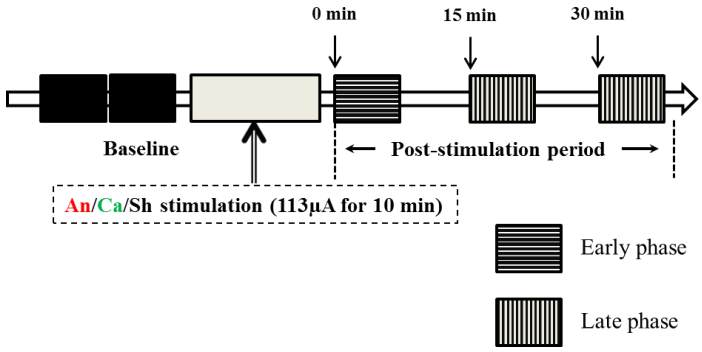

Figure 1: Schematic diagram of the experimental paradigm.

Each smaller rectangular block represents a 5 minute of electrophysiological recording. The animal is awake but not performing any task. After a baseline recording session, the animals are randomly assigned to the anodal (*An*), cathodal (*Ca*) or sham (*Sh*) stimulation group. The first 5 minutes post-stimulation are considered as DCS dependent early-phase modulation and 15 minutes onwards is considered as the DCS dependent late-phase modulation.

In this study, our goal was to apply a low-amplitude constant electric field to a population of neurons in the cerebellum of awake mice in which specific plasticity mechanisms are genetically ablated. The investigation of the effect of stimulation in different genetic mutations will enable us to decipher the neuronal pathways through which DCS exerts polarity specific effects on the cerebellum. We used C57BL/6 mice (wild type), L7-PP2B mice (impaired postsynaptic long-term potentiation (LTP) in PC, Schonewille *et al.*, 2010) and GluR2Δ7 mice (lacking parallel fiber (PF)-PC long-term depression (LTD), Schonewille *et al.*, 2011) and were able to observe the neuronal activity before and after the stimulation. The main finding emerged; that DCS showed no polarity effect in the neuronal activity of wild type and GluR2Δ7 mice. Moreover, preliminary data suggest that the effects of anodal stimulation on the early-phase multi-unit activity (MUA) is reversed in late-phase MUA when the LTP pathway of PC is compromised in L7-PP2B mice.

4.2 Methods

4.2.1 Summary of methodology:

Acute extracellular signals from the cerebellum were recorded with a glass micropipette before, during and after DCS (at 0, 15 and 30 min post-stimulation) on awake but non-behaving mice. Spike-sorting was performed off-line using a custom built in-house MATLAB (The MathWorks

Inc., Natick, MA, USA) program. Firing rate modulation in multi-unit activity (MUA) was compared at the different time points. Change from baseline was assessed in groups receiving anodal/cathodal and sham stimulation. Post-stimulation 0-5 min and 15 – 35 min neuronal activity were categorized as early- and late-modulation, respectively (Figure 1). Modulation of firing rate was then compared for the different stimulation conditions across wild type and mutant mice.

4.2.2 Experimental paradigm

The effect of DCS on cerebellar neurons was examined before and after the stimulation (at 0, 15 and 30-minute post-stimulation, Figure 1). After a stable recording of baseline activity for 10 minutes, DCS (anodal/cathodal or sham) was applied for 10 minutes. Post-stimulation effects were assessed by recording from the same neuron or neurons. An hour later, if the recording was stable, DCS with opposite to previous stimulation polarity was applied. If the recording was no longer stable, a new stable population was sought by changing the depth of the microelectrode.

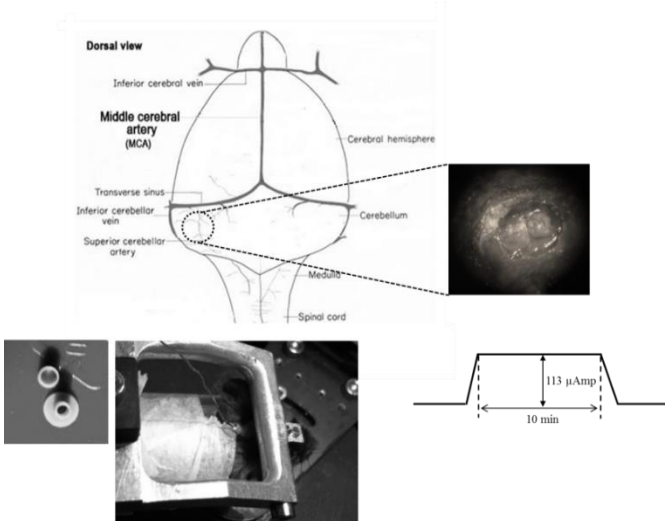

Figure 2: DCS location and procedure

A) Schematic representation of craniotomy for placement of implant over the cerebellum of a mouse brain. B) Craniotomy. Anatomical location for the DCS-implant placement. **C) DCS implant.** The DCS chamber to bridge the stimulating electrode and the brain, above is the cap to cover the implant to protect the brain from infection. **D) Stimulating the mice cerebellum.** The DCS chamber is filled with saline (0.9% NaCl) solution. A silver wire that touches the saline solution but not the dura directly is connected to the current generator (SUI-91, Isolated current source). During stimulation of the mouse is awake but head restrained. **E) Stimulation paradigm.** DCS is ramped up to 113 µAmp. The current is maintained at its peak value for 10 mins. After the stimulation, the current is ramped down.

4.2.3 Experimental procedure

4.2.3.1 Animals

C57BL/6 (N = 14) mice were acquired from Charles River laboratories, Inc. (Wilmington, Massachusetts). L7-PP2B (N = 21) and GluR2Δ7 (N = 16) mutants were bred in Erasmus MC, Rotterdam. Details of the mouse lines used in this study have been described previously (Schonewille *et al.*, 2010; Schonewille *et al.*, 2011). Three to four mice were caged together in temperature-regulated (22 ± 1° C) housing with a 12:12 light-day cycle. All experiments were done in the light cycle. Food and water was provided *ad libitum*. All experiments were conducted in accordance with Animal Welfare Committee of the Erasmus University and the European Communities Council Directive (86/609/EEC).

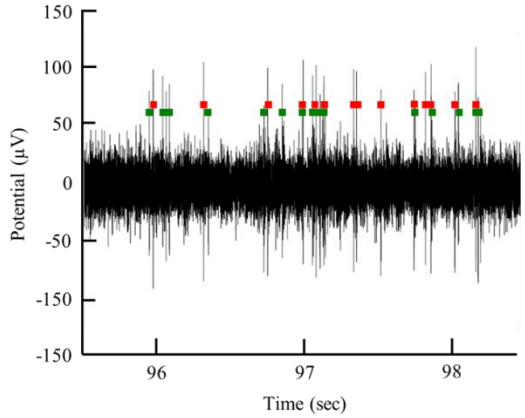

Figure 3: Neuronal activity recorded from cerebellar cortex

The multiunit activity (MUA) of the cerebellar cortex. Detected spikes are clustered and put as different class of units (red and green). In this case, red and green units are considered for the MUA analysis

4.2.3.2 Surgery

Mice, aged 10-12 weeks, were handled for 2 days before the surgery in order to habituate the animal with the experimenter. The surgical procedure was performed under sterile conditions. Isoflurane (5% induction, 1.5% in 0.5 L/m O_2 and 0.2 L/m air) was administered as an anesthetic while body temperature was regulated around 36.5 ± 0.5° via a feedback-controlled heating pad. Breathing profile was continually monitored. After shaving the head, a 1 cm long mid-sagittal incision was performed. The bone was etched (37.5% phosphoric acid, Kerr) and a primer (Optibond, Kerr) was applied. To immobilize the animal's head during electrophysiological recording, a pedestal containing two M1.4 nuts was glued to the skull using dental acrylic (Charisma, Flowline, Hereaus Kulzer) which could then be attached to a custom made fixed arm.

The DCS implant was placed on a circular craniectomy (approx. 2 mm in diameter) on the left occipital bone from where the neck-muscles (vertical and horizontal) were carefully removed (Figure 2 A, B). A lubricating ointment (Duratears, Alcon) was applied epidurally to protect the exposed area of brain from drying. The DCS implant (Figure C) was placed identically in all animals using an anatomical marker (Figure B) and then glued to the skull using cyanoacrylate gel (Plastic One Inc., USA).

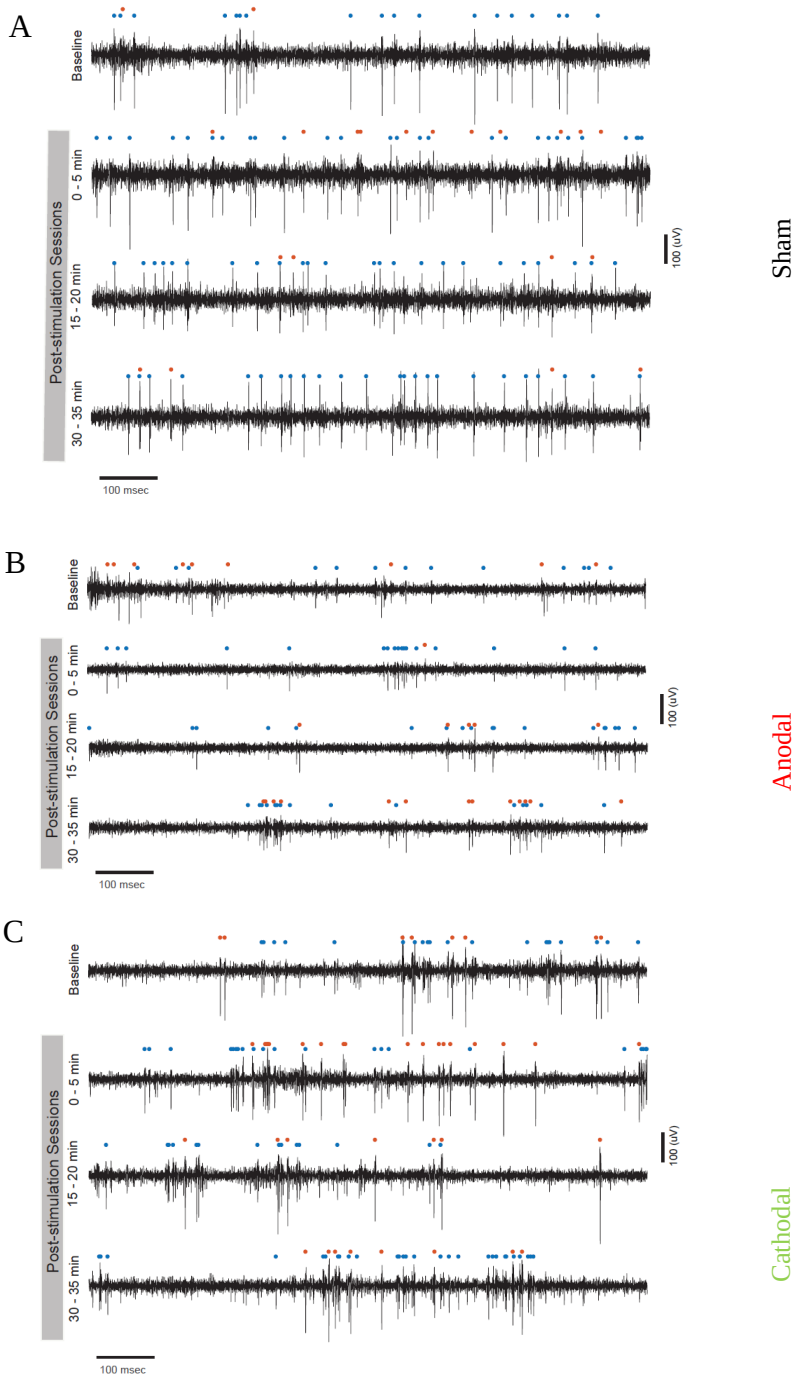

Figure 4: Neuronal data recorded from C57BL/6 control mice

(A) Sham stimulation; (B) Anodal stimulation and (C) Cathodal stimulation conditions
Two units those are taken for MUA, marked as blue and red

The mice were given an analgesic (0.1 ml/mg of body weight Buprenorphine/Temgesic) and placed under an infrared heating lamp until the animal started to move. Mice were allowed to recover for at least 4-5 days before recordings were performed.

4.2.4 Apparatus

4.2.4.1 In *vivo* electrophysiology

Electrophysiology was performed on awake restrained mice, in a quiet dark room. Glass microelectrodes (tip diameter 1.5 ± 0.5 µm) were prepared from custom-made borosilicate glass capillaries (Harvard apparatus, USA) using a vertical pipette-puller (Narishige Co. Ltd, Japan). Pipettes were filled with 3 M KCl solution. Impedance of electrodes

varied from 3 to 5 MΩ. A platinum wire was inserted into the glass electrode to make contact between the electrode and the 16-channel head-stage (AlphaLab SnR™, Israel). Data was acquired with a 24 kHz sampling frequency and digitized at the head-stage before sending to the main processing unit through a signal integration unit (AlphaLab SnR™, Israel). Raw electrophysiology data was stored for offline processing and analysis.

In our superficial recordings in the cerebellar lobules, electrodes with flexible long tips were lowered using a one-axis oil hydraulic micromanipulator (MO-10, Narishige Co. Ltd, Japan). Based on existing literature and signal properties, we performed recordings only from the cerebellar cortex (depths of 0 - 1500 µm). Total distance travelled by the electrode from the surface of the brain was noted for all recordings (track-length). Neurons were held for at least 10 minutes to ensure stability before we started the experimental paradigm (Figure 1).

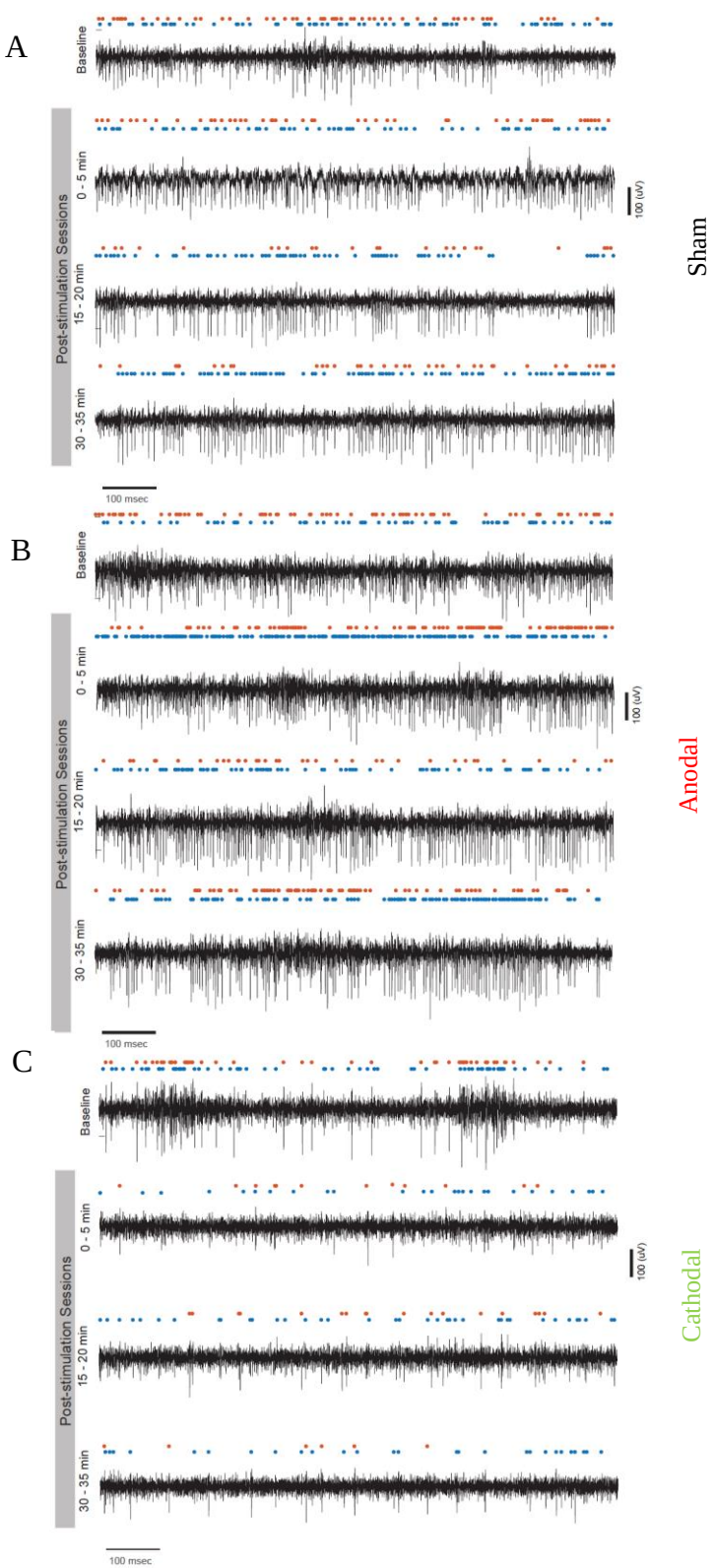

Figure 5: Neuronal data recorded from L7-PP2B mice

(A) Sham (B) Anodal and (C) Cathodal stimulation conditions Two units those are taken for MUA, marked as blue and red

4.2.4.2 *Direct current stimulation*

A low amplitude of continuous DCS (113 µA) was applied using a constant current stimulator (SUI-91, Isolated current source, Cygnus Technology Inc., USA; range = 0.1 µA - 10 mA). Currents were applied to the surface of the dura above the cerebellar cortex through a circular DCS implant with a defined contact area (2 mm inner diameter). Prior to stimulation, the stimulation electrode was filled with saline solution (0.9% NaCl). A silver wire electrode connected to the stimulation box was attached to the DCS implant such that the tip of the silver wire touched the top level of the saline solution but did not touch the brain directly (Figure 2). This circular active electrode (Figure 2C) was chosen to create a symmetric current density with the highest density directly beneath the stimulating electrode. A disposable foam electrode (Kendall Medi-Trace mini resting ECG electrode, Davis medical predicts Inc., USA), was placed onto the ventral thorax of the animal to complete the circuit. The entire circuit was connected through a multi-meter to check current amplitude online. Mice were awake during DCS. To avoid stimulation break effects (Gandiga *et al.,* 2006; Liebetanz *et al.*, 2009), the current intensity was ramped up to its maximal value gradually over 30 s.

4.2.4.2 Electrophysiological data analysis

Spike sorting was performed off line using a custom built in-house MATLAB program. The raw signal was filtered with a band-pass Butterworth filter (4 pole, range 500 to 8500 Hz) with additional hum-noise reduction by applying a comb filter at 50 Hz and its harmonic frequencies (ranging from 25 to 20000 Hz). From the filtered signal, large movement artefacts were removed using an in-house built GUI designed for this purpose. Potential spikes were detected when the processed signal crossed a threshold of 2.5 times the standard deviation of the mean signal amplitude. The peak in every segment was determined, and spikes were aligned to the minimum point and 1.5 ms of signal was kept before and after the peak. Spike sorting was then based on k-means and principle component analysis (PCA). The first three principle components were used to classify the neuron clusters.

All the sorted spikes were used for multi-unit analysis (MUA), (Figure 3). The entire recording session was divided into 100 ms bins for further analysis. The MUA activity in the 10 minutes pre-stimulation was used as a measure of baseline activity. We used the z-score because MUA can

vary greatly in the absolute value, imagine an MUA consisted of 2 units firing at 100Hz, and then another MUA recording with 2 units at 30Hz, plotting both of those on the same graph would be difficult because of the scale (Figure 4, 5, 6). Instead using a z-score normalises everything to its own baseline so that everything can be plotted in a comparable manner (Figure 7, 8). The advantage of the z-score over just subtracting the baseline mean is that it also takes into account baseline variability, so that a z-score of 1 indicates an increase in activity of exactly 1 standard deviation of the baseline variability from the baseline mean.

Z-scores for each recording session were calculated by subtracting the baseline mean and dividing by the standard deviation. In order to validate the stability of the baseline session the first 5 minutes of baseline activity from a recording session was used to calculate the z-score of the last 5 minutes baseline activity. Fluctuations in the last 5-minute period of baseline recording was considered as unstable recording and excluded from further analysis. This early baseline activity was also used to calculate the post-stimulation z-score values.

The offline after-effects of DCS could be based on two mechanisms: (i) early phase - changes in synaptic strength involving the modulation of GABAergic and glutamatergic activity (Nitsche *et al*., 2003; Stagg and Nitsche, 2011), and (ii) late phase - Ca^{2+} dependent long-term plasticity (Fritsch *et al.*, 2010; Islam *et al.*, 1995;). It has been shown that large post-synaptic calcium level increases long-term potentiation (LTP), which produces after-effects lasting for several hours (Cho *et al.*, 2001; Lisman, 2001).

We, therefore, divided the post-stimulation recording session into early and late phases (Figure 1). The early phase consisted of post-DCS 0 - 5 minutes of neuronal activity. The late z-score consisted of post-DCS 15 - 30 minutes and 30 - 35 minutes of neuronal activity. From z-score values of each 100ms bin, we extracted mean z-score value of the early and late phase, respectively, for further analysis. Then we compared the mean z-score values based on the stimulation polarity and genetic background.

4.2.5 Statistical analysis

Statistical analysis of the data was performed using SPSS 20.0 (SPSS, Chicago, IL). In order to test for differences between the groups an ANOVA was performed with stimulation type and

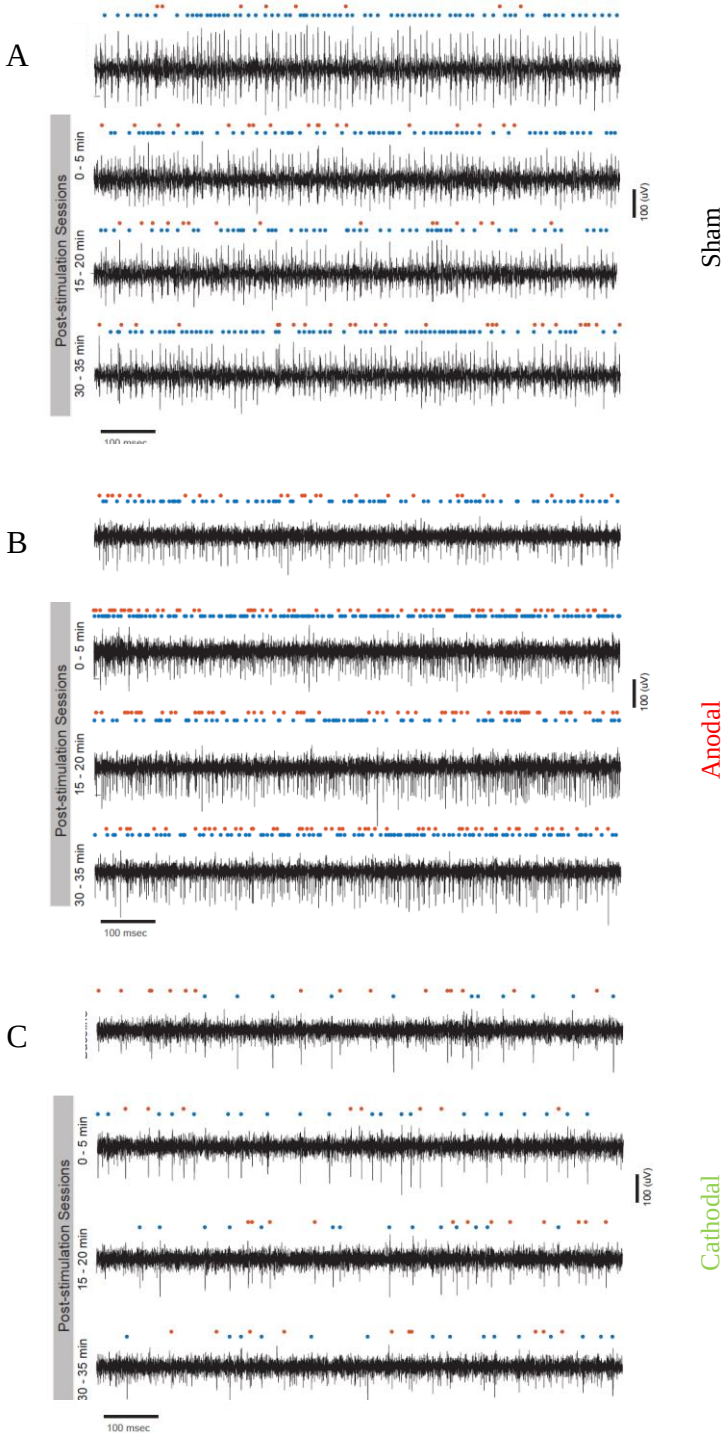

Figure 6: Neuronal data recorded from GluR2Δ7mice

(A) Sham stimulation; (B) Anodal stimulation and (C) Cathodal stimulation conditions

Two units those are taken for MUA, marked as blue and red

genetic background as within subject factors. Significance levels were set to 0.05. Later on, a Bonferroni-Holm Correction for Multiple Comparisons corrected post-hoc analysis was applied to find intra- / inter-group interactions. The values are represented here as mean ± SEM. We pooled the wild type C57BL/6, littermates of GluR2Δ7 and littermates of L7-PP2B data into the control group (WT) based on the polarity of DCS, as statistical analysis revealed no difference between these three groups ($p = 0.8$). Thus, in total we had 9 groups to compare. The nomenclatures of the groups are described in the table 1.

To check the long-term effect, we did linear regression analysis.

4.3 Results

4.3.1 DCS has no polarity specificity in the modulation of MUA of wild type control mice

Surprisingly, either polarity of DCS can increase of decreased the firing rate of MUA (Figure 9). This can be seen in the positive and negative z-scores we see in each stimulation

condition. The mean of absolute z-scores of the early phase was higher for the anodal (0.25 ± 0.82) and cathodal (-0.22 ± 0.44) stimulation conditions compared to sham (-0.38 ± 0.54) stimulation condition in the wild type mice. A Wilcoxon signed-rank test with Holm-Sidak correction showed a significant different between cathodal and sham stimulation conditions ($p < 0.01$).

The correlation of early vs late z-score was significant and positive in all 3 stimulation conditions (anodal condition ($r = 0.83$, $p < 0.001$), cathodal condition ($r = 0.94$, $p < 0.001$) and sham condition ($r = 0.60$, $p = 0.042$)) (Figure 9). Anodal and cathodal condition had higher tendency of modulation than sham condition. This indicates that the direction of modulation was consistent over time within a single recording.

4.3.2 DCS dependent modulation of the early and late-phase MUA in GluR2Δ7 and L7-PP2B mice

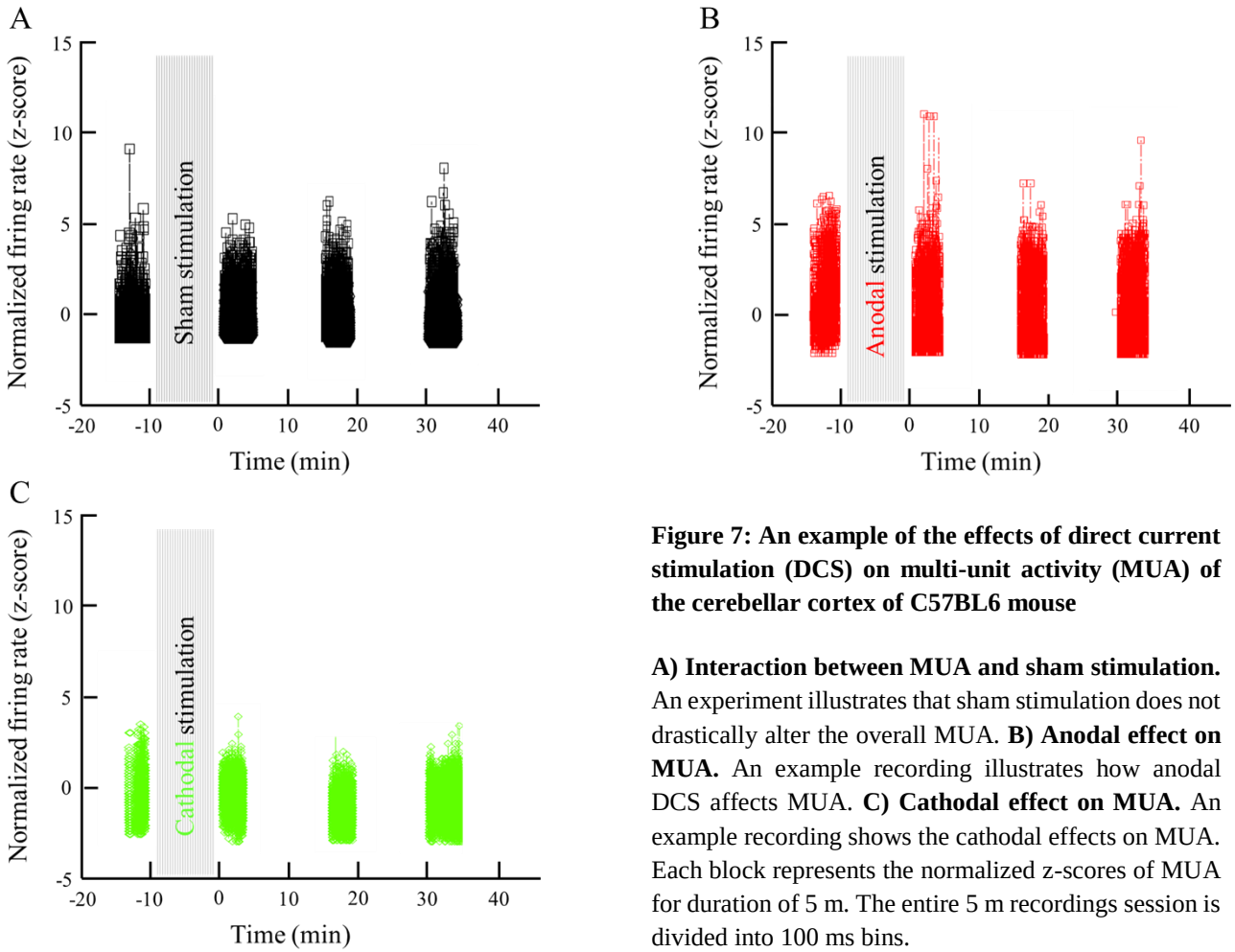

Figure 7: An example of the effects of direct current stimulation (DCS) on multi-unit activity (MUA) of the cerebellar cortex of C57BL6 mouse

A) Interaction between MUA and sham stimulation. An experiment illustrates that sham stimulation does not drastically alter the overall MUA. **B) Anodal effect on MUA.** An example recording illustrates how anodal DCS affects MUA. **C) Cathodal effect on MUA.** An example recording shows the cathodal effects on MUA. Each block represents the normalized z-scores of MUA for duration of 5 m. The entire 5 m recordings session is divided into 100 ms bins.

In our experiment, the group size of L7PP2B and GluR2Δ7 were small. While wild type mice had a positive correlation of early phase and late phase MUA modulation, in L7PP2B mice anodal stimulation caused a negative correlation (Figure 9B). Comparison between wild type and L7-PP2B anodal groups showed a significant difference in the slope ($p < 0.001$; Table 2). However, cathodal dependent modulation of the early vs later phase MUA remained alike to the wild type mice anodal stimulation condition ($p < 0.001$; Table 2) in terms of a positive correlation and a near zero intercept.

The anodal and cathodal stimulation had similar modulatory effects on MUA, in terms of a positive correlation and near 0 intercept, of GluR2Δ7 mice, despite of the fact that LTD at PC-PF synapses was absent in these mice (Figure 9C). Moreover, the effects of DCS in GluR2Δ7 MUA were similar to the effects of DCS in wild type control mice.

The statistical analysis confirmed the effects of DCS in terms of slope was significantly dependent on the genetic background of the mice $F(4, 46) = 2.71$, $p < 0.05$. In addition, the polarity specific effects of DCS and genetic background of the mice had a significant interaction $F(8, 36) = 2.32$, $p < 0.05$.

We found a significant difference between WtAn and LtpAn. As a result, we compare LtpAn to LtpCa and found a significant difference there as well. In the following paragraphs, we will discuss these group specific results in more detail.

4.3.3 DCS has no polarity specific effects at the population activity in the wild type mice

As described above, DCS had no polarity specific effects on the population activity of cerebellar cortical neurons in awake wild type mice. Our statistical analysis (linear regression) confirmed that in the wild type mice sham, anodal and cathodal stimulation groups had similar slope i.e., 0.73, 0.79, 0.76, respectively. In addition, there was no significant difference in the intercept ($p = 0.68$). Table 2 details the statistical analysis and displays no significant difference between the stimulation groups in control mice (Figure 9A).

4.3.4 Ablation of LTD at PF-PC synapses tends not to alter the effects of DCS

Statistical analysis comparing the slope of early vs late modulation of population activity was not significantly different between anodal and cathodal stimulation group in GluR2Δ7 mice; $F(1, 52) = 0.14$, $p = 0.71$ (Figure 9C, Table 2). In addition, comparing the control mice anodal group to the LTD anodal and cathodal groups indicated no difference ($p < 0.001$, Table 2).

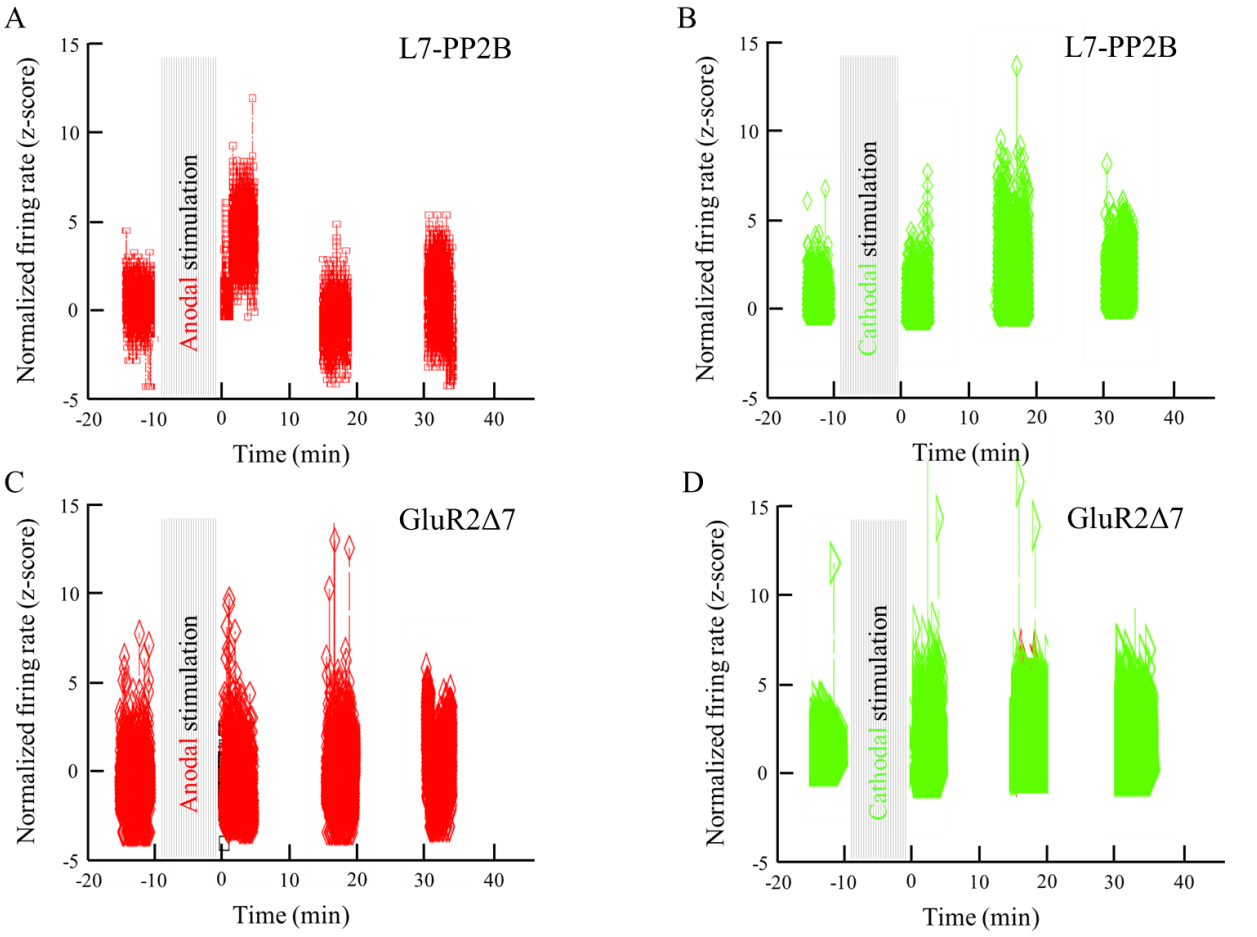

Figure 8: Examples of the effects of direct current stimulation (DCS) on multi-unit activity (MUA) of the cerebellar cortex of L7-PP2B and GluR2Δ7 mice

A) Anodal induced acute change in MUA. In this example, anodal DCS leads to an acute increment in MUA of the L7-PP2B mouse. The effect does not persist long after the stimulation. **B) Cathodal effect on MUA.** An example recording illustrates that cathodal DCS does not have an acute effect on the MUA of L7-PP2B mouse. **C) Anodal DCS does not alter MUA in GluR2Δ7.** An example recording in which the anodal stimulation does not have any acute effect on MUA. Moreover, the early and late-phase of MUA do not differ greatly. **D) Cathodal DCS does not alter early vs late - MUA differentially in GluR2Δ7.** The example recording illustrates that post-stimulation the MUA has increased. However, this increment in MUA stays high throughout the recording duration.
Each block represents normalized z-score of MUA for a duration of 5 m. Entire 5 m recordings session is divided into 100 ms bins.

4.3.5 Anodal DCS indicates sensitive towards the potentiation pathway of PCs in L7-PP2B mice

L7-PP2B mice tends to show a significantly different response when compared to the anodal control group. We observed a reverse correlation in anodal group (Figure 9B, Table 2). However,

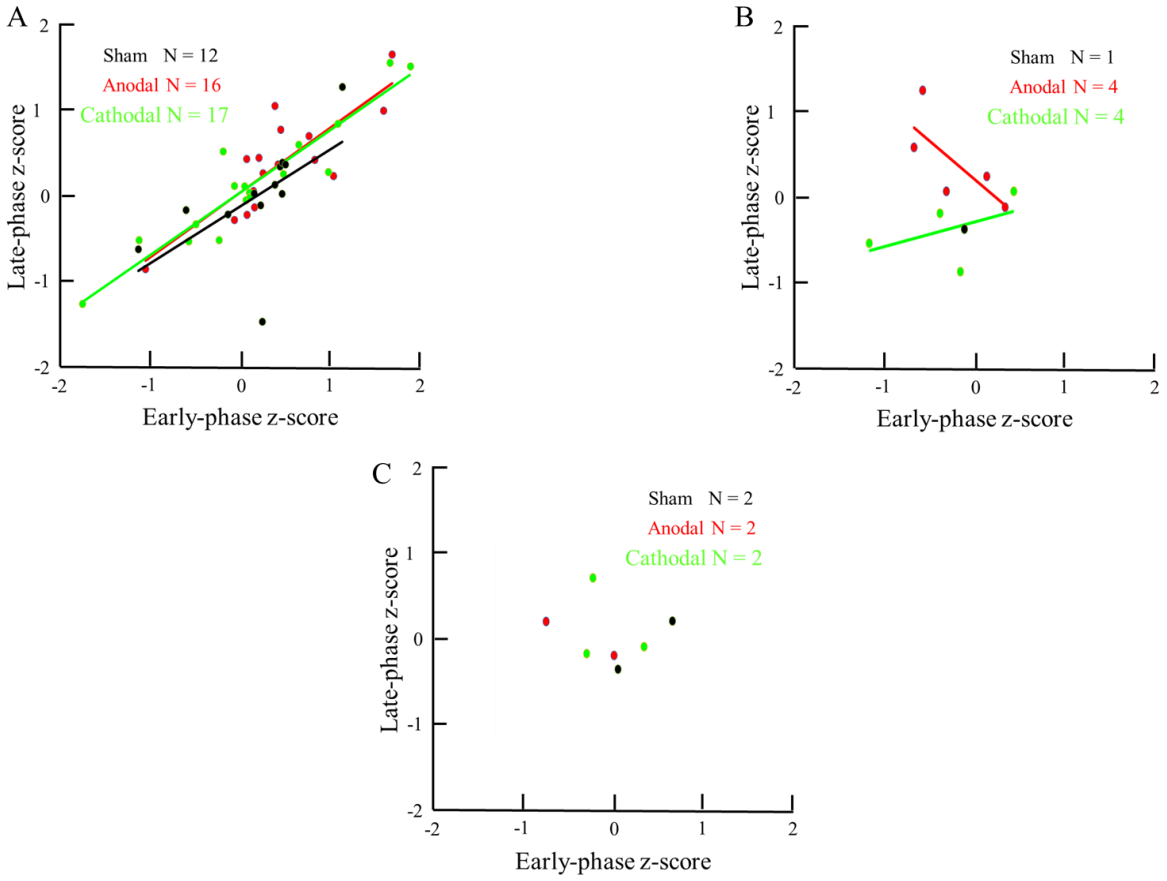

Figure 9: Scatter diagram of polarity dependent modulation of early vs late MUA

Each dot represents the early vs late phase s-score value of MUA from an experimental session. They are color coded according to the stimulation conditions. The line illustrates the linear fit for all the dots from a stimulation polarity of a specific type of mouse. Line follows the same color code. The length of the line depicts the range of a group.
A) DCS has polarity independent effects on control mice. Sham stimulation and DCS group do not have difference in terms of late vs early change in MUA. Only cathodal group shows greater distribution (or variation is higher). **B) Anodal effects suggest a reverse correlation in L7-PP2B mice.** The plot depicts that early vs late phase MUA modulation is different in the anodal group. When early MUA increases the late MUA decreases and vice versa. Cathodal stimulation has a positive correlation. The slope of the cathodal fit shows lesser change in early vs late phase MUA. **C) The effects of DCS on the cerebellar cortex of GluR2Δ7 mice.** Despite lack of parallel fiber Purkinje cell long-term depression, the effects of DCS shows a control like trend in these mice. The liner fit is not depicted here as the sham and anodal group has only 2 samples.
Each plot represents the z-score of MUA. The x and y-axis represent early and late phase MUA modulation, respectively. The color code: Black = sham stimulation; Red = anodal stimulation and Green = cathodal stimulation.

cathodal stimulation group had similar effects compared to the control anodal stimulation group (Table 2). Once again, we must consider that the group size is small in both anodal and cathodal stimulation groups.

4.4 Discussion

Our study suggests three major effects of DCS on cerebellar neuronal activity. First, DCS has no effects on neuronal activity in the wild type mice: it causes naturally occurring modulation to become persistent. Second, despite genetic deletion of the LTD at PF-PC synapses (GluR2Δ7 mice), both anodal and cathodal effects on neuronal activity seems to stay similar to the effects of stimulation in the control mice. Third, our preliminary data suggests that when PC LTP is genetically ablated (in the L7PP2B mutation), anodal stimulation is prone to induce an acute modulation, although effects of cathodal stimulation remained the same.

Strikingly, we observed that both anodal and cathodal stimulation can increase or decrease the MUA in the wild type mice. A similar result was reported in a human study where both polarities enhanced motor evoked potential (Wiethoff *et al.*, 2014) and semantic processing (Brückner, Kammer, 2017). Due to the lobular and highly foliated structure of the cerebellar cortex, the orientation of PCs within lobules can vary greatly. Since neuronal orientation has a major role in determining the effects of the current on neuron (Rahman *et al.*, 2014), stimulation of a given polarity can act like an excitatory or inhibitory stimulation on different neurons in the same lobule. Possibly, this is why either polarity stimulation can increase or decrease the MUA. Moreover, previous reports have used isolated, flattened the cerebellum (Parazzini *et al.*, 2013; Rahman *et al.*, 2014) to measure effects of electrical stimulation. We are the first to record from an *in vivo* preparation, but it should be noted that the animal was at rest and not performing a task. Many of the reported behavioral effects of tDCS are only observed when stimulation is applied concurrently with a behavioral task and therefore a next step would be to do recording while the animal is performing.

Cathodal stimulation leads to a higher early-phase MUA compared to the sham stimulation condition in wild type mice. The outcome of applying DCS depends on the noise present in the system and the level (stimulus intensity and duration) of DCS, rather than solely on the stimulation polarity (Miniussi *et al.*, 2013). For instance, Batsikadze *et al.*, (2013) showed that 20 min of

cathodal stimulation at 2 mA applied to the motor cortex significantly increased MEP amplitudes, while 1 mA of the same stimulation decreased the excitability. In our experiment, it is possible that cathodal stimulation reduces overall variability in the early-phase MUA by reducing the inherent noise of the system.

Anodal stimulation may enhance global inhibition that leads to a negative slope in early vs late phase neuronal activity in L7-PP2B mutant (Figure 9B, 10). If it is indeed the case, we propose that PCs in the L7-PP2B mutants may receive more background inhibition during anodal stimulation that could lead to an acute reduction of neuronal activity. When acute reduction is gone, a higher late phase activity is observed. This acute inhibition can be generated by subthreshold depolarization dependent GABA release from molecular layer interneurons (MLI) (Christie *et al.*, 2011) that increases inhibition on PCs. Perhaps, cathodal stimulation reduces this inhibitory tone and therefore we see consistent effects in neuronal activity. Our experimental power is not sufficient to resolve which mechanism plays the largest role in preventing an effect

Group code	Mouse type	Stimulation type
WtSh	C57BL/6 and wild type littermates of L7-PP2B and GluR2Δ7	Sham DCS
WtAn	C57BL/6 and wild type littermates of L7-PP2B and GluR2Δ7	Anodal DCS
WtCa	C57BL/6 and wild type littermates of L7-PP2B and GluR2Δ7	Cathodal DCS
LtpSh	L7-PP2B	Sham DCS
LtpAn	L7-PP2B	Anodal DCS
LtpCa	L7-PP2B	Cathodal DCS
LtdSh	GluR2Δ7	Sham DCS
LtdAn	GluR2Δ7	Anodal DCS
LtdCa	GluR2Δ7	Cathodal DCS

Table 1: Description of the group-code abbreviation used in the result section

of anodal DCS stimulation on cerebellar plasticity. Further work using techniques sensitive to membrane dynamics may be the best way forward in addressing this important question.

The sensitivity towards DCS remains unaltered in mice lacking PF-PC LTD (GluR2Δ7 mice); Figure 9C. The possible reasons could be due to – (i) PF driven rise in firing rate is unaltered in PC of these mice (Schonewille *et al.*, 2011) (ii) PF can suppress PCs firing rate through PF-MLI

LTP (Jörntell *et al.*, 2003) and (iii) intrinsic potentiation of PCs is possible (Gao *et al.*, 2012). Thus, the network functions may have a similarity to the wild type network.

In summary, we developed a mouse model of cerebellar DCS, allowing us to present the first demonstration of cerebellar DCS driven neuronal changes in awake non-behaving rodents. The results presented here suggest that anodal effects may depend on PC LTP pathway whereas cathodal effects not. Future research must address the specific mechanisms through which DCS has its effects during active behavior.

Compared groups	F-stat	DoF1	DoF2	P value	Holm significance
WtAn - WtSh	0.066370526	1	52	0.797713311	0
WtAn - WtCa	0.046953485	1	52	0.829299752	0
WtCa - WtSh	0.011834636	1	52	0.913790056	0
WtAn - LtpAn	34.84834755	1	52	2.73611e-07	1
WtAn - LtpCa	1.259356436	1	52	0.266928091	0
WtAn - LtdAn	7.183410004	1	52	0.009832548	0
WtAn - LtdCa	5.256224255	1	52	0.025944847	0
WtAn - LtdSh	0.944534853	1	52	0.335613552	0
LtpAn - LtpCa	18.93279903	1	52	6.35113e-05	1
LtdAn - LtdCa	0.136408979	1	52	0.713377162	0

Table 2: ANOVA analysis of the linear model

The first column depicts the group and conditions those are compared (group-code is similar to the Table 1). Second column shows the F-value. The third and fourth column corresponds to the hypotheses degree of freedom and error degree of freedom, respectively. Fifth column demonstrated the P value between the groups. Finally, the sixth column shows the actual significance after Holm's correction as few groups have low number of N. Here, 1 means significance.

References:

Bastian, A.J. (2011) Moving, sensing and learning with cerebellar damage. *Curr. Opin. Neurobiol.* 21, 596–601

Batsikadze *et al.* (2013) Partially non-linear stimulation intensity-dependent effects of direct current stimulation on motor cortex excitability in humans. *J. Physiol*. 591, 1987–2000

Boggio, P.S. *et al.* (2007) Repeated sessions of noninvasive brain DC stimulation is associated with motor function improvement in stroke patients. *Restor. Neurol. Neurosci.* 25, 123–129

Brunelin, J. *et al.* (2012) Efficacy and safety of bifocal tDCS as an interventional treatment for refractory schizophrenia. *Brain Stimul* 5, 431–432

Buttkus, F. *et al.* (2011) Single-session tDCS-supported retraining does not improve fine motor control in musician's dystonia. *Restor Neurol Neurosci* 29, 85–90.
Chan, C.Y. and Nicholson, C. (1986) Modulation by applied electric fields of Purkinje and stellate cell activity in the isolated turtle cerebellum. *J. Physiol. (Lond.)* 371, 89–114
Chan, C.Y. *et al.* (1988) Effects of electric fields on transmembrane potential and excitability of turtle cerebellar Purkinje cells in vitro. *J. Physiol. (Lond.)* 402, 751–771
Cho, K. *et al.* (2001) An experimental test of the role of postsynaptic calcium levels in determining synaptic strength using perirhinalcortex of rat. *J Physiol.* 532, 459–466
Christie, J.M. *et al.* (2011) Ca(2+)-dependent enhancement of release by subthreshold somatic depolarization. *Nat. Neurosci.* 14, 62–68
Fregni, F. and Pascual-Leone, A. (2007) Technology insight: noninvasive brain stimulation in neurology-perspectives on the therapeutic potential of rTMS and tDCS. *Nat Clin Pract Neurol* 3, 383–393.
Fritsch, B. *et al.* (2010) Direct current stimulation promotes BDNF-dependent synaptic plasticity: potential implications for motor learning. *Neuron* 66, 198–204
Galea, J.M. *et al.* (2009) Modulation of cerebellar excitability by polarity-specific noninvasive direct current stimulation. *J. Neurosci.* 29, 9115–9122
Galea, J.M. *et al.* (2011) Dissociating the roles of the cerebellum and motor cortex during adaptive learning: the motor cortex retains what the cerebellum learns. *Cereb. Cortex* 21, 1761–1770
Gandiga, P.C. *et al.* (2006) Transcranial DC stimulation (tDCS): a tool for double-blind sham-controlled clinical studies in brain stimulation. *Clin Neurophysiol* 117, 845–850
Herzfeld, D.J. *et al.* (2014) Contributions of the cerebellum and the motor cortex to acquisition and retention of motor memories. *Neuroimage* 98, 147–158
Islam, N. *et al.* (1995) Increase in the calcium level following anodal polarization in the rat brain. *Brain Res.* 684, 206–208
Jayaram, G. *et al.* (2012) Modulating locomotor adaptation with cerebellar stimulation. *J Neurophysiol* 107, 2950–2957
Liebetanz, D. *et al.* (2006a) After-effects of transcranial direct current stimulation (tDCS) on cortical spreading depression. *Neurosci. Lett.* 398, 85–90
Liebetanz, D. *et al.* (2006b) Anticonvulsant effects of transcranial direct-current stimulation (tDCS) in the rat cortical ramp model of focal epilepsy. *Epilepsia* 47, 1216–1224
Liebetanz, D. *et al.* (2009) Safety limits of cathodal transcranial direct current stimulation in rats. *Clin Neurophysiol* 120, 1161–1167
Lisman, J.E. (2001) Three Ca2+ levels affect plasticity differently: the LTP zone, the LTD zone and no man's land. *J Physiol* 532 (Pt 2), 285.
Márquez-Ruiz, J. *et al.* (2012) Transcranial direct-current stimulation modulates synaptic mechanisms involved in associative learning in behaving rabbits. *Proc Natl Acad Sci U S A* 109, 6710–6715
Miniussi, *et al.* (2013) Modelling non-invasive brain stimulation in cognitive neuroscience. *Neurosci Biobehav Rev* 37, 1702–1712
Murphy, D.N. *et al.* (2009) Transcranial direct current stimulation as a therapeutic tool for the treatment of major depression: insights from past and recent clinical studies. *Curr Opin Psychiatry* 22, 306–311
Nitsche, M. A. *et al.* (2003) Pharmacological modulation of cortical excitability shifts induced by transcranial direct current stimulation in humans. *J. Physiol* 553, 293–301.
Parazzini, M. *et al.* (2013) Computational model of cerebellar transcranial direct current stimulation. , in *2013 35th Annual International Conference of the IEEE Engineering in Medicine and Biology Society (EMBC)*, pp. 237–240
Rahman, A. *et al.* (2014) Polarizing cerebellar neurons with transcranial Direct Current Stimulation. *Clin Neurophysiol* 125, 435–438

Sabrina *et al.* (2010) Both anodal and cathodal transcranial direct current stimulation improves semantic processing. Neurosc 343, 269-275

Schonewille, M. *et al.* (2010) Purkinje cell-specific knockout of the protein phosphatase PP2B impairs potentiation and cerebellar motor learning. *Neuron* 67, 618–628

Schonewille, M. *et al.* (2011) Reevaluating the role of LTD in cerebellar motor learning. *Neuron* 70, 43–50

Stagg, C.J. and Nitsche, M.A. (2011) Physiological basis of transcranial direct current stimulation. *Neuroscientist* 17, 37–53

Takano, Y. *et al.* (2011) A rat model for measuring the effectiveness of transcranial direct current stimulation using fMRI. *Neurosci. Lett.* 491, 40–43

Wiethoff, S. *et al.* (2014) Variability in response to transcranial direct current stimulation of the motor cortex. *Brain Stimul* 7, 468–475

Chapter Five

An optimal control model of the compensatory eye movement system

Peter Holland, Tafadzwa M. Sibindi, Marik Ginzburg, Suman Das, Kiki Arkenstein, Opher Donchin , Maarten A. Frens

An optimal control model of the compensatory eye movement system

Abstract

We proposed in 2009 that a state-predicting feedback control (SPFC) framework could apply the elegance of optimal control models to the compensatory eye movement system. Here, we present a working version of the SPFC. We challenge our model by comparing the output to the eye movements of mice (n = 34). The model reproduces behavior across a range of frequencies (0.1-3.2 Hz) and amplitudes (0.5-8°) for primary reflexes (optokinetic response (OKR) and vestibulo-ocular reflex (VOR)) as well as for two conditions where the reflexes function simultaneously (a matrix of 144 conditions). We also reproduced the response of the system to complex stimuli such as sums of sines. Moreover, we challenge the anatomical basis for the model: removal of output from specific parts of the model are compared with the known effects of neural lesions. In our model, the OKR system learns to compensate for inaccuracies of the VOR. This explains the non-linear summation of the VOR and OKR systems across different stimulus conditions. Since adaptation then changes the OKR compensation, this also explains how flocullar lesions abolish VOR adaptation but not VOR performance.

5.1 Introduction

Optimal control models are the dominant paradigm in current studies of motor control. They combine strong theoretical foundations with elegant explanatory power, and the ideas have been successfully applied to research in the study of cerebellum and basal ganglia. Indeed, one appeal of these models is the connections that have been made between the physiology of specific motor systems and the functional pieces of an optimal controller (Frens and Donchin, 2009; Shadmehr and Krakauer, 2008). However, while these connections make sense intuitively, it has proved very difficult to build optimal control models that make specific predictions for real, physiological motor circuits.

In this paper, we address this gap by building a working model of the compensatory eye movement (CEM) system starting from the ideas developed in the Frens and Donchin state predicting feedback control (SPFC) scheme (Frens and Donchin, 2009). In implementing the model, we developed our ideas significantly relative to the earlier work, but many of the basic ideas driving the two works are the same, and we consider both models to be within the SPFC framework, as defined below.

We challenge our model in a broad range of experimental conditions and find that the model successfully predicts the behaviour of the CEM system in all tested conditions. We chose to model and do experiments in mice, because mice are afoveate and hence lack a confounding smooth pursuit system. Furthermore mice are becoming a model of choice in oculomotor research because of the availability of genetic techniques and because it is now feasible to record mouse eye movements precisely in all dimensions (van Alphen *et al*., 2004). Technical details of the current model are provided in the supplementary material.

5.1.1 CEM system: what it is and how it has been modeled previously

Compensatory eye movement is a general term for several reflexes whose goal is to maintain a stable image on the retina during movements of the head, by moving the eyes in the opposite direction (Delgado-Garcia *et al*., 2000). In other words, these reflexes serve to reduce retinal slip (movement of the visual image across the retina). In afoveate animals like mice, the vestibulo-

ocular reflex (VOR) uses vestibular input to compensate retinal slip and the optokinetic reflex (OKR) is driven by the retinal slip itself.

OKR originates in velocity sensitive neurons of the retina, which project through the Accessory Optic System (AOS) and Nucleus Reticularis Tegmenti Pontis (NRTP) to the vestibular nucleus (VN) and the vestibulo-cerebellum (Gerrits *et al.*, 1984; Glickstein *et al.*, 1988; Langer *et al.*, 1985). The VN output is sent to the brainstem nuclei, which drive the extra-ocular muscles. In the case of horizontal eye movements, these are the abducens nucleus (Ab), the oculomotor nucleus (OMN) and nucleus prepositus hypoglossi (NPH; Buttner-Ennever *et al.*, 1992). While oculomotor proprioceptive signals may play a role in CEM circuitry (Donaldson *et al.*, 2000; Wang *et al.*, 2007), this possibility remains controversial and is not considered in our model.

The OKR has a species-dependent response delay of 70-120ms (Collewijn *et al.*,1969; van Alphen *et al.*, 2001; Winkelman and Frens, 2006) primarily caused by the visual processing in the pathway from retina to VN (Graf *et al.*, 1988). The retinal afferents saturate at high velocities (Oyster *et al.*, 1972; Soodak and Simpson, 1988), causing non-linearities in the OKR in this range (Collewijn *et al.*, 1969; van Alphen *et al.*, 2001). Thus, the OKR is ineffective in compensating high velocity (and thus often high frequency) visual stimuli.

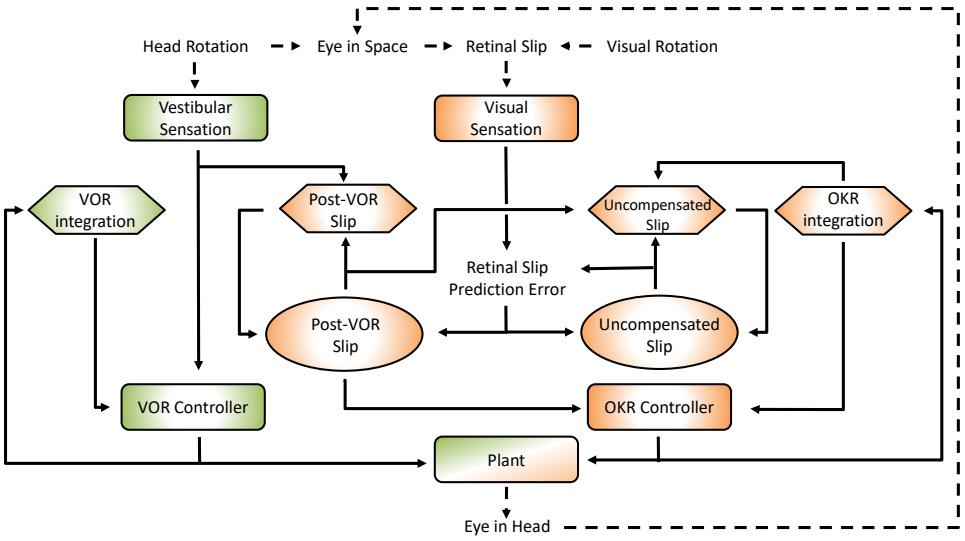

Figure 1: General layout of the model presented in this chapter.

Green areas are vestibular, orange areas are optokinetic. Hexagons represent Forward Models, ellipses are State Estimators. Dashed arrows indicate processes in the real world, solid arrows are neural processes. Details of the model are specified in the text.

The vestibulo-ocular reflex (VOR) uses vestibular input from the semi-circular canals (labyrinth) to compensate head movement (Delgado-Garcia, 2000). Vestibular afferents from the labyrinth project directly to VN with a small delay (2ms; Glasauer, 2007) . Their activity accurately reflects head velocity at high frequencies but not at low frequencies (Robinson, 1981) due to filtering properties of the vestibular labyrinth (Yang and Hullar, 2007). From the VN, the VOR and OKR pathways are identical.

Thus, the OKR and VOR reflexes have roughly complementary properties. The OKR works well in low velocities, and the VOR works well at high frequencies. The existence of these reflexes allows accurate compensation of the retinal slip velocity in normal behaviour. The CEM system has a number of properties that make it a popular candidate for quantitative modeling of sensorimotor processes. First, its goal, minimizing retinal slip, is clear and invariant over time. Second, the dynamics of the system as a whole are close to linear. Third, the output only has 3 degrees of freedom. Moreover, horizontal CEM can be isolated from the other two degrees of freedom and treated as a system with a single degree of freedom. This is commonly done in the experimental literature, and it is our approach as well.

5.1.2 SPFC model: basic architecture and predictions

Theories of motor control are primarily based on one of two main architectures. One theory suggests that the motor system relies on generating an ideal "desired movement" or "desired trajectory" that serves as a basis for subsequent control. Such an architecture faces a number of key challenges: generating the desired trajectory, translating it into motor commands, and correcting for deviations during online control. At the heart of such a system is an "inverse model" which translates desired movement into motor commands (Jordan and Rumelhart, 1992). Traditional models of CEM all have this form (see Glasauer, 2007 for review). In general, a desired motor command is fed to the brainstem, which then acts as an ‘inverse plant’, i.e. it processes the command in order to overcome the low-pass properties of the extraocular muscles and tissues that are connected to the eye.

An alternative architecture that has served as a basis for recent work suggests, instead, that the system operates in a "full feedback" mode: generating motor commands in response to the best guess regarding the current situation as opposed to using a pre-defined plan (Todorov and Jordan,

2002). Frens and Donchin (2009) used this architecture in their analysis of the CEM, which they called the state-predicting feedback control, SPFC, framework. Here, we develop a quantitative model with this architecture inspired by their earlier work (Fig. 1).

The SPFC framework has three types of components: a forward model, a state estimator, and a controller. Given the control delays of the biological motor system, feedback is feasible only if the system relies on a "forward model" that predicts the current state with reasonable accuracy based on the best previous estimate and on-going motor commands (Todorov and Jordan, 2002). In the SPFC framework, the flocculus serves this role. The forward model's prediction is then input to a state estimator (the vestibular nucleus), which integrates the prediction with delayed sensory inputs. This internal state estimation is the "best guess regarding the current situation". The feedback controller uses the current estimate of state in order to decide what motor commands to generate. It either replaces or incorporates the inverse model on which tradition has focused. Anatomically, the feedback controller would incorporate the Abducens nucleus and the NPH, if one pertains to the view that the NPH provides an efference copy signal (Green *et al*., 2007). In a more classical view, the NPH integrates the oculomotor command and is thus part of the forward model stage (Cannon and Robinson, 1987; Robinson, 1981).

This approach was shown to be relevant in explaining various other motor control tasks, like reaching movements (Todorov and Jordan, 2002).

In developing a computational model of the SPFC framework and fitting it to real data, we realized a number of ways in which our earlier thinking had missed details that were of key importance. We also introduced a new, and completely innovative, understanding of the role of adaptation in the CEM system. First, our original conception of the CEM system, following the ideas in Shadmehr and Krakauer (2008) (Shadmehr and Krakauer, 2008), was of a single optimal feedback loop. This proved inadequate. Our current implementation is essentially hierarchical, with the vestibular and the visual components of the CEM handled in two distinct loops (see Fig 1). This is closer to a traditional view of CEM which also incorporates two more or less separate mechanisms for the VOR and OKR. The VOR operates in a partially open-loop fashion with feedback used to drive only the forward model of the eye without modifying processing of the vestibular state itself. The OKR loop, on the other hand, incorporates forward models of the eye,

the visual input, and also the VOR system. That is, the OKR not only predicts current retinal slip based on models of the environment and the eye movements, it also incorporates a model of the residual retinal slip that remains after the actions of the VOR loop. Thus, the transition to two separate loops brings our model closer to the classical model of the CEM while maintaining the essential structure of the SPFC. However, it also allows to introduce a key innovation. We postulate that the primary adaptation of the CEM system is in the OKR part of the system. These are consistent with experimental findings (as reviewed below) and also with our hypothesis that the OKR loop is more dependent on forward model prediction than the VOR loop. Further, we predict that the adaptation of the CEM system (at least to first approximation) is mostly adaptation of the OKR model of VOR inaccuracies (Fig1; Post-VOR Slip). While the reality may be more complex, the idea that the OKR models the VOR was the only way that we could explain the relatively high gains of both the OKR and VOR systems in isolation with the veridical gain of the two systems combined.

5.1.3 Sensory signals

Compensatory eye movements are driven by two different sensory signals – vestibular and retinal. In this section we describe the biological processes behind these feedback signals and the numerical models that can be used to describe them.

Vestibular input is created by semi-circular canals in the inner ear. At high frequencies, canals sense head rotation velocity with high accuracy. However due to the physical properties of the sensor, the accuracy is poor at low frequencies (Robinson, 1981). Thus, the semi-circular canals act as a high-pass filter that outputs the neural vestibular velocity feedback signal ($V^{(1)}$) on the basis of the actual head velocity ($\dot{H}$). The corresponding differential equation can be found in the supplementary material (Eq 3).

Visual input is provided by motion sensitive neurons in the retina (Yoshida *et al*., 2001). Those neurons sense retinal slip, the velocity of the image on the retina, where

$$R^* = \dot{H} + \dot{E} - \dot{T} \qquad (1)$$

Here R^* is retinal slip, $\dot{T}$ is the velocity of the visual surroundings, and $\dot{E}$ is the velocity of the eye relative to the head (all in in °/s). The linear response of the motion sensitive neurons has a limited range that effectively makes it a low-pass filter (see Eq 8 in the Supplementary Material). There is no data currently available on the precise saturation point for the motion processing system of the mouse.

In addition, the processing of visual signals adds substantial delay to the retinal feedback (Collewijn, 1969). Our model uses the value of δ_R = 70ms proposed for the delay in mice (van Alphen *et al*., 2001).

5.1.4 Motor Command Signals

Output of the OMN/Ab innervates the horizontal rectus muscles, which are responsible for horizontal eye movements. These nuclei are reciprocally activated and project to muscles that move the eyes in opposite directions. Hence eye velocity depends on the difference between OMN and AB activities. The transfer function of the oculomotor plant, i.e. the muscles and elastic tissue in the orbit, can be described as a low pass filter (Eq 2 in Supplementary Material) with a time constant of T_p , which we set at 0.5s (Stahl and Simpson, 1995; Stahl *et al*., 2015).

5.1.5 Forward Model and State Estimation

Forward models allow the observer to predict the current state of the system according to the previous state and command signals available through efference copy. Frens and Donchin (2009) and Green *et al.*, (2007) both proposed that the floccular vestibular area generates a forward model of the compensatory eye movement system. We denote the output of the forward model at time step k as $\hat{x}_k$ and the state estimate that combines forward model output and sensory feedback, as $\tilde{x}_k$. The output of a forward model is given by:

$$\hat{x}_{k+1} = A'\tilde{x}_k + Bu_k \qquad (2)$$

Hence, the values represented in the forward model are a weighted sum of the efference copy and the previous optimal estimation of state.

5.1.6 Model Architecture

Our model assumes that VOR and OKR involve separate neural processing. In the case of VOR, the processing is quite simple (green areas in Fig 1). The internal state needs only have three elements: head velocity, eye position, and eye velocity. Since the system has no access to the actual head velocity, we use the vestibular signal as an approximation of the head velocity. Neither system dynamics nor the oculomotor command affects head dynamics. Note therefore that this model currently does distinguish between active and passive head movements, i.e. it does not incorporate efference copy or proprioceptive information about head movement.

Eye movements and eye position have standard dynamics; the motor command drives them directly. The flocculus is not critical for VOR performance, as animals lacking Purkinje cells do have an intact VOR although the amplitude of the response is significantly higher (van Alphen *et al*., 2001). While our model does include a forward model and state estimator for head velocity, this is only a formal result of the structure of the model. In fact, our model ignores the results of the forward model and uses the sensory information exclusively to determine head velocity. Thus, the role of the forward model (green hexagon in Fig 1) in this system is actually only to integrate eye velocity into eye position.

The job of the second part of the control loop is to estimate the retinal slip that will be uncompensated by the VOR (Post-VOR Slip) and then compensate for it. Post-VOR slip arises from two sources: from changes in the velocity of the visual stimulus and from head movements not compensated by the VOR. These signals represent the predicted retinal slip for which the OKR needs to correct. We use the symbol $\hat{R}_k^*$ for the forward model of this this signal and $\tilde{R}_k^*$ for the state estimate. The combination of this latter signal (how much the visual environment would be moving in the absence of OKR) and estimate of how much the OKR is moving the eye, $\hat{\dot{E}}_{R,k}$, gives the OKR's prediction of uncompensated retinal slip (right orange hexagon in Fig 1):

$$\hat{R}_k = \hat{\dot{E}}_{R,k} + \tilde{R}_k^* \qquad (3)$$

The OKR system assumes that VOR compensates for some fraction of the head movement, and it models the effect of VOR as a gain applied to the sensed head velocity. Thus, our forward model

estimate of movement of the visual surrounding (left orange hexagon in Fig 1) will be updated by a factor proportional to head acceleration (See also Eq 29 in Supplementary text). ζ , the constant of proportionality, will be further discussed in the section on VOR adaptation below.

$$\hat{R}^*_{k+1} = \tilde{R}^*_k + \zeta\left(\hat{\dot{H}}_k - \hat{\dot{H}}_{k-1}\right) \qquad (4)$$

As one can see in Fig 1, state estimation produces estimates of both Post-VOR slip, and uncompensated retinal slip (oval boxes). Post-VOR slip is retinal slip after VOR compensation and uncompensated slip is that remaining after the action of both systems. The state estimator is a Kalman filter. Parameters of the Kalman gain were selected by hand to match the data (see Supplementary Material, Eq 42). Thus, through the model architecture, vestibular input only affects our estimate of the head velocity, and retinal input affects both our estimate of retinal slip, and our estimate of uncompensated retinal slip.

It is worth noting that in our earlier discussion (Frens and Donchin, 2009), we argued that a Kalman filter was unrealistic because it would require a delay line for dealing with the visual feedback delay. We posited that delay lines are non-physiological. To keep the current model manageable, we do not address this important caveat. The model uses both a delay line and a Kalman filter. We did not attempt a model with more realistic internal models of delay, although this is clearly an important next step.

Note that in calculating state estimation for the OKR system, we must take into account the non-linearity of the retinal processing before comparing the predicted uncompensated retinal slip to the sensory input. To produce a combined system, we simply combine the descriptions of the OKR and VOR systems above.

5.1.7 Costs

We assumed that the primary goal of the optimal controller of the CEM in afoveate species (like rabbit and mouse) is to minimize motion of the visual field on the retina in order to stabilize the retinal image. We make the assumption that this cost is considered separately for VOR and OKR because we are assuming that these reflexes are supported by separate neural substrates. Thus, the

overall cost of the system is the linear sum of the vestibular (C_{V}) and retinal costs (C_{R}; see Eq 43 in Supplementary Materials).

Each of the two sub costs is concerned with a different retinal slip: C_{V} relates to $\dot{H}_k + \tilde{\dot{E}}_{\mathrm{V},k}$, i.e. retinal slip due to uncompensated head motion, whereas C_{R} relates to $R^*_k + \tilde{\dot{E}}_{\mathrm{R},k}$, retinal slip due to uncompensated motion of the visual environment.

In addition to the cost associated with retinal slip, each cost function includes a cost associated with eye eccentricities (this can be considered an "action" cost since eye eccentricity leads to extra muscle activity and energy expenditure). Finally, both cost functions discount future costs, as is common for an infinite horizon feedback controller (see Supplementary Material, Eq 44).

5.1.8 VOR adaptation

VOR adaptation occurs when the vestibular and visual sensory motion signals about self-motion mismatch (Blazquez *et al*., 2004; Schonewille *et al*., 2010). In a laboratory environment, this can occur if an animal is rotated in a non-earth-stationary visual environment (as described in the Methods below). This leads to persistent changes in the VOR output that are optimized for the new situation. In the structure of the model, such a mismatch would affect the proportionality constant ζ. This is because the OKR system's first assumption is that retinal slip is the result of inaccuracies in the VOR loop (see Supplementary Material).

5.1.9 Model Parameters

In the model only a few parameters were set to match the data, and the same parameters were used for all conditions. Most variables were either taken from literature, or experimentally derived by us in separate experiments. Interestingly, it turned out that the exact values of most parameters was not critical (see table 1 in Supplementary Material). For example, we determined the VOR and OKR gains from our own data, using high frequency stimulation to determine the maximum gain of the VOR and low velocity stimulation to determine the maximum gain of the OKR. The form of the non-linearity in processing of retinal slip was fit to published results (Oyster *et al*., 1972; Soodak and Simpson, 1988). The filtering of vestibular stimulation, however, was shaped to

achieve the best fit to the data. Ultimately, the filter that fit our data best was also compatible with the literature. We used a first order high pass filter with a time constant of 4s (Yand and Hullar, 2007). Similarly, drift velocity and VOR adaptation speed were fit to the data, and then found to be compatible with results in the literature.

5.1.10 Predictions

We consider the model to function well, if the main characteristics of OKR and VOR are reflected in the model output, without the need to specifically tweak the model parameters. Furthermore, the same set of parameters should then result in good predictions of responses in additional conditions, i.e. the visuo-vestibular ocular reflex (vVOR; rotation of the animal in the dark, providing simultaneous visual and vestibular stimulation), suppressed VOR (sVOR; simultaneous rotation of the animal and its visual surroundings), and responses to non-sinusoidal stimuli.

Furthermore, in order to test the relation between the different pieces of the model and the underlying anatomy, lesions in specific parts of the model, should mimic actual lesions in the associated brain structures. Finally, it should be possible to set the value of ζ adaptively, thus mimicking VOR adaptation.

5.2 Methods

5.2.1 Animals

In order to test the model we recorded CEM in 13 C57Bl/6J mice. All mice were housed on a 12h light / 12h dark cycle with unrestricted access to food and water. Experiments were done during their light phase. All experiments were done with approval of the local ethics committee and were in accordance with the European Communities Council Directive (86/609/EEC).

5.2.2 Surgery

Animals were prepared for head fixation by attaching two metal nuts to the skull using a construct made of a micro glass composite. The full procedure is described in van Alphen *et al*., (2009). Mice were given at least 3 days following surgery to recover before the start of any experimental paradigm.

5.2.3 Stimulus setup

Optokinetic stimuli were created using a modified Electrohome Marquee 9000 CRT projector (Christie Digital Systems, Cypress CA, USA) with a spatial resolution of at least 0.1 degrees and a temporal resolution of 0.01 s. The average luminance was kept constant at 17.5 cd/$m^{2.}$ The stimuli were projected via mirrors onto three transparent anthracite-coloured screens (156*125 cm), which were placed in a triangular formation around the recording setup (Fig 2A). This created a green monochrome panoramic stimulus fully surrounding the animal. The stimuli were programmed in C++ and rendered in openGL. They each consisted of 1592 green dots (2 degrees diameter) equally spaced on a virtual sphere with its centre at eye height above the centre of the table. Moving stimuli were generated by rotating the virtual sphere around its vertical axis in sinusoidal patterns of different frequency and amplitude, so that all the dots moved coherently and in phase.

Vestibular stimulation was given by means of a motorized (Mavilor-DC motor 80) vestibular table that had its axis aligned with the centre of the visual stimulus. The driving signal of both the visual and vestibular stimulation, which specified the required position, was computed and delivered by a CED Power1401 data acquisition interface (Cambridge Electronic Design) with a resolution of 0.1 º and 0.01 s.

5.2.4 Eye movement recordings

Mice were immobilized by placing them in a plastic tube, with the head pedestal bolted to a restrainer that allowed translations in three dimensions such that the eye of the mouse was placed in the centre of the visual stimulus and thus above the rotation axis of the turn table, in front of the eye position recording camera.

Eye movements were recorded with an infrared video system (Iscan ETL-200). Images of the eye were captured at 120 Hz with an infrared sensitive CCD camera [see van Alphen *et al*. (2009) for more details]. To keep the field of view as free from obstacles as possible, the camera and lens were mounted under the table surface, and recordings were made with a hot mirror that was transparent to visible light and reflective to infrared light (Fig. 2B). The eye was illuminated with two infrared LEDs at the base of the hot mirror. The camera, mirror and LEDs were all mounted

on an arm that could rotate about the vertical axis over a range of 26.12º (peak to peak). Eye movement recordings and calibration procedures were similar to those described by Stahl *et al*., 2000. Eye position was stored, along with the stimulus traces on hard disk for offline analysis.

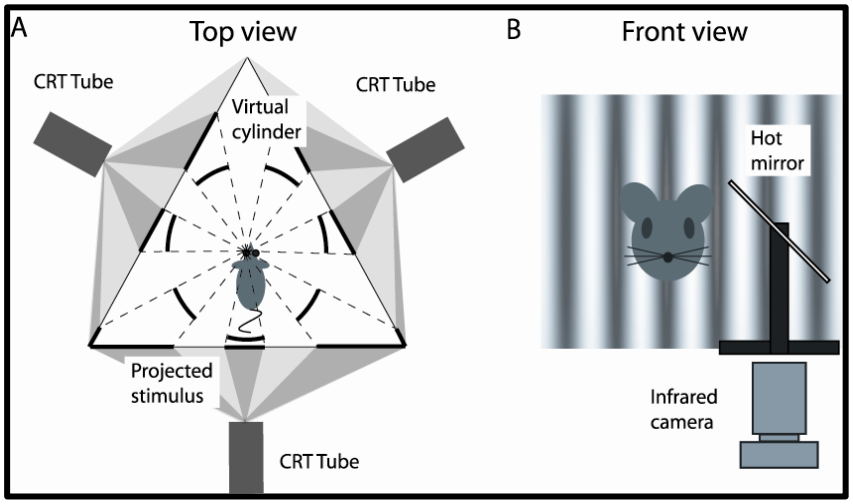

Figure 2. Schematic representation of the experimental setup.

(A) Top view. A mouse in the setup, with its left eye in the center and surrounded by three screens on which the visual stimuli are projected. The visual stimuli were programmed in such a way that from the point of view of mouse it appeared as a virtual sphere. (B) Front view. A mouse placed in front of a hot mirror, which enabled the infrared camera underneath the table to record the eye movements.

5.2.5 Experimental Paradigms

5.2.5.1 Optokinetic Reflex

The OKR (N=9) was tested using visual stimuli, while the mouse was kept stationary. We presented sinusoidal stimuli containing a wide range of frequencies (0.1, 0.2, 0.4, 0.8, 1.6 and 3.2 Hz) and amplitudes (0.5, 1.0, 2.0, 4.0, 6.0 and 8.0º), all about the earth vertical axis.

5.2.5.2 Vestibulo-ocular Reflex

The VOR (N=9) was tested with vestibular stimulation in the dark. Stimulus amplitudes and frequencies were identical to those used for the OKR, except that stimuli with a peak velocity higher than 60 º/s were discarded, because of mechanical considerations. Again, only rotations about the vertical axis were made.

5.2.5.3 Visually enhanced VOR and suppressed VOR

The vVOR (N=9) and the sVOR (N=6) protocols were identical to the VOR stimulation, except for the visual stimulation. During vVOR the visual stimulus was on, but stationary; during sVOR the visual stimulus was on and moved in phase and at the same amplitude as the turn table.

These four stimulus protocols were presented blockwise in 1 or 2 experimental sessions. Within each protocol the stimulus conditions were presented in random order to prevent effects of either learning or fatigue. All stimuli were presented for at least 5 cycles. The other protocols were performed separately.

5.2.5.4 Non-periodic stimulation

For non-periodic stimulation we opted to give Sum-of-Sine (SoS) stimuli. In these SoS conditions, the two constituent frequencies were chosen that had no harmonic relation. Four SoS frequency combinations were used in this study: 0.6/0.8 Hz, 0.6/1.0 Hz, 0.8/1.0 Hz and 1.0/1.9 Hz. Amplitude was either one or two degrees for each frequency component. Either both frequencies had the same amplitude (both 1º or both 2º) or they had different amplitude (one at 1º and the other at 2º). This led to a total of 24 types of stimuli in each of the OKR, VOR, vVOR and sVOR SoS conditions. 8 mice were used in this paradigm and they all performed all conditions.

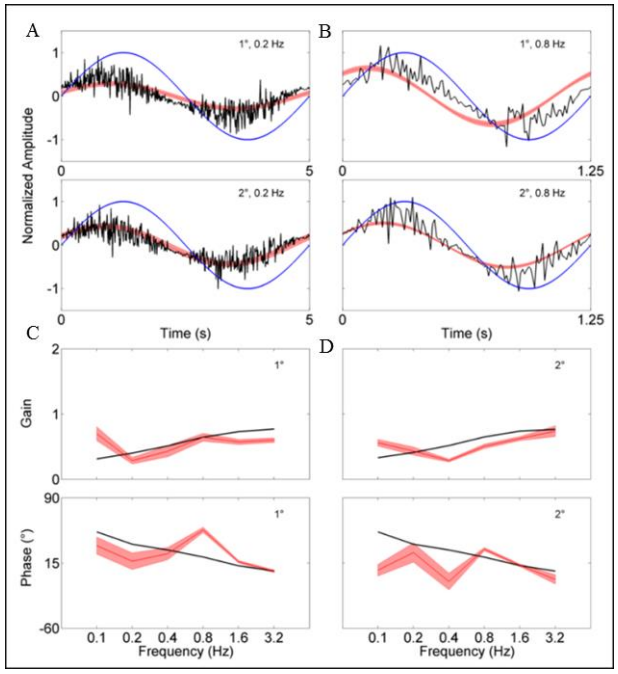

Figure 3. Summary of VOR data and simulation.

The upper row gives results for 1° stimuli, the lower row for 2° stimuli. Panel A gives a 0.2Hz stimulus (black), with the simulated response (blue) and the mean measured responses (red) with confidence limits. Panel B does the same for a 0.8 Hz stimulus. Panel C and D are Bode plots for Gain and Phase respectively. Other stimulus conditions fitted equally well.

5.2.6 Drift in the dark

In order to compute the plant time constant (see Supplementary Material, eq 15), we needed the mouse eye to drift in the dark from an eccentric position to the center of the oculomotor range. To do so, a visual scene moved slowly horizontal, thus making the eye move eccentrically. Subsequently, the light was turned off, and the mouse was in complete darkness. We then recorded the drift towards the centre of the eye. By fitting an exponential function to this drift, the plant time constant was calculated. 6 mice were measured over a range of drift amplitudes between 4 and 10 degrees, the number of drift repetitions was on average around 6 per amplitude per mouse.

4.2.7 VOR adaptation

VOR gain down adaptation (N=7) experiments consisted of 6 testing sessions and 5 training trials. Duration of each testing / training trial was 60s / 300s respectively. Sinusoidal (1 Hz, 5°) vestibular stimulation was applied in the dark for the testing sessions. During training sessions, vestibular stimulation was accompanied by optokinetic sinusoidal stimulation of the same amplitude, phase and frequency (thus resulting in a stable head fixed visual surrounding).

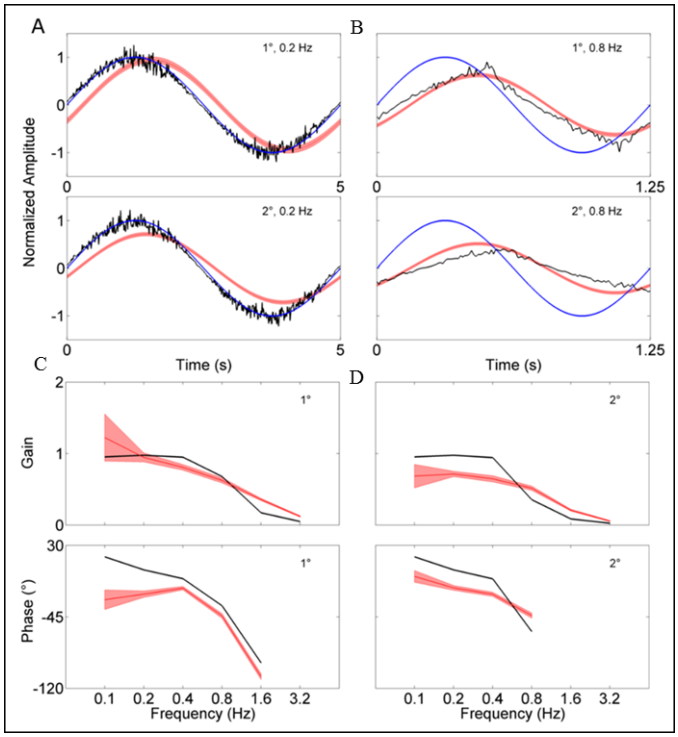

Figure 4. Summary of OKR data and simulation.

The upper row gives results for 1° stimuli, the lower row for 2° stimuli. Panel A gives a 0.2Hz stimulus (black), with the simulated response (blue) and the mean measured responses (red) with confidence limits. Panel B does the same for a 0.8 Hz stimulus. Panel C and D are Bode plots for Gain and Phase respectively. Other stimulus conditions fitted equally well. Note that responses with Gains < 0.25 have been removed, since the phases could not reliably be determined. Note that at low frequencies the model matches the stimulus slightly better than the mice.

5.2.8 Model

The model was implemented in Matlab (The MathWorks, Natick, MA) and calculations were performed via matrix multiplication. Details are given in the Supplementary Material.

5.2.9 Data Analysis

Measured eye responses were analyzed offline (Matlab; The MathWorks, Natick, MA). Position signals were transformed into velocity signals by a Savitski-Golay differentiating filter (cut-off frequency 50 Hz with a 3° polynomial) and were then smoothed with a median Gaussian filter (width 50ms). Nystagmus fast phases and saccades were removed with a velocity threshold of 150°/s and with an FIR Butterworth low pass filter optimized to the stimulus frequency (cutoff at 3x stimulus frequency). There were two primary outcome measures in this study: gain and phase.

Gain and phase was extracted from the sinusoidal data by fitting a sinusoid and then using the gain and phase of the fit. The fit was done using a hierarchical Bayesian analysis using OpenBugs (Version 3.2.3, http://www.openbugs.net). The precise details of the model used, as well as the parameters supplied to the OpenBugs algorithm, and a full presentation of the results of the fit are all provided in the Supplementary Material. In brief, the data for each trial for each mouse was assumed to be the result of a specific gain and phase specific to that trial, generated according to a distribution of gains and phases that were specific to the mouse. This distribution was, itself, generated according to hyper-parameters that characterize the population of mice. In addition, the noise in each trial was the result of a noise distribution characteristic of the mouse, which was generated according to hyper-parameters that characterized the population. Because our data was messy -- some mice had far more noise than others and some mice provided much more stable recording of eye movements than others -- the Bayesian approach allowed to incorporate all of the data in a robust manner, discounting the noisy or incomplete data when making estimates of the population parameters. Ultimately, we report the mean and confidence intervals for the gain and phase of the population from which each individual mouse's behavior was drawn. This is essentially equivalent to reporting the population mean and confidence intervals across mice in a mixed-model regression, without the sensitivity to assumptions to which mixed-model regressions are susceptible. In order to quantify the similarity between model response and experimental data the response of the model was compared to the mean and standard deviation of the mouse population response and expressed as a z-score (the number of standard deviations from the mean).

For the non-periodic data, gain and phase information were obtained by fitting two sine waves to the stimuli and the data in custom-made Matlab curve fitting routines.

For all experiments, the fits of the sine waves to the eye movement data provided the amplitude and phase of the eye movements. The gain was calculated as the ratio of the amplitude of eye movement compared to the amplitude of the stimulus, phase was calculated by subtracting the phase of the stimulus from the movement. Thus, a positive phase value indicates a lagging eye position signal.

5.3 Results

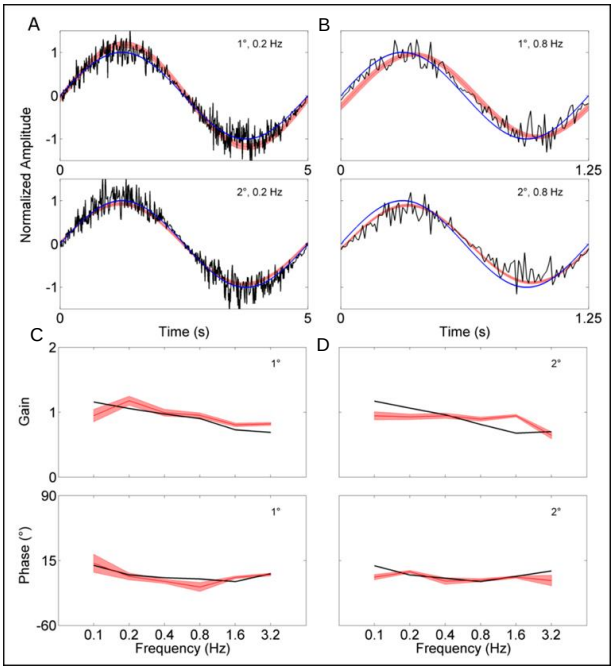

Figure 5. Summary of vVOR data and simulation

The upper row gives results for 1° stimuli, the lower row for 2° stimuli. Panel A gives a 0.2Hz stimulus (black), with the simulated response (blue) and the mean measured responses (red) with confidence limits. Panel B does the same for a 0.8 Hz stimulus. Panel C and D are Bode plots for Gain and Phase respectively. Other stimulus conditions fitted equally well.

5.3.1 Responses to sinusoidal stimulation

The behavioral data that we present are in agreement with the values that have been published earlier for the C57BL/6 mouse strain (van Alphen *et al.*, 2010; Faulstich *et al.*, 2004; Stahl *et al.*, 2000). The VOR in the dark responded to high frequency stimulation, and the OKR was mainly active in response to low velocity stimuli (van Alphen *et al.*, 2001). The vVOR was more or less perfect over the whole stimulus range, while suppression in the sVOR paradigm mainly happened at low frequency/velocity conditions.

In Fig 3 we show a comparison of experimental and simulated VOR. We see that there is a good match between simulation and average experimental response over the whole stimulus range. First, there is a high gain at high frequencies and lower gain at low frequencies is clearly observable. Furthermore, we see a phase lead at low frequencies which diminishes with increasing stimulus frequency.

Fig 4 follows the same format as Fig 3, but compares simulation to experimental results for the OKR response. The simulation nicely predicts the main features of the OKR response. The gain decreases and the phase lag increases with increasing stimulus velocity.

Figure 5 shows how well simulations predict experimental data for combined visual and vestibular stimulation (vVOR). In both the simulation and experimental data, we observe high gain and almost no phase lead or lag between response and the stimulus. These results show that VOR and

OKR have complementary results, which allows the combined system to produce excellent compensation of the retinal slip.

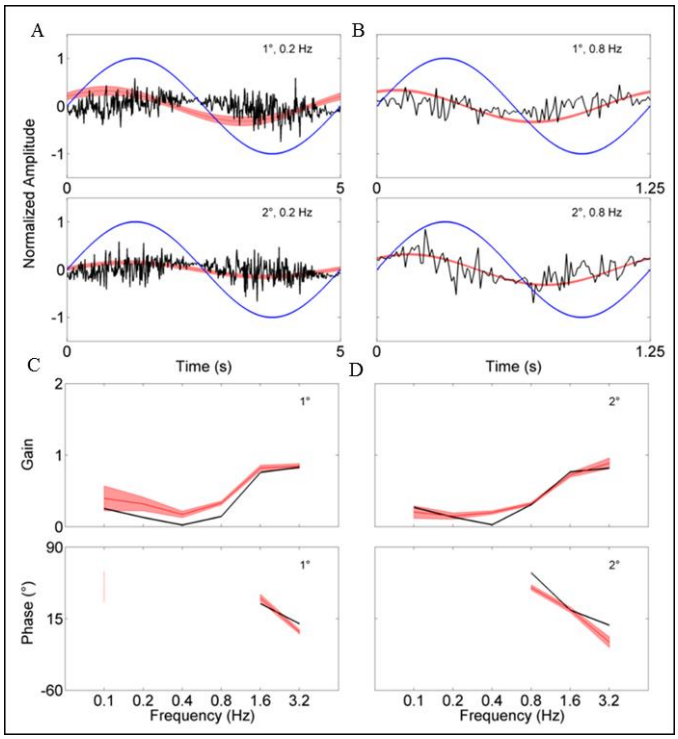

Figure 6. Summary of sVOR data and simulation.

This figure follows the format of Fig 3. Note that responses with Gains < 0.25 have been removed, since the phases could not reliably be determined.

Fig 6 shows how the model fits experimental data generated during sVOR – suppression of the VOR response with visual input. The response in high frequencies looks very similar to that in VOR because OKR is not responsive in high frequencies (see Fig. 3 and 4), and hence cannot suppress vestibular triggered response. We see that effect in both simulation and experiment. At low frequencies, there is a very small response, because VOR has low gain and is suppressed by OKR. The model reproduces all of these results.

In order to examine the overall quality of fit in each of the four experimental conditions above, we calculated the Z-scores of the overall fitting errors. These are shown in Fig 7. Note how the overall fit quality is good ("cool" colors in the heat map), with some poorer fits in the low frequency/high amplitude range of the sVOR condition.

5.3.2 Sum of Sines

When the OKR responds to SoS stimuli, we observed relative gain suppression of the lower frequency in the SoS stimulus, irrespective of the absolute frequency. Conversely in SVOR and VOR, results showed gain enhancement in the lower frequency component and an overall decrease in phase lead. VVOR results showed a trend for overall gain suppressions and delay decrease. For more details see (Sibindi *et al*. in press).

When applying identical stimuli to the model, the main pattern of effects is reproduced. Thus, we find qualitatively similar changes in both gain and phase of the constituting frequencies (see Fig 8).

5.3.3 VOR Adaptation

Perhaps counterintuitively, VOR adaptation occurs as a result of changes in the OKR's model of VOR. Adaptation modifies the OKR's prediction of post-VOR slip. Thus, adaptation in our model involved allowing the parameter ζ to vary in response to retinal slip as reported by the afferents using gradient descent. As derived in the supplementary material, the gradient is in the direction that decorrelates head acceleration and retinal slip. The minimum error had a broad basin of attraction. Thus, regardless of what the starting value of ζ was, it always converged to the same value of -0.6, if the stimulation frequency was kept constant. The value to which ζ converged depended on stimulus frequency but not amplitude. Nevertheless, there was a broad range of frequencies for which ζ was relatively stable.

The adaptation protocol reduced the gain of the VOR in mice to around 50% of its original value within 1 hour, comparable to that which has been previously described in literature (Schonewille *et al*., 2011). When presented with an identical stimulation protocol, the model was able to produce adaptation dynamics that match the experimentally derived data (Fig 10).

5.3.4 Effects of lesions

In the model, we simulated a lesion of the flocculus and a lesion of the NPH. The way of how this is done in the model depends on the role that is assigned to either structure (see Introduction). If one considers the NPH to be part of the controller (Green *et al*., 2007), a lesion of the NPH equals removing the inputs of the two outer hexagonal Forward Model boxes of Fig 1. A lesion of the flocculus is than equal to setting the values of all Forward Model boxes to a constant value of 0.

Alternatively, if the NPH is the oculomotor integrator (Cannon and Robinson, 1987), an NPH lesion equals setting the output of (outer, hexagonal [Fig 1]) integration boxes to 0. A floccular lesion in that respect only affects the two inner FM boxes of Fig 1 (“post-VOR slip” and “uncompensated slip”).

Since we did not want to make an a priori choice between both options, we performed both lesion types.

5.3.4.1 NPH lesions

Both types of lesion of the NPH resulted in exactly the same result. This is not surprising, since

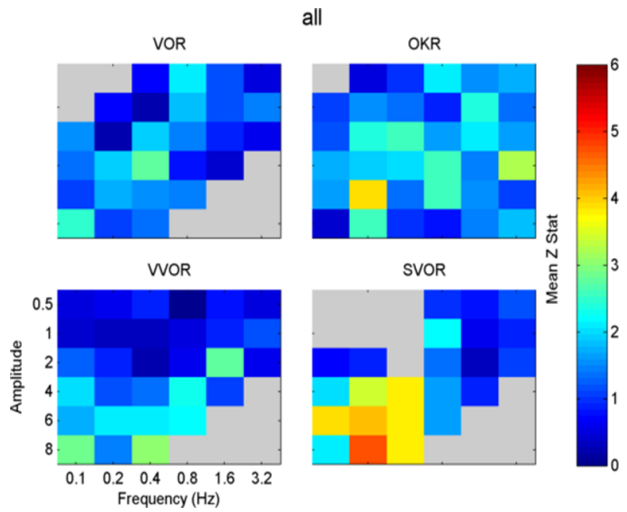

Figure 7. Summary of the degree to which the model matches the behavioral data across all amplitudes, frequencies and conditions tested.

The goodness of fit is summarized as a z-score representing the number standard deviations away from the mean population of mice response. In cases in which the gain was < 0.25 the results are omitted due to unreliable phase and appear as grey boxes in the figure. Cooler colors represent a closer match of model to data and this is the case in almost all tested conditions. One exception is the high amplitude low frequency sVOR in which the match is poorer but still within 2.5 standard deviations

setting the input to the integration step to 0, or setting the output to 0 lead to exactly the same result. As expected (see discussion) the lesion had an effect on the drift of the eyes back to the centre in the dark, decreasing the time constant from 2.56 to 0.29.

5.3.4.2 Flocculus lesions

Figure 9 shows the result of a flocculus lesion on the CEM that incorporated all Forward Model boxes. The OKR is virtually gone. Meanwhile the VOR gain is increased, and the VOR phases are substantially lagging. The gain responses were identical for the lesion of only the “post-VOR slip” and “uncompensated slip” boxes, but in the latter case the VOR phase was unaltered, compared to the unlesioned situation.

Following a model floccular lesion, the VOR did not adapt, regardless of the type of flocculus lesion that was applied (see above). However, partial lesions of the floccular processes (that have no real life equivalent) revealed that lesioning the “post-VOR slip” was fully responsible for the observed performance effects, and lack of adaptation (Fig 10). On the other hand a lesion of the

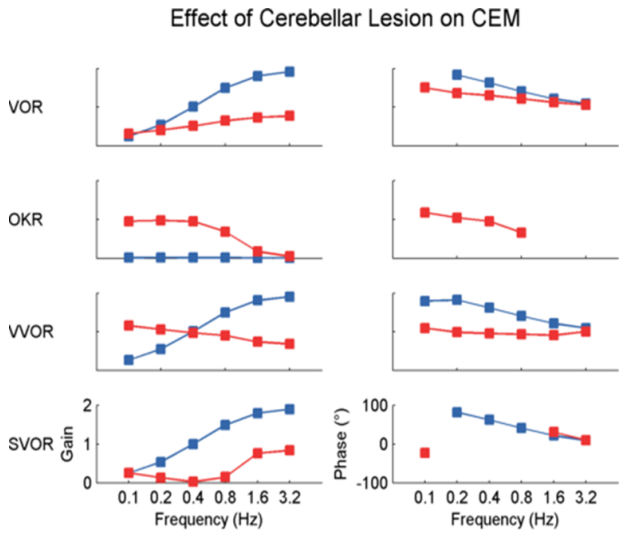

Figure 8. Bode plots summarizing the effect of lesioning all four forward models on the model response.

The intact model response (red) and lesioned response (blue) show clear differences; an increase in VOR gain and phase and an almost complete loss of the OKR response. Stimulation that combines the two reflexes (sVOR and vVOR) also display the effects on the two primary reflexes.

"uncompensated slip" resulted in mild performance effects and slowing but not completely absent adaptation.

5.4 Discussion

In Frens and Donchin, 2009, we proposed that CEM are generated by a SPFC framework where specific functional roles can be ascribed to specific nuclei in the CEM circuitry. Here, we implement the SPFC framework in a detailed computational model which can, with a single set of parameters, mimic the behaviour of OKR and VOR. With the same set of parameters, the model also reproduces vVOR, sVOR and non-periodic SoS-stimuli. Furthermore, it successfully predicts the effects of lesions, and it is capable of showing adaptive behaviour, similar to VOR learning (Schonewille *et al*., 2011).

The strength of this model is that it has relatively few critical parameters (see table 1, supplement), and that the critical parameters can be straightforwardly experimentally derived. This is an advantage over other SPFC-like models that address other motor systems (Shadmehr and Krakauer, 2008).

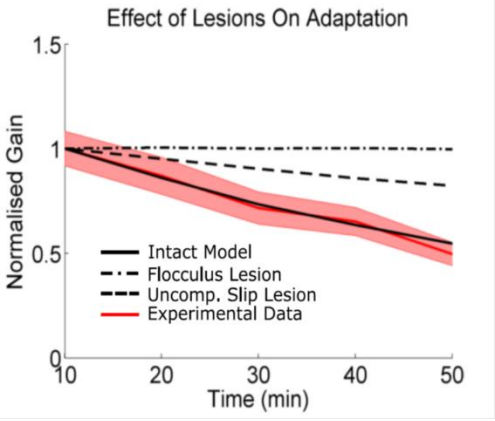

Figure 9. Comparison of gain down VOR adaptation in experimental data to the model with different lesions.

The model is able to reproduce the adaptation seen in experimental mice as well as the lack of adaptation as seen experimentally with a lesion of the flocculus. Interestingly a lesion of only the forward model of uncompensated slip dramatically slows adaptation but does not prevent it. Shaded regions represent SEM.

Key to the model are two distinct circuits for VOR and OKR. As described in the introduction, the VOR loop is relatively simple, and mainly consists of an integration step. In traditional models, the OKR responds to actual retinal slip. However, due to the relatively long delay of the visual processing, the OKR response would then typically respond late. OKR state estimation in our model resolves this by predicting retinal slip. Both the VOR and the OKR loop contribute to this internal estimate of (uncompensated) retinal slip. This combined contribution is necessary, since the OKR assumes that the vestibular system will only partially resolve the retinal slip. Finally, our model implements adaptation as a recalibration of the OKR estimate of VOR slip compensation. This helps explain why floccular lesions have a stronger direct effect on OKR but also disrupt VOR adaptation.

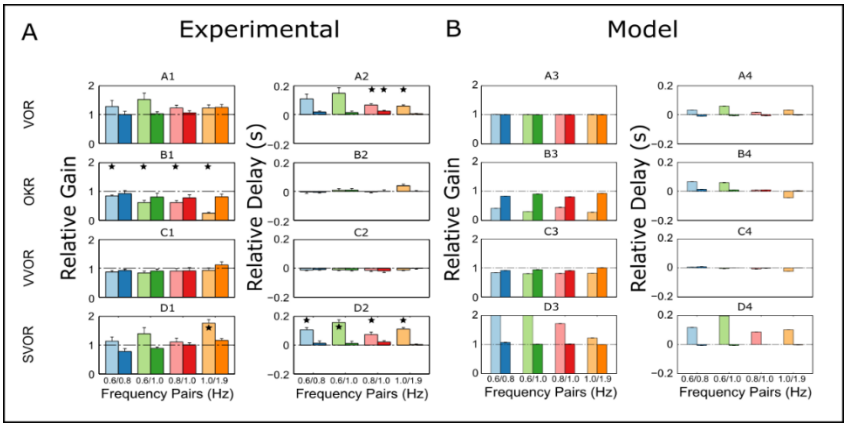

Figure 10. Comparison of the relative gains and delays in response to SoS stimuli in mice (A) and the model (B)

Experimental data is reproduced from Sibindi et al (2016, in press), stars above the bars indicate responses that were significantly different from that predicted by a linear system. Whilst the model does not reproduce exactly the size of the nonlinearities the pattern (effects on relative gain in OKR and sVOR and relative delay in VOR and vVOR) is effectively reproduced.

5.4.1 The non-linear response to SoS stimulation

In addition to its capability to respond to sinusoidal stimulation under several conditions, the model also responded accurately to SoS-stimuli, similar to those previously used by Sibindi *et al*. 2016, in press. Strikingly, two non-linearities in the results of Sibindi were reproduced: The first one is that when confronted with a stimulus that consists of two non-harmonic optokinetic sinusoids, the amplitude of the lower frequency is suppressed, independent of the absolute value of the constituent frequencies. This then also results in changes in the amplitudes in vVOR and sVOR conditions. The second one is that the lag of the response to especially the lower frequency is

larger, resulting in a delayed overall response. This can be seen for both VOR, OKR and its combinations.

The model has one non-linearity specifically built in: the saturation of the visual motion sensitive neurons in the retina (see Eq 8 in the Supplementary Material). Explicitly removing this saturation abandoned the gain decrease and delay increase of the OKR and vVOR, but left the increased delays in the VOR and sVOR unaffected (Fig 11).

This supports the conclusion of Sibindi *et al* that such increased delays may be a result of the circuit properties, e.g. when the forward models fail to predict upcoming retinal slip. The changes in gain, however, can simply be understood from the non-linear properties of the retina.

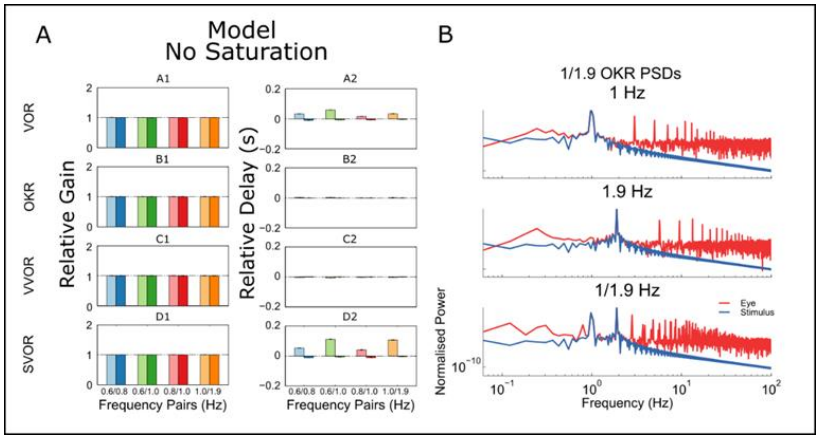

Figure 11. The effect of removing the retinal saturation on the model in response to SoS stimuli in terms of relative gains and phases (A) and the power spectra of the response in an example of single sine and SoS stimuli (B).

It can be seen from for the relative gains that the removal of retinal saturation removes the nonlinearities expressed in the relative gain of components of sVOR and OKR. However, the nonlinearities observed in the relative delays are not affected and therefore likely represent a nonlinear interaction between the OKR and VOR reflexes. Saturation of retinal input causes the appearance of power at frequencies in the eye movement response (red) other than those in the stimulus (blue), in the original data these were too small to detect but the model allowed us to interrogate this further and determine conclusively the source of the nonlinearity.

5.4.2 Lesioning the flocculus: effects on OKR and VOR

We mimicked lesioning the flocculus by removing the output of the "Post-VOR slip" and "Uncompensated slip" forward models, thus effectively removing the capability of the system to predict upcoming retinal slip. This virtually abolished the optokinetic response, whereas the VOR substantially increased. Both of these findings are compatible with existing literature: lesions of the flocculus dramatically decrease the OKR gain. As lurcher-mice, a mutant strain that lacks Purkinje cells, have substantially lower OKR gains than their wild type littermates (van Alphen *et al*., 2002). Like in our model after removal of the floccular output, the VOR-gain of these animals however is increased, a finding

that never has been fully explained. From our model we can understand this in the following terms: The OKR generally acts to suppress the VOR and loss of this suppression with a flocculus lesion leads to increased VOR gains.

5.4.3 Lesioning the NPH: effects on drift

This model provides a potential resolution to a debate about the role of the NPH in eye movement generation. In Robinson's inverse-model framework, the NPH is thought to act as the neural integrator for horizontal eye position. Such an integrator is necessary to provide the abducens nucleus with both velocity and position commands that are needed to overcome the low-pass filtering properties of the plant (Robinson, 1981). This view has been widely adopted by researchers in the oculomotor system. A critical finding supporting this view is from Cannon and Robinson (1987) showing that lesions of the NPH cause the eye to drift towards the center of the oculomotor range. This is compatible with the loss of an integrator that opposes the elastic restoring forces of the plant. However, more recently Green *et al*., (2007) showed that the burst tonic neurons of the NPH have activity that is nearly identical to that of the motor neurons in the abducens nucleus. Furthermore these neurons have direct projections to the flocculus (Belknap and McCrea, 1988; Blazquez *et al*., 2003; Langer *et al*., 1985; McCrea and Baker, 1985). Therefore, they propose that the NPH provides efference copy input to a cerebellar forward model (Ghasia *et al*., 2008; Green *et al*., 2007). This view was also incorporated in our SPFC (Frens and Donchin, 2009). However, when we lesioned the NPH projection in our simulation (by removing efferent copy to the forward model or by removing its output), we found a smaller drifting time constant. Hence, a lesion of the efference copy projection can manifest behaviorally as the lesion of an integrator.

5.4.4 VOR Adaptation

Within this framework, VOR adaptation can be achieved by adaptively changing the estimate of this vestibular contribution to the total CEM output. Determining the proportionality constant robustly led to the same value regardless of stimulus amplitude, and for a wide range of frequencies. When challenged with an adaptation stimulus (see Methods) the model gradually changed its gain. Setting the adaptation parameter to a value of 0.009 led to an adaptation speed

that is very similar to what we experimentally found in mice under identical experimental conditions.

5S Supplementary Material – An optimal control model of the compensatory eye movement system

5S.1 Overview

This chapter describes the details of the model of the CEM described in the main text. The description provides all of the equations used in sufficient detail for the model to be implemented, although the actual Matlab code is available on our website (spfc.neuro.nl). The model was implemented in Matlab R2012b (Mathworks, 2012). The time step for the simulation used was 1 ms.

This chapter is divided into sections that describe the implementation of the plant and the control system. In the section on the plant, we describe both the effector and input implementations. The effector implementation is a model of how firing in the oculomotor nuclei affects muscle activation, and how that drives eye movement. The inputs we model are the vestibular and the retinal inputs to the system. The description of the control system is divided into three parts: the actual state dynamics; the system's estimate of state; and the transformation of state estimate into motor command.

5S.2 The plant

In this section we describe the dynamics of eye movement as a function of the firing rate of neurons in motor nuclei (OMN/AB) that project to eye muscles. Output of the OMN/AB innervates the horizontal rectus muscles, which are responsible for horizontal eye movements. These nuclei are reciprocally activated and project to muscles that move the eyes in opposite directions. Hence eye velocity depends on the difference between OMN and AB activities. The transfer function of these nuclei for monkey has been described using the formula (207):

$$T_p \dot{E} + E = Cu \qquad (1)$$

(Where E is eye position, u is motor command from the OMN/AB, and C and T_p are the gain and time constants, respectively). The motor commands from the two nuclei were not separately modelled, but rather their activity was represented in a combined manner as the sum of two oppositely signed command signals.

Eq. (1) describes a leaky integrator with leakage time (in s). In monkey, T_p has been estimated at 0.24s and in rabbits it can be estimated from the work of Stahl & Simpson (1995) and more recently for mice in Stahl et al., (2015) to be 0.5s . We ran our simulation both with $T_p = 0.24\,\mathrm{s}$ and with $T_p = 0.5\,\mathrm{s}$, and saw no difference in the results. For this paper, we present results using $T_p = 0.5\mathrm{s}$ (see Table 1). For the purpose of the model, we absorbed the constant C into the definition of u, so that our motor command was specified in °/s rather than in units of firing rate:

$$\dot{E} = u - \frac{1}{T_p} E \qquad (2)$$

5S.3 Sensory Signals

Compensatory eye movements are driven by two different sensory signals – vestibular and retinal. In this section we describe the biological processes behind these sensory signals and the numerical models that can be used to describe these processes.

5S.4 Vestibular input

Vestibular input is created by the semicircular canals in the inner ear. We transformed the head velocity to sensory signal in three steps: linear filtering, velocity-sensitive transformation, and delay. At high frequencies, canals sense head rotation velocity with high accuracy. However due to the physical properties of the sensor, the accuracy is not good at low frequencies (Robinson, 1981). Thus, the semicircular canals can be best described as a high pass filter that acts on head velocity:

$$\dot{V}^{(1)} = -\frac{1}{T_v} V^{(1)} + \dot{H} \qquad (3)$$

Where $V^{(1)}$ is the first stage of the neural signal generated by the velocity sensitive vestibular afferents (as opposed to V, the internal representation of head velocity) that are driven by the actual rotational head velocity, $\dot{H}$, and T_V is the filter constant that defines the effective sensitivity range of the afferents. The value of T_V differs between different species. In mice this constant was measured in (Yang and Hullar, 2007).While they fit their data using a fairly complex transfer function (here reproduced in its original Laplace-domain notation):

$$0.09\frac{3.0s}{(3.0s+1)(0.007s+1)}(0.2s+1)^{0.03} \qquad (4)$$

a first order approximation of the formula, and neglecting the leading constant, gives us Eq. (3). This approximation is justified by Fig. **Error! Reference source not found.**, which shows that over the relevant frequency range, the two functions are nearly identical, with $T_v = 3\text{sec}$ for regular afferents of the horizontal semicircular canal that project to the vestibular nucleus. Van Alphen, Stahl and De Zeeuw (2001) found that a lower time constant is needed to explain VOR experimental data. It is possible that additional filtering in the input synapses of the vestibular nucleus explains the difference between the constant measured in the afferents and that seen behaviorally. However, we found that our behavioral data was best matched by a constant very close to that found by Yang and Hullar (2007) $T_v = 4\text{sec}$.

Subsequently, we introduced a delay and added noise:

$$\dot{V}_k^+ = \dot{V}_{k-\delta_v}^{(1)} + n_{V,k} \qquad (5)$$

The vestibular delay ($\delta_V = 2$ ms) represents the physical response time of the semi-circular canal and the neuronal transmission delay (Sohmer *et al.*, 1999). The noise ($n_{V,k}$) has a standard deviation proportional to the size of the vestibular signal (with constant of proportionality a_V, with the tilde, $\sim$, meaning "distributes as" and $N(\mu,\sigma^2)$ is the normal distribution with mean μ and variance σ^2.):

$$n_{V,k} \sim N\left(0, a_V^2 \dot{V}_k^2\right) \qquad (6)$$

Since vestibular inputs depend only on head movement and head movement is determined by the experiment, the behaviour of the system has no effect on vestibular inputs. Thus, we calculated these signals offline before running the simulations and introduced them directly as input.

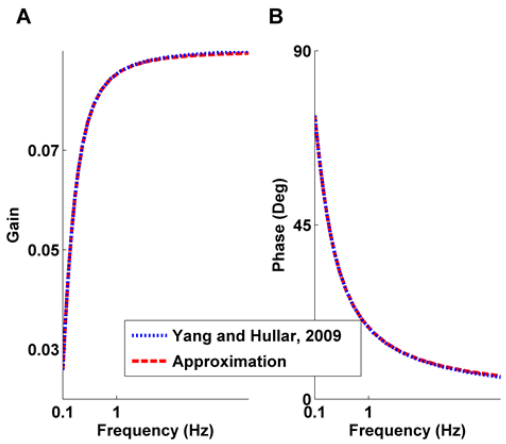

Fig. 1: (A) Amplitude and **(B)** phase response of the vestibular filter as modeled by (217; blue dashes) and the first order linear approximation (red larger dashes) used in our model in the frequency ranges we tested. The two are nearly indistinguishable.

5S.5 Retinal Input

Visual information is provided by motion sensitive neurons in the retina (Yoshida *et al*., 2001). Those neurons sense local velocity of the image on the retina (often called retinal slip). In our experiments, the entire retina experiences the same retinal slip, and it is equal to:

$$R_k = \dot{H}_k + \dot{E}_k - \dot{T}_k \qquad (7)$$

Where R is retinal slip velocity, in °/s, $\dot{T}$ the velocity of the visual surroundings in °/s, and $\dot{E}$ is the velocity of the eye relative to the head (generated as described above in Eq. (2).

The retinal motion sensitive neurons are linear in a limited range. In rabbits, sensitivity peaks at about 0.6 °/s (Oyster *et al*., 1972), with neuron firing rates increasing through this range, but then dropping off for higher velocities. At 10 °/s the neurons are unresponsive. Neurons in the AOS (the retinal target driving OKR) have shown similar properties (Soodak and Simpson, 1988). Currently available data does not give the precise saturation point for the motion processing system of the mouse. In order to fit our data, our model assumes saturation of $R_{\max} = 0.65$ deg/sec and a piece-wise linear response function, representing a population code of neurons that individually drop off at values between 0 and R_{max}:

$$h(R_k) = \begin{cases} R_k & -R_{\max} \le R_k \le R_{\max} \\ R_{\max} & R_k \ge R_{\max} \\ -R_{\max} & R_k \le -R_{\max} \end{cases} \qquad (8)$$

The processing of visual signals adds substantial delay to the retinal feedback (Collewijn, 1969). Our model uses the value of $\delta_R = 70$ ms proposed for the delay in mice (van Alphen *et al*., 2001):

$$R_k^+ = h\left(R_{k-\delta_R}\right) + n_{R,k} \tag{9}$$

With R_k^+ the current internal representation of retinal slip, and $n_{R,k}$ the retinal noise, which has standard deviation proportional to the retinal activation (with a constant of proportionality a_R^2):

$$n_{R,k} \sim N\left(0, a_R^2 R_k^2\right) \tag{10}$$

5S.6 Full system dynamics

The above descriptions of the oculomotor plant and the retinal and vestibular input are combined to make a linear state equation for the plant. Thus, we use a standard linear systems formulation (Frens and Donchin, 2009) with the state of the system at time k, x_k, undergoing a particular dynamics specified by the matrix A. In addition, the state is influenced by three factors: the command signal, u_k, affects the state through a matrix, B, that specifies how each part of the command signal influences each element of the state; the external input, z_k, represents the influence of the external world on the state; also, the state is influenced by noise, n_k. Finally, this state leads to sensory input (often called the observation), y_k, through a matrix, D. Altogether, this leads to what is called the system equations:

$$\begin{aligned} x_{k+1} &= Ax_k + Bu_k + z_k + n_k \\ y_k &= Dx_k \end{aligned} \tag{11}$$

These system equations are linear. Each piece of this equation is treated in detail in the paragraphs that follow.

The state at time step k is represented by the following vector:

$$x_k = \left[H_k \quad \dot{H}_k \quad V_k \quad E_{V,k} \quad \dot{E}_{V,k} \quad T_k \quad \dot{T}_k \quad E_{R,k} \quad \dot{E}_{R,k} \quad R_k \quad R_{k-1} \quad \cdots \quad R_{k-70} \quad V_{k-1} \quad V_{k-2}\right] \tag{12}$$

The state includes time-delayed versions of the retinal and vestibular sensory signals. R_k represents the retinal input being generated at this instant (based on the current eye velocity) and R_{k-1} through R_{k-70} represent increasingly delayed versions. The observation matrix, Eq. (20), is such that only the fully delayed retinal slip, R_{k-70}, is available to the state estimation. The vestibular input is not affected by the behaviour of the system, so it was generated offline according to Eq. (3) and delayed by 2 ms according to Eq. (5).

z_k is the external input and includes the change in the actual head velocity, vestibular sensory signal, and movement of the visual stimulus. These signals can all be generated offline before running the simulation. The vector can be written as:

$$z_k = \begin{bmatrix} 0 & \Delta\dot{H}_k & \Delta V_k & 0 & 0 & 0 & \Delta\dot{T}_k & 0 & 0 & 0 & 0 & 0 & \cdots & 0 & 0 & 0 & 0 \end{bmatrix}$$

(13)

n_k is the noise in the system. It affects eye velocity as well as vestibular and retinal input, so it can be written as (where $[\ ]^T$ indicates a transformed matrix):

$$n_k = \begin{bmatrix} 0 & 0 & n_V & 0 & n_u & 0 & 0 & 0 & n_u & n_R & 0 & 0 & \cdots & 0 & 0 & 0 & 0 \end{bmatrix}^T \quad (14)$$

In modelling the noise, we opted for model simplicity over realistic modelling of the noise. We followed the general idea in (Harris and Wolpert, 1998; Todorov, 2004) and of having the size of the noise be proportional to the signal. Vestibular noise and retinal noise have already been described in Eqs. (6) and (10) respectively. The standard deviation of the motor noise is similarly proportional to the motor command (with constant of proportionality a_u)

$$\dot{E}_{k+1} = u_k - \frac{1}{T_p} E_k + n_u$$
$$n_u \sim N\left(0, a_u^2 u_k^2\right) \quad (15)$$

We ran the model with different constants of proportionality for the noise (a_u , a_R , and a_V) up to 0.5 and did not see a change in the results. Given that we have no available data on amount of sensory or motor noise in the system we used values well in the middle of stable range, i.e:

$$a_u = a_R = a_V = 0.1 \tag{16}$$

A is the matrix describing the state dynamics and is written as

$$A = \begin{bmatrix}
1 & dt & 0 & 0 & 0 & 0 & 0 & 0 & 0 & 0 & 0 & 0 & \cdots & 0 & 0 & 0 & 0 \\
0 & 0 & 0 & 0 & 0 & 0 & 0 & 0 & 0 & 0 & 0 & 0 & \cdots & 0 & 0 & 0 & 0 \\
0 & 0 & 0 & 0 & 0 & 0 & 0 & 0 & 0 & 0 & 0 & 0 & \cdots & 0 & 0 & 0 & 0 \\
0 & 0 & 0 & 1 & dt & 0 & 0 & 0 & 0 & 0 & 0 & 0 & \cdots & 0 & 0 & 0 & 0 \\
0 & 0 & 0 & -1/T_P & 0 & 0 & 0 & 0 & 0 & 0 & 0 & 0 & \cdots & 0 & 0 & 0 & 0 \\
0 & 0 & 0 & 0 & 0 & 1 & dt & 0 & 0 & 0 & 0 & 0 & \cdots & 0 & 0 & 0 & 0 \\
0 & 0 & 0 & 0 & 0 & 0 & 0 & 0 & 0 & 0 & 0 & 0 & \cdots & 0 & 0 & 0 & 0 \\
0 & 0 & 0 & 0 & 0 & 0 & 0 & 1 & dt & 0 & 0 & 0 & \cdots & 0 & 0 & 0 & 0 \\
0 & 0 & 0 & 0 & 0 & 0 & 0 & -1/T_P & 0 & 0 & 0 & 0 & \cdots & 0 & 0 & 0 & 0 \\
0 & 1 & 0 & 0 & 1 & 0 & 1 & 0 & 1 & 0 & 0 & 0 & \cdots & 0 & 0 & 0 & 0 \\
0 & 0 & 0 & 0 & 0 & 0 & 0 & 0 & 0 & 1 & 0 & 0 & \cdots & 0 & 0 & 0 & 0 \\
0 & 0 & 0 & 0 & 0 & 0 & 0 & 0 & 0 & 0 & 1 & 0 & \cdots & 0 & 0 & 0 & 0 \\
\vdots & \vdots & \vdots & \vdots & \vdots & \vdots & \vdots & \vdots & \vdots & \vdots & \vdots & \vdots & \ddots & \vdots & \vdots & \vdots & \vdots \\
0 & 0 & 0 & 0 & 0 & 0 & 0 & 0 & 0 & 0 & 0 & 0 & \cdots & 0 & 0 & 0 & 0 \\
0 & 0 & 0 & 0 & 0 & 0 & 0 & 0 & 0 & 0 & 0 & 0 & \cdots & 1 & 0 & 0 & 0 \\
0 & 0 & 1 & 0 & 0 & 0 & 0 & 0 & 0 & 0 & 0 & 0 & \cdots & 0 & 0 & 0 & 0 \\
0 & 0 & 0 & 0 & 0 & 0 & 0 & 0 & 0 & 0 & 0 & 0 & & 0 & 0 & 1 & 0
\end{bmatrix} \tag{17}$$

Rows 2, 3 and 7 (velocity of the surroundings and of the head and the vestibular signal) are all just equal to 0. This reflects the fact that these variables are controlled by the inputs and not part of the dynamics of the system, in our model. Row 4 (eye position) simply includes the change in eye position caused by eye velocity (column 5), which needs to be scaled by $d = 0.001$ because eye velocity is in units of °/s and the time step is 1 millisecond. It is worth noting that row 8 also describes eye dynamics (just like row 4). These representations are separated because in the internal controller they reflect different estimates. The simulation code keeps them in register by replacing them with the sum of the two values on each time step. Row 5 (and row 9) describe the tendency of the eye to drift back to centre (the position dependent part of Eq. 2. Row 10 says that current retinal slip is equal to head velocity plus eye velocity minus stimulus velocity (Eq. 7). The

rest of the dynamics matrix (rows 13 through 78, not shown) simply shifts previous measured retinal input backwards in time

(eg. $R_k \to R_{k-1},\ R_{k-1} \to R_{k-2}$).

State transition is not, however, strictly linear. This non-linearity is represented by the function $h(Ax_k)$ in Eq. (11) so that,

$$h(Ax_{k+1}) = \begin{bmatrix} H_k & \dot{H}_k & V_k & E_{V,k} & \dot{E}_{V,k} & T_k & \dot{T}_k & E_{R,k} & \dot{E}_{R,k} & h(R_k) & R_k & R_{k-1} & \cdots & R_{k-69} & R_{k-70} & V_{k-1} & V_{k-2} \end{bmatrix} \quad (18)$$

Where $h(R)$ describes the saturation of the retinal sensory signal (Eq. 8). That is, every element of the state vector is preserved by h except the retinal slip which saturates. Non-linearity of the vestibular inputs does not affect linearity of the system, since it is handled in generation of the input.

Since the motor command, u_k, is a scalar, the control matrix B of Eq. (11) is a vector with the same size as the state. Because the command affects eye velocity directly, the only non-zero element of B is in the row representing eye velocity. Units are adjusted so that 1 unit of motor command (neural activation) causes an acceleration of 1 °/ms, so B is:

$$B = \begin{bmatrix} 0 & 0 & 0 & 0 & 1 & 0 & 0 & 0 & 0 & 0 & \cdots & 0 & 0 \\ 0 & 0 & 0 & 0 & 0 & 0 & 0 & 0 & 1 & 0 & \cdots & 0 & 0 \end{bmatrix} \quad (19)$$

The second equation in Eq. (11) describes the observation, which is the part of the state available to the controller. The observation vector, y_k, contains delayed retinal and vestibular inputs. Thus, it can be calculated linearly using the observation matrix D (which is simply a 2x82 matrix of zeros with ones at locations (1, 82) and (2, 80) for vestibular and retinal input respectively). The D matrix is applied to the retinal slip after saturation, and we also add in sensory noise at this stage.

$$y_k = Dh(x_k) + \eta = \begin{bmatrix} \dot{V}_{k-\delta_V} + \eta_V \\ h(R_{k-\delta_R}) + \eta_R \end{bmatrix}^T = \begin{bmatrix} \dot{V}^+_{k-\delta_V} \\ R^+_{k-\delta_R} \end{bmatrix}^T \quad (20)$$

5S.7 Control system

In this section we describe an optimal feedback controller for the compensatory eye movement system. This controller includes a forward model and a process of combining forward model prediction with sensory input, called state estimation. We will use the hat notation, $\hat{x}$, for estimates produced by the forward model and the tilde notation, $\tilde{x}$, for the combined state estimate.

The operation of the controller can be described globally with the following equations:

$$\begin{aligned} \hat{x}_{k+1} &= A'\tilde{x}_k + Bu_k \\ \tilde{x}_{k+1} &= \hat{x}_{k+1} + K\left(y_k - h\left(D'\hat{x}_{k+1}\right)\right) \\ u_{k+1} &= -L\tilde{x}_{k+1} \end{aligned} \qquad (21)$$

The first equation says that the forward model uses the previous state estimate and the previous motor command to generate a prediction of the next state. The second equation says that the estimate of the next state is generated by correcting this prediction for discrepancies between predicted and experienced retinal slip. The last equation says that motor command will be a linear function of the state. The tags on some symbols result from the fact that the controller's internal representation of state is different from the actual system state. Thus, A' is the internal representation of system dynamics and D' selects the appropriate sensory inputs from the internal system state.

5S.7.1 VOR control

Our model assumes that VOR and OKR involve separate neural processing. Thus, it will be clearest if the operation of each is described separately, and then the combined matrix equations will be easier to follow.

The architecture of the VOR is the same as the overall architecture of the system:

$$\begin{aligned} \hat{x}_{\mathrm{V},k+1} &= A'_{\mathrm{V}}\tilde{x}_{\mathrm{V},k} + B_{\mathrm{V}}u_{\mathrm{V},k} \\ \tilde{x}_{\mathrm{V},k+1} &= \hat{x}_{\mathrm{V},k+1} + K_{\mathrm{V}}\left(\dot{V}_k^{+} - D'_{\mathrm{V}}\hat{x}_{k+1}\right) \\ u_{\mathrm{V},k+1} &= -L_{\mathrm{V}}\tilde{x}_{\mathrm{V},k+1} \end{aligned} \qquad (22)$$

In the case of VOR, since we have no access to the actual head velocity, we use the vestibular signal as an approximation of the head velocity. Thus, the state needs only have five elements:

$$\hat{x}_{V,k} = \begin{bmatrix} \hat{H}_k & \hat{\dot{H}}_k & \hat{\dot{V}}_k & \hat{E}_{V,k} & \hat{\dot{E}}_{V,k} \end{bmatrix} \tag{23}$$

The forward model is quite simple. The head velocity is not affected by either system dynamics or command (row 1 of Eq. 24 and the first 0 in Eq. 25). Eye movements have the usual plant dynamics (rows 4 and 5, which are taken from Eq. 2) and are affected directly by the motor command (the 1 in the fifth position of Eq. 25):

$$A'_V = \begin{bmatrix} 1 & dt & 0 & 0 & 0 \\ 0 & 1 & 0 & 0 & 0 \\ 0 & 1 & 0 & 0 & 0 \\ 0 & 0 & 0 & 1 & dt \\ 0 & 0 & 0 & -1/T_P & 0 \end{bmatrix} \tag{24}$$

$$B_V = \begin{bmatrix} 0 & 0 & 0 & 0 & 1 \end{bmatrix} \tag{25}$$

The observation matrix returns the estimated head velocity (which is what we expect the vestibular input to be):

$$D'_V = \begin{bmatrix} 0 & 1 & 0 & 0 & 0 \end{bmatrix} \tag{26}$$

which is compared to the actual vestibular input, $\dot{V}_k$. Because a flocullar lesion does not eliminate VOR performance, we set $K_V = \begin{bmatrix} 0 & 1 & 1 & 0 & 0 \end{bmatrix}$. That is, the sensory feedback completely replaces the forward model in our knowledge of head velocity. The role of the forward model in this system is actually to integrate eye velocity into eye position.

Finally, the actual motor command is generated (again, see below for how these values are determined) using the equation $u_{V,k+1} = -L_V \tilde{x}_V$ with $L_V = \begin{bmatrix} 0 & 0.972 & 0 & -1.7669 & 0.0002 \end{bmatrix}$ so that, ultimately:

$$u_{V,k+1} = -0.97\tilde{\dot{H}}_{V,k} + 1.77\tilde{E}_{V,k} - 0.0002\tilde{\dot{E}}_{V,k} \tag{27}$$

5S.7.2 OKR control

The job of the second part of the control loop is to estimate uncompensated retinal slip and compensate for it. Uncompensated visual slip arises from three sources: changes in the velocity of the visual stimulus, noises in the system, and head movements not compensated by the VOR. Importantly, the system cannot distinguish changes in the velocity of the visual stimulus from noises in the system. We use the symbol $\tilde{R}_k^*$ for the system's estimate of all three of these quantities together: the retinal slip uncorrected by VOR. We also call this the post-VOR slip, and it represents how much the visual environment would be moving in the absence of OKR.

The OKR's prediction of uncompensated retinal slip is thus the difference of two quantities: the post-VOR slip and the estimate of how much the OKR is moving the eye, $\hat{\dot{E}}_{R,k}$:

$$\hat{R}_k = \hat{\dot{E}}_{R,k} - \tilde{R}_k^* \qquad (28)$$

The OKR system assumes that some amount of head movement will be compensated for by the VOR. Its estimate of uncompensated visual input generated by sensed head velocity is proportional to the actual sensed head velocity. Our forward model estimate of post-VOR retinal slip will be different from our previous estimate because it is updated by a factor proportional to head acceleration:

$$\hat{R}_{k+1}^* = \tilde{R}_k^* + \zeta\left(\hat{\dot{H}}_k - \hat{\dot{H}}_{k-1}\right) \qquad (29)$$

(where ζ is the constant of proportionality and is discussed in the section on VOR adaptation below). We then use a Kalman filter to incorporate sensory prediction error and produce a final estimate of post-VOR retinal slip:

$$\tilde{R}_{k+1}^* = \hat{R}_{k+1}^* + K_{T,R_k}\left(R_k - \tilde{R}_{k+1}\right) \qquad (30)$$

K_{T,R_k} represents the appropriate term in the Kalman gain matrix (specified fully below). Our data was best fit by using $\zeta = -0.6$ and $K_{T,R_k} = 0.05$ which means that that OKR has a tendency to overcompensate for head rotation and that it estimates that 5% of unexpected retinal slip represents

real movement of the visual surroundings. Note that Eq. (30) uses R_k and $\tilde{R}_k$ which are the currently available retinal slip and its estimate while Eq. (28) used $\tilde{R}_k^*$ which is the estimate of the retinal slip happening right now. This estimate will be delayed for 70 ms before it becomes available as $\hat{R}_k$.

With this understanding in place, we can describe the OKR control system. It has the same overall architecture as the full system:

$$\begin{aligned}\hat{x}_{\mathrm{R},k+1} &= A_{\mathrm{R}}\tilde{x}_{\mathrm{R},k} + B_{\mathrm{R}}u_{\mathrm{R},k}\\ \tilde{x}_{\mathrm{R},k+1} &= \hat{x}_{\mathrm{R},k+1} + K_{\mathrm{R}}\left(R^{+}_{k-\delta_R+1} - h\left(D_{\mathrm{R}}\hat{x}_{\mathrm{R},k+1}\right)\right)\\ u_{\mathrm{R},k+1} &= -L_{\mathrm{R}}\tilde{x}_{\mathrm{R},k+1}\end{aligned} \tag{31}$$

With function h representing the saturation of the retinal input (Eq. 8). The state vector includes everything needed to calculate retinal slip, movement of the visual world, and head acceleration:

$$\hat{x}_{R,k} = \begin{bmatrix}\hat{H}_k & \hat{\dot{H}}_k & \hat{V}_k & \hat{T}_k & \hat{\dot{T}}_k & \hat{E}_{R,k} & \hat{\dot{E}}_{R,k} & \hat{R}^*_k & \hat{R}_k & \hat{R}_{k-1} & \cdots & \hat{R}_{k-69} & \hat{R}_{k-70}\end{bmatrix}$$

(32)

The forward dynamics matrix, A'_R, look like this:

$$A'_R = \begin{bmatrix}
1 & dt & 0 & 0 & 0 & 0 & 0 & 0 & 0 & 0 & \cdots & 0 & 0\\
0 & 1 & 0 & 0 & 0 & 0 & 0 & 0 & 0 & 0 & \cdots & 0 & 0\\
0 & 1 & 0 & 0 & 0 & 0 & 0 & 0 & 0 & 0 & \cdots & 0 & 0\\
0 & 0 & 0 & 1 & dt & 0 & 0 & 0 & 0 & 0 & \cdots & 0 & 0\\
0 & \zeta & 0 & 0 & 0 & 0 & 0 & 0 & 0 & 0 & \cdots & 0 & 0\\
0 & 0 & 0 & 0 & 0 & 1 & dt & 0 & 0 & 0 & \cdots & 0 & 0\\
0 & 0 & 0 & 0 & 0 & -1/T_P & 0 & 0 & 0 & 0 & \cdots & 0 & 0\\
0 & \zeta & 0 & 0 & -1 & 0 & 0 & 1 & 0 & 0 & \cdots & 0 & 0\\
0 & 0 & 0 & 0 & 0 & 0 & 1 & 1 & 0 & 0 & \cdots & 0 & 0\\
0 & 0 & 0 & 0 & 0 & 0 & 0 & 0 & 1 & 0 & \cdots & 0 & 0\\
\vdots & \vdots & \vdots & \vdots & \vdots & \vdots & \vdots & \vdots & \vdots & \vdots & \ddots & \vdots & \vdots\\
0 & 0 & 0 & 0 & 0 & 0 & 0 & 0 & 0 & 0 & \cdots & 0 & 0\\
0 & 0 & 0 & 0 & 0 & 0 & 0 & 0 & 0 & 0 & \cdots & 1 & 0
\end{bmatrix} \tag{33}$$

These rows accomplish: calculation of post-VOR retinal slip (row 8, implementing Eq. 29, shifting of current vestibular input to previous vestibular input (rows 4-5), modelling of the eye plant (row 6-7, implementing Eq. 2), calculation of the uncompensated retinal slip (row 9, implementing Eq. 28. The rest of the A'_{R} matrix takes care of the delay of the estimated retinal slip.

The B_{R} matrix simply copies the motor command into the eye velocity vector, just as with the VOR system:

$$B_R = \begin{bmatrix} 0 & 0 & 0 & 0 & 0 & 0 & 1 & 0 & 0 & 0 & \cdots & 0 & 0 \end{bmatrix} \quad (34)$$

In calculating state estimation for the OKR system, we must take into account the non-linearity of the retinal processing before comparing the predicted retinal slip to the sensory input. We first use the matrix D_{R} to select only the uncompensated retinal slip, $\hat{R}_{k-70}$, from out of the state vector, as in Eq. (26) but with a larger state vector. Then, the uncompensated retinal slip is cut off with the saturation function of the retinal input, as specified in Eq. (8). This can be compared to the true retinal input R_k , providing unexpected retinal slip. Unexpected retinal slip updates the estimated state values of post-VOR retinal slip and uncompensated retinal slip. Our data was best fit by using:

$$K_R = \begin{bmatrix} 0 & 0 & 0 & 0 & 0 & 0 & 0 & 0 & 0.05 & 0.05 & \cdots & 0.05 & 0.05 \end{bmatrix} \quad (35)$$

Finally, the motor command is generated by using the equation $u_{R,k+1} = -L_R \tilde{x}_R$ just like in the case of VOR (again, see below for derivations), with $L_R = \begin{bmatrix} 0 & 0 & 0 & 0 & 0 & -1.767 & 0.0002 & 0.972 & 0 & 0 & \cdots & 0 & 0 \end{bmatrix}$ so that the motor command is:

$$u_{R,k+1} = -0.97\tilde{R}^*_{R,k} + 1.77\tilde{E}_{R,k} - 0.0002\tilde{\dot{E}}_{R,k} \quad (36)$$

5S.7.3 The combined controller: forward model

To produce a combined system, as described in Eqs. (21), in our calculations we simply combine the descriptions of the OKR and VOR systems above. The only state variable that overlaps in the two systems is the head velocity. However, this poses no difficulties.

$$\hat{x}_k = \left[\hat{H}_k \quad \hat{\dot{H}}_k \quad \hat{V}_k \quad \hat{E}_{V,k} \quad \hat{\dot{E}}_{V,k} \quad \hat{T}_k \quad \hat{\dot{T}}_k \quad \hat{E}_{R,k} \quad \hat{\dot{E}}_{R,k} \quad \hat{R}^*_k \quad \hat{R}_k \quad \hat{R}_{k-1} \quad \cdots \quad \hat{R}_{k-69} \quad \hat{R}_{k-70} \quad \hat{V}_{k-1} \quad \hat{V}_{k-2} \right] \quad (37)$$

And the dynamics and command matrixes can be copied from the two systems described above (the last sets of rows just shift the retinal slip back in time):

$$A' = \begin{bmatrix}
1 & dt & 0 & 0 & 0 & 0 & 0 & 0 & 0 & 0 & 0 & 0 & \cdots & 0 & 0 & 0 & 0 \\
0 & 1 & 0 & 0 & 0 & 0 & 0 & 0 & 0 & 0 & 0 & 0 & \cdots & 0 & 0 & 0 & 0 \\
0 & 1 & 0 & 0 & 0 & 0 & 0 & 0 & 0 & 0 & 0 & 0 & \cdots & 0 & 0 & 0 & 0 \\
0 & 0 & 0 & 1 & dt & 0 & 0 & 0 & 0 & 0 & 0 & 0 & \cdots & 0 & 0 & 0 & 0 \\
0 & 0 & 0 & -1/Tp & 0 & 0 & 0 & 0 & 0 & 0 & 0 & 0 & \cdots & 0 & 0 & 0 & 0 \\
0 & 0 & 0 & 0 & 0 & 1 & dt & 0 & 0 & 0 & 0 & 0 & \cdots & 0 & 0 & 0 & 0 \\
0 & \zeta & 0 & 0 & 0 & 0 & 0 & 0 & 0 & 0 & 0 & 0 & \cdots & 0 & 0 & 0 & 0 \\
0 & 0 & 0 & 0 & 0 & 0 & 0 & 1 & dt & 0 & 0 & 0 & \cdots & 0 & 0 & 0 & 0 \\
0 & 0 & 0 & 0 & 0 & 0 & 0 & -1/Tp & 0 & 0 & 0 & 0 & \cdots & 0 & 0 & 0 & 0 \\
0 & \zeta & 0 & 0 & 0 & 0 & -1 & 0 & 0 & 1 & 0 & 0 & \cdots & 0 & 0 & 0 & 0 \\
0 & 0 & 0 & 0 & 0 & 0 & 0 & 0 & 1 & 1 & 0 & 0 & \cdots & 0 & 0 & 0 & 0 \\
0 & 0 & 0 & 0 & 0 & 0 & 0 & 0 & 0 & 0 & 1 & 0 & \cdots & 0 & 0 & 0 & 0 \\
\vdots & \vdots & \vdots & \vdots & \vdots & \vdots & \vdots & \vdots & \vdots & \vdots & \vdots & \vdots & \ddots & \vdots & \vdots & \vdots & \vdots \\
0 & 0 & 0 & 0 & 0 & 0 & 0 & 0 & 0 & 0 & 0 & 0 & \cdots & 0 & 0 & 0 & 0 \\
0 & 0 & 0 & 0 & 0 & 0 & 0 & 0 & 0 & 0 & 0 & 0 & \cdots & 1 & 0 & 0 & 0 \\
0 & 1 & 0 & 0 & 0 & 0 & 0 & 0 & 0 & 0 & 0 & 0 & \cdots & 0 & 0 & 0 & 0 \\
0 & 0 & 0 & 0 & 0 & 0 & 0 & 0 & 0 & 0 & 0 & 0 & \cdots & 0 & 0 & 1 & 0
\end{bmatrix}$$

(38)

The internal representation of the command is two dimensional, with separate command for the VOR (dimension 1) and OKR (dimension 2), and each is added into the appropriate eye velocity:

$$B = \begin{bmatrix} 0 & 0 & 0 & 0 & 1 & 0 & 0 & 0 & 0 & 0 & 0 & 0 & \quad & 0 & 0 & 0 & 0 \\ 0 & 0 & 0 & 0 & 0 & 0 & 0 & 0 & 1 & 0 & 0 & 0 & \quad & 0 & 0 & 0 & 0 \end{bmatrix} \qquad (39)$$

5S.7.4 The combined controller: state estimation

In the second equation of the set in Eq. (21), the observation matrix, D', selects the vestibular and retinal input appropriately:

$$D' = \begin{bmatrix} 0 & 1 & 0 & 0 & 0 & 0 & 0 & 0 & 0 & 0 & 0 & 0 & \cdots & 0 & 0 & 0 & 0 \\ 0 & 0 & 0 & 0 & 0 & 0 & 0 & 0 & 0 & 0 & 0 & 0 & \cdots & 0 & 1 & 0 & 0 \end{bmatrix} \quad (40)$$

Note that the first row of D' is different than the first row of D. This comes from the fact that the internal system maintains an ongoing estimate of head velocity that is influenced by the input while the real system does not maintain such an ongoing estimate. The only representation of the delayed head velocity is the actual delayed head velocity. $h'(x)$ applies the retinal saturation non-linearity, $h(R)$ from Eq. (8), to the retinal slip and does not change the vestibular input:

$$h'\begin{pmatrix} \hat{\dot{H}} \\ \hat{R} \end{pmatrix} = \begin{pmatrix} \hat{\dot{H}} \\ h(\hat{R}) \end{pmatrix} \quad (41)$$

Parameters of the Kalman gain were selected by hand to match the data. We assumed that vestibular input only affects our estimate of the head velocity, $\tilde{\dot{H}}$, and that retinal input affects both our estimate of post-VOR retinal slip, $\tilde{R}^*$, and our estimate of uncompensated retinal slip ($\tilde{R}_k$) and it's delayed versions. This gave the Kalman gain matrix the following form:

$$K = \begin{bmatrix} 0 & 1 & 1 & 0 & 0 & 0 & 0 & 0 & 0 & 0 & 0 & 0 & \cdots & 0 & 0 & 0 & 0 \\ 0 & 0 & 0 & 0 & 0 & 0 & 0 & 0 & 0 & 0.05 & 0.05 & 0.05 & \cdots & 0.05 & 0.05 & 0 & 0 \end{bmatrix}$$

(42)

We set κ_V to 1, in order match the experimental finding that floccular lesion does eliminate VOR performance. We set the other values to match the behavioural data. That is, the larger the value of κ_T and $\kappa_{R,k}$, the more quickly new retinal input affects our estimates. This leads to a degradation in our match to the OKR data (since the OKR data has low gain when the amplitude and frequency of the stimulus are both high). Balancing these two considerations, we got the best match for our data at $\kappa_T = \kappa_{R,69} = \kappa_{R,68} = \cdots = \kappa_{R,1} = \kappa_{R,0} = 0.05$.

5S.7.5 The combined controller: cost function

We assumed that the primary goal of the optimal controller of the CEM in afoveate species (like rabbit and mouse) is to minimize motion of the visual field on the retina in order to stabilize the

retinal image. We make the assumption that this cost is considered separately for VOR and OKR because we are assuming that these reflexes are supported by separate neural substrates.

Thus, the overall cost of the system can be broken down into two parts, vestibular and retinal:

$$C = C_{\mathrm{V}} + C_{\mathrm{R}} \tag{43}$$

Each of the two sub costs is concerned with a different retinal slip: C_{V} relates to $\tilde{\dot{H}}_k + \tilde{\dot{E}}_{\mathrm{V},k}$, retinal slip due to uncompensated head motion, while C_{R} relates to $\tilde{R}^*_k + \tilde{\dot{E}}_{\mathrm{R},k}$, retinal slip due to uncompensated motion of the visual environment. In addition to the cost associated with retinal slip, each cost function includes a cost associated with eye eccentricities (this can be considered an "action" cost since eye eccentricity leads to extra muscle activity and energy expenditure). Finally, both cost functions discount future costs, as is common for an infinite horizon feedback controller: Thus, the two cost functions required for creating the two motor commands are:

$$\begin{aligned} C_{\mathrm{V}} &= \sum_{k=0}^{\infty} \gamma^{-k} \left(\left(\dot{E}_{\mathrm{V},k} + \dot{H}_k \right)^2 + \theta E_{\mathrm{V},k}^2 \right) \\ C_{\mathrm{R}} &= \sum_{k=0}^{\infty} \gamma^{-k} \left(\left(\dot{E}_{\mathrm{R},k} + R^*_k \right)^2 + \theta E_{\mathrm{R},k}^2 \right) \end{aligned} \tag{44}$$

The parameter θ balances between eccentricity and retinal slip costs. The parameter γ is the discount parameter (Bradtke, 1993) used to reduce the influence of increasingly distant costs. These two parameters were needed to match the drift of the eyes in the dark and were set to $\theta = 2$ and $\gamma = e^{\frac{1}{150}}$. The sum was approximated and we kept the first 100,000 terms.

5S.7.6 The combined controller: the motor command

If our system had a linear plant (L), quadratic cost function (Q) and independent, identically distributed (i.i.d.) Gaussian noise, it would be called an LQR system (Aström and Murray, 2010). For such systems, it can be proven that the optimal controller can be separated in two independent parts – an observer and a simple controller – using the Ricatti equations (Lancaster and Rodman, 1995). We do not go into the details of these equations here, but we note that the CEM system, as described above, is not linear (because of non-linearities in the inputs) and does not have i.i.d.

noise (since we use signal dependent noise). Nevertheless, the convenience of the LQR formulas has led to their frequent use in systems that are close to being LQR (Burns and Ou, 1994). Previous experience is that this leads to nearly optimal controllers, and we followed this strategy here.

However, before we apply Ricatti equations, we make one additional assumption. We assume that for the purposes of this solution, the controller assumes full correction of the head velocity by the VOR system. That is, we set $\zeta = 0$ in the matrix A', Eq. (38).

Applying the equations of Lancaster & Rodman (1995) to our system, Eq. (21), we derive a solution for the control policy, L.

$$L = \begin{bmatrix} 0 & 0.972 & 0 & -1.7669 & 0.00023313 & 0 & 0 & 0 & 0 & 0 \\ 0 & 0 & 0 & 0 & 0 & 0 & 0 & -1.7669 & 0.00023313 & 0.972 \end{bmatrix} \quad (45)$$

This can be more clearly written in terms of the final results for the motor commands:

$$u_{R,k+1} = -0.97\tilde{R}^*_{R,k} + 1.77\tilde{E}_{R,k} - 0.0002\tilde{\dot{E}}_{R,k}$$

$$u_{V,k+1} = -0.97\tilde{\dot{H}}_{V,k} + 1.77\tilde{E}_{V,k} - 0.0002\tilde{\dot{E}}_{V,k} \quad (46)$$

The first term in both Eqs 46 compensates for retinal slip. The second term combines compensation for the "drift to centre" generated by the elastic properties of the plant (Eq. 2). This activity is apparently generated by the "neural integrator" produced by the firing of the tonic and burst-tonic premotor cells (Robinson, 1981). Experimental results presented in this article and in other works (Cannon and Robinson, 1987) show the elastic properties of the plant are not fully compensated for by the controller; i.e the neural integrator is leaky, and this leakage has a much higher time constant than the elastic term of the plant. The last term in equation (46) term represents this failure to compensate.

5S.8 VOR adaptation

The parameter ζ (introduced in Eq. 29) represents the extent to which the OKR system assumes head movements will go uncompensated. We model CEM adaptation as adaptation of this

parameter so as to accurately predict retinal slip. The forward model prediction of retinal slip is given by Eq. (28).

Where we recall that the star indicates that this is the estimate of the retinal slip that is we predict that is happening right now (post-VOR slip), as opposed to the estimate of the available retinal slip (with a 70 ms delay) which is indicated by $\hat{R}_k$ (Eq. 9).

We want to minimize the error in predicted (post-VOR) retinal slip:

$$m = \left(R_k^* - \hat{R}_k^* \right)^2 \tag{47}$$

So we can calculate:

$$\frac{\partial m}{\partial \zeta} = -2\left(R_k^* - \hat{R}_k^* \right) \frac{\partial}{\partial \zeta} \hat{R}_k^* \tag{48}$$

And then using the definition of $\hat{R}_k^*$ (Eq. 28 and Eq. 29), we get:

$$\frac{\partial m}{\partial \zeta} = 2\left(R_k^* - \hat{R}_k^* \right)\left(\hat{\dot{H}}_{k-1} - \hat{\dot{H}}_{k-2} \right) \tag{49}$$

To decrease m we have to change parameter ζ in direction of minus the derivative:

$$\zeta_{\text{new}} = \zeta_{\text{old}} - \eta * \left(R_k^* - \hat{R}_k^* \right)\left(\hat{\dot{H}}_{k-1} - \hat{\dot{H}}_{k-2} \right) \tag{50}$$

where η specifies the rate of adaptation. For the results presented here ζ was updated every 4 cycles of the stimulus (although this value is not critical and adaptation functions correctly with a wide range of update schedules) and $\eta = 0.009$ to match the rate of adaptation in the experimental data.

5S.9 Bayesian Fitting Procedure

The gains and phases of the single sine experimental data were estimated using a Bayesian fitting procedure using OpenBugs (version 3.2.3). The model used is specified in full form below:

```
model{
    for( rat in 1 : n.Rats ) {
        for( bin in 1 : n.Bins ) {
            for( rep in 1 : n.Reps ) {
                Vel[rep , bin , rat] ~ dnorm(sint[bin , rat], tau.Vel.rat[rat])
            }
            sint[bin , rat] <- A.rat[rat] * sin(w * dT * bin - phi.rat[rat])
        }
        A.rat[rat] ~ dnorm(A.mu, A.tau)C(0,)
        phi.rat[rat] ~ dnorm(phi.mu, phi.tau)C(-π,π)
        tau.Vel.rat[rat] ~ dgamma(tau.Vel.shape, tau.Vel.scale)
    }
    A.mu ~ dunif(A.mu.lower, A.mu.upper)
    A.tau ~ dgamma(A.tau.shape, A.tau.scale)
    phi.mu ~ dnorm(phi.mu.mu, phi.mu.tau)C(-π,π)
    phi.tau ~ dgamma(phi.tau.shape, phi.tau.scale)
}
```

The fitting procedure was run with 1000 samples with a burn in of an additional 500 samples in 3 chains. The initial values of the amplitude and phase of the fits were estimated from the data and each chain was initialised with a different precision (an order of magnitude between each).

Table of Parameters

	Value	Eq.	Meaning	Is it critical?	How was it set?
	1 ms		Time step		
T_p	0.5 sec	1	Leaky integrator time constant for motor nuclei	No	(Stahl and Simpson, 1995; Stahl *et al.*, 2015)
T_v	4sec	3	Low pass filter constant for the vestibular inputs	Yes	Fit to data. Close to value found for actual vestibular afferents by Yang, 2009 (3 sec).
δ_V	2ms	5	Vestibular sensory delay	No	Sohmer *et al.*, 1999
a_V	0.1	6	Vestibular sensory noise proportionality constant	No	Middle of the stable range
$R_{\max}$	0.65 deg/sec	8	Retinal saturation	Yes	Oyster *et al.*, 1972
δ_R	70 ms	9	Visual processing delay	Yes	van Alphen *et al.*, 2001
a_R	0.1	10	Visual sensory noise proportionality constant	No	Middle of the stable range.
a_u	0.1	15	Motor noise	No	Middle of the stable range
T_n	4.13 sec	27	Time constant of the neural integrator	No	Set by the Riccati equations.
Z	-0.6	29	Assumed VOR inaccuracy	No	Fit to match VOR performance in the dark.

κ_V	1	42	Kalman gain of vestibular input	No	Set so VOR is not affected by flocullar lesion
κ_T	0.05	42	Kalman gain for the effect of retinal slip prediction error on post-VOR retinal slip	No	Fit to width of correlation between forward model and actual eye movements
$\kappa_{R,k}$	0.05	42	Kalman gain for the effect of retinal slip prediction error on estimate of uncompensated retinal slip	No	Fit to width of correlation between forward model and actual eye movements
γ	$e^{\frac{1}{150}}$	44	Discount parameter for cost function	No	Fit to produce credible drift in the dark
θ	2	44	Weight of position factor in cost function	No	Fit to produce credible drift in the dark
	100,000		Number of terms kept in infinite cost function sum	No	Arbitrary

Table 1.

Overview of all parameters used in this chapter, their values, the equation they are first used, a short description of their meaning. The last two columns describe whether they are critical, and how they were set. We determined how critical the parameters were, by varying them over an order of magnitude, and observing the changes in results.

References:

van Alphen, A.M. *et al.* (2001) The dynamic characteristics of the mouse horizontal vestibulo-ocular and optokinetic response. *Brain Res* 890, 296–305
van Alphen, B. *et al.* (2009) Age- and Sex-Related Differences in Contrast Sensitivity in C57Bl/6 Mice. *Investig Opthalmology Vis Sci* 50, 2451
van Alphen, B. *et al.* (2010) Three-Dimensional Optokinetic Eye Movements in the C57BL/6J Mouse. *Investig Opthalmology Vis Sci* 51, 623
Belknap, D.B. and McCrea, R.A. (1988) Anatomical connections of the prepositus and abducens nuclei in the squirrel monkey. *J Comp Neurol* 268, 13–28

Blazquez, P.M. *et al.* (2003) Cerebellar signatures of vestibulo-ocular reflex motor learning. *J. Neurosci.* 23, 9742–9751

Blazquez, P. *et al.* (2004). The vestibulo-ocular reflex as a model system for motor learning: what is the role of the cerebellum? *The Cerebellum* 3, 188–192

Bradtke, S. (1993) Reinforcement learning applied to linear quadratic regulation. *Adv. Neural Inf. Process. Syst* http://citeseerx.ist.psu.edu/viewdoc/download?doi=10.1.1.42.3939&rep=rep1&type=pdf

Burns, J. and Ou, Y. (1994) Feedback control of the driven cavity problem using LQR designs. Decis. Control Proc.

Büttner-Ennever, J.A., and Büttner, U. (1992) Neuroanatomy of the ocular motor pathways. *Baillières Clin Neurol* 1, 263–287

Cannon, S.C., and Robinson, D.A. (1987) Loss of the neural integrator of the oculomotor system from brain stem lesions in monkey. *J Neurophysiol* 57, 1383–1409

Collewijn, H. (1969). Optokinetic eye movements in the rabbit: Input-output relations. *Vision Res* 9, 117–132

Delgado-García, J.M. (2000) Why move the eyes if we can move the head? *Brain Res Bull* 52, 475–482

Donaldson, I.M.L. (2000) The functions of the proprioceptors of the eye muscles. *Philos. Trans R Soc Lond B Biol Sci* 355, 1685–1754

Faulstich, B.M. *et al.* (2004) Comparison of plasticity and development of mouse optokinetic and vestibulo-ocular reflexes suggests differential gain control mechanisms. *Vision Res* 44, 3419–3427

Frens, M.A. and Donchin, O. (2009) Forward models and state estimation in compensatory eye movements. *Front Cell Neurosci* 3, 13

Gerrits, N.M. *et al.* (1984) The mossy fiber projection of the nucleus reticularis tegmenti pontis to the flocculus and adjacent ventral paraflocculus in the cat. *Neurosc* 11, 627–644

Ghasia, F.F. *et al.* (2008) Neural Correlates of Forward and Inverse Models for Eye Movements: Evidence from Three-Dimensional Kinematics. *J Neurosci* 28, 5082–5087

Glasauer, S. (2007) Current models of the ocular motor system. *Dev Ophthalmol* 40, 158–174

Glickstein, M. *et al.* (1994) Visual pontocerebellar projections in the macaque. *J Comp Neurol* 349, 51–72

Graf, W. *et al.* (1988) Spatial organization of visual messages of the rabbit's cerebellar flocculus. II. Complex and simple spike responses of Purkinje cells. *J Neurophysiol* 60, 2091–2121

Green, A.M. *et al*. (2007) A Reevaluation of the Inverse Dynamic Model for Eye Movements. *J Neurosci* 27, 1346–1355

Harris, C.M. and Wolpert, D.M. (1998) Signal-dependent noise determines motor planning. *Nature* 394(6695): 780–784.

Jordan, M.I. and Rumelhart, D.E. (1992) Forward Models: Supervised Learning with a Distal Teacher. *Cognitive Science* 16, 307–354

Lancaster, P., and Rodman, L. (1995). Algebraic riccati equations. [Online]. Available: http://www.mathos.unios.hr/matjsus/literatur.pdf.

Langer, T. *et al*. (1985) Afferents to the flocculus of the cerebellum in the rhesus macaque as revealed by retrograde transport of horseradish peroxidase. *J Comp Neurol* 235, 1–25

Lopez-Martinez, M. and Diaz, J. (2004) Control of a laboratory helicopter using switched 2-step feedback linearization Semantic Scholar Available: https://www.semanticscholar.org/paper

McCrea, R.A. and Baker, R. (1985) Anatomical connections of the nucleus prepositus of the cat. *J Comp Neurol* 237, 377–407

Oyster, C.W. *et al*. (1972) Direction-selective retinal ganglion cells and control of optokinetic nystagmus in the rabbit. *Vision Res* 12, 183–193

Robinson, D.A. (1981) The Use of Control Systems Analysis in the Neurophysiology of Eye Movements. *Annu Rev Neurosci* 4, 463–503

Schonewille, M. *et al.* (2010) Purkinje cell-specific knockout of the protein phosphatase PP2B impairs potentiation and cerebellar motor learning. *Neuron* 67, 618–628

Schonewille, M. *et al.* (2011) Reevaluating the role of LTD in cerebellar motor learning. *Neuron* 70, 43–50

Shadmehr, R. and Krakauer, J.W. (2008) A computational neuroanatomy for motor control. *Exp Brain Res* 185, 359–381
Sohmer, H. *et al*. (1999) Effect of noise on the vestibular system - Vestibular evoked potential studies in rats. *Noise Health 2*, 41
Soodak, R.E. and Simpson, J.I. (1988) The accessory optic system of rabbit. I. Basic visual response properties. *J Neurophysiol* 60, 2037–2054
Stahl, J.S. and Simpson, J.I. (1995) Dynamics of abducens nucleus neurons in the awake rabbit. *J Neurophysiol* 73, 1383–1395
Stahl, J.S. *et al.* (2000) A comparison of video and magnetic search coil recordings of mouse eye movements. *J. Neurosci. Methods* 99, 101–110
Stahl, J.S. *et al.* (2015) Mechanics of mouse ocular motor plant quantified by optogenetic techniques. *J Neurophysiol* 114, 1455–1467
Todorov, E. and Jordan, M.I. (2002) Optimal feedback control as a theory of motor coordination. *Nat. Neurosci.* 5, 1226–1235
Todorov, E. (2004) Optimality principles in sensorimotor control. *Nat Neurosci* 7, 907–915
Van Alphen, A.M. *et al.* (2002) Motor Performance and Motor Learning in Lurcher Mice. *Ann NY Acad Sci* 978, 413–424
Wang, X. *et al.* (2007) The proprioceptive representation of eye position in monkey primary somatosensory cortex. *Nat Neurosci* 10, 640–646
Winkelman, B. and Frens, M. (2006) Motor Coding in Floccular Climbing Fibers. *J Neurophysiol* 95, 2342–2351
Yang, A. and Hullar, T.E. (2007) Relationship of Semicircular Canal Size to Vestibular-Nerve Afferent Sensitivity in Mammals. *J Neurophysiol* 98, 3197–3205
Yoshida, K. *et al.* (2001) A Key Role of Starburst Amacrine Cells in Originating Retinal Directional Selectivity and Optokinetic Eye Movement. *Neuron* 30, 771–780

General Discussion

In this thesis, we have explored the effects of transcranial direct current stimulation (tDCS) on cerebellar network through behavioral and electrophysiological assessments. Simultaneously we have tried to validate Frens and Donchin state predicting feedback control (SPFC) scheme of the compensatory eye movement (CEM) system. We have performed tDCS behavioral experiments not only in control and genetically modified mice but also in healthy human subjects. We have introduced multidimensional approach to tackle the complexity of polarity specific effects of tDCS on cerebellar functions. For the first time, we have established a mouse model of cerebellar direct current stimulation (DCS) during vestibulo-ocular reflex (VOR) gain down adaptation as well as explored the learning rate of acute VOR gain down training in humans while coupled to tDCS. Furthermore, we have assessed *in vivo* short vs long term effects of DCS on cerebellar neuronal activity. We have also simulated behavioral data acquired during a wide range of CEM paradigms to increase understanding of the motor control system regulating CEM.

tDCS, a noninvasive brain stimulation technique, modulates neuronal excitability and promises treatment of several neurological and psychiatric disorders. The simplicity and ease of use have led to a great interest in its clinical potential. However, it seems highly sensitive to the stimulation parameters and there has been difficulty in determining ways to maximize the technique's effectiveness. The effects of stimulation are often claimed to be reversed with change in polarity, though this idea has been challenged in several studies. A real understanding can only be accomplished by accumulating evidence of how tDCS modulates a group of neurons, what the impact of tDCS has on the local network and how tDCS can alter the inter-network signal processing. There is no available animal model of cerebellar DCS although a rodent model of DCS has been validated in various cortical functional studies. As the plasticity mechanisms of the cerebellar cortex are different from those in neocortex, there is ample of justification for having a separate animal model of cerebellar DCS. Therefore, we have focused not only on developing an animal model of cerebellar DCS but also unraveling the role of PC LTP in mediating DCS effects on cerebellar dependent motor adaptation. We have used a gain down VOR adaptation task to probe this (**Chapter 2**).

Furthermore, it is important to translate the findings from animal studies to humans in order to justify the role of tDCS in rehabilitation therapy for certain cerebellar degenerative diseases. Therefore, we have chosen a similar gain down VOR adaptation behavioral paradigm to probe the

effects of tDCS in healthy human subjects. To date, numerous animal and human studies have allowed researchers to delineate the role of tDCS in modulating neuronal processes underlying specific behaviors. At the same time, studies showing the ambiguous effects of tDCS on various behaviors have generated controversy. Behavioral modulation depends on changes in the neuronal firing rate and pattern. Moreover, changes in individual neurons ultimately express themselves as network effects that can be local or spread across multiple brain regions. In this study, we have tried to find an optimal stimulation paradigm to modulate human VOR gain down adaptation task (**Chapter 3**).

In order to optimize cerebellar tDCS, we require a clear vision of the polarity specific effects of tDCS on the cerebellar neuronal network. In addition, we need to explore the role of tDCS in different cerebellar disorders. As PCs are the sole output neurons of the cerebellar cortex, we have investigated the effects of DCS on the cerebellum of mice in which LTP or LTD of PC is genetically altered. Our preliminary data suggest that the PC LTP may be crucial in determining the effects of anodal stimulation (**Chapter 4)**.

Computational modelling techniques can be used to increase understanding of the neural circuitry involved in a process and the functions performed by specific anatomical locations. Optimal control models are the dominant paradigm in current studies of motor control. We have employed a quantitative version of the Frens and Donchin SPFC scheme of the CEM system. In our model, we proposed that CEM are generated by a SPFC framework where specific functional roles can be ascribed to specific nuclei in the CEM circuitry. We have challenged our model in a broad range of experimental conditions to establish the robustness of performance and compare the effects of lesions in the model to their real-world counterparts (**Chapter 5**).

6.1 tDCS modulates cerebellar functions

It is of vital import to explore whether tDCS can modulate the function of the cerebellum, a crucial structure involved in movement control and cognitive processing. Human study reports that both anodal and cathodal tDCS delivered over the cerebellum impairs the practice-dependent increase in verbal working memory task proficiency (Ferrucci *et al.*, 2008; Ferrucci *et al.*, 2015). This finding implies that tDCS of both polarities could alter the fine-tuning ability of the cerebellar cortex. Galea *et al.*, 2009 finds that cathodal tDCS can decrease and anodal tDCS can increase the

inhibitory tone the cerebellum exerts over the motor cortex (M1). To this point, it seems that tDCS has polarity specific effects on cerebellar excitability which can directly modulate cerebellar dependent motor learning tasks. More precisely, one can predict that anodal stimulation of cerebellum should facilitate cerebellar dependent motor tasks where the region specific plasticity needs to be facilitated. As predicted, anodal stimulation facilitates locomotor (Jayaram *et al.*, 2012), force field (Herzfeld *et al.*, 2014) adaptation and eye-blink conditioning (Zuchowski *et al.*, 2014) tasks while cathodal stimulation hinders leaning in all these tasks. Similarly, cerebellar tDCS shows a polarity specific effect in executing cognitive tasks. Cathodal tDCS applied over the right cerebellum facilitates performance on an arithmetic and verb generating task that both required a high level of cognitive load compared with arithmetic and reading tasks that require less effort, in which tDCS has no added benefit (Pope and Miall, 2012). In this case, cathodal stimulation might reduce cerebellar inhibition on higher brain centers (such as prefrontal cortex) and, in turn, elevates the performance. Surprisingly, both faciliatory and inhibitory cerebellar stimulation resulted in similar modulation in ankle visuomotor learning after 15 min of combined tDCS and motor practice (Shah *et al.*, 2013). These all findings have motivated us to unravel the pathway through which tDCS modulate cerebellar functions. We believe that polarity dependent modulation of the cerebellar task is dependent on the nature of the task and also the regions which are involved during that specific task along with the cerebellum.

Animal study demonstrates acute effects of stimulation

We have selected relatively simple behavioral task (VOR gain down adaptation) to probe the effects of tDCS on cerebellar dependent adaptation. In the animal model, we have applied current directly on the dura because of this we term it DCS rather tDCS. From the VOR adaptation study in mice, we concluded that DCS has an acute modulatory role in cerebellar motor learning but no long-lasting effects as such. We have captured this important aspect by - (i) exploring the temporal pattern of post-stimulation effects on VOR adaptation and (ii) investigating the effects of DCS in control and disrupted neuronal network. Our study was focused on assessing the post-stimulation effects on training and testing sessions, whereas most of the reports available today are based on stimulation applied during learning (Herzfeld *et al.*, 2014; Jayaram *et al.*, 2012; Zuchowski *et al.*, 2014). The DCS dependent long-lasting change that is important for use in rehabilitation therapy can be dissected temporally in our study. We have shown that the total learning is similar in the anodal and the cathodal stimulation conditions although the gain reduction at the early phase is

clearly different in C57BL/6 control mice (Figure 1). Plausibly, DCS has limited scope in augmenting a motor learning task when it is not coupled to the learning phase. This notion is supported by other studies as well. The post-stimulation deadaptation curve (Herzfeld *et al.*, 2014; Jayaram *et al.*, 2012) or extinction rate (Zuchowski *et al.*, 2014) shows no difference across various stimulation groups. This is remarkable because irrespective of altered rate and total amount of learning, polarity has no effect on post-stimulation de-adaptation/ learning processes. Clearly, our study inspects an important temporal aspect of post-stimulation effects of DCS on cerebellar dependent VOR adaptation. The temporal profile depicts that both anodal and cathodal stimulation have short-lasting effects on gain down adaptation. However, these short-lasting effects are abolished in L7-PP2B mice those who do not have potentiation at the PCs. This part of the study brings us to the point where we can say that tDCS should not be administered to improve motor functions in ataxic patients having impairment in PC potentiation.

Human study defines the limits of cerebellar tDCS

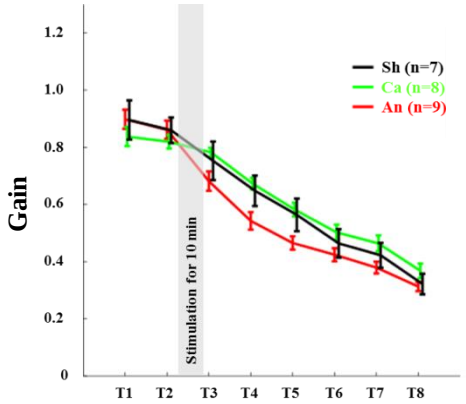

Figure 1: Anodal stimulation accelerates gain down adaptation in C57BL/6 mice.

Trial-to-trial changes in mean VOR gain during VOR-decrease training. The VOR was tested pre- and post-training by measuring the eye movement response to the vestibular stimulus.
Black, Green and Red lines are for sham, cathodal and anodal stimulation conditions respectively. n depicts number of animals used in the group. The grey bar indicates the stimulation period. Error bars represent SEM.

Interestingly, we observed that anodal stimulation can lead to the reduction of VOR gain before any training session. It looks like anodal stimulation has acutely increased PC driven inhibitory activity that suppressed VOR amplitude. Probably, anodal stimulation makes PC more active and therefore there is an acute effect on the VOR. To understand this, we need to study a gain up VOR paradigm with DCS. Otherwise, contralateral DCS while animal will perform the similar VOR gain down paradigm. The idea is that as cerebellum projects to the unilaterally so the eye amplitude of the non-stimulated side will be unaffected.

We have extended our search from animal to human by using a similar behavioral task, in order to understand how tDCS can modulate VOR adaptation in healthy human subjects. This is altogether

a fast approach to translate the findings from animal experiments to human. In this process, we have found two key features which determine the modulatory role of tDCS in human VOR gain down adaptation – (i) sensitivity of tDCS depends on the anatomical location of the interested brain structure and (ii) the nature of a task regulates the effects of tDCS.

Our results indicate that tDCS over the cerebellum does not modulate VOR adaptation in human (Figure 2a). This is in contradiction to the observations from mice experiment. Moreover, our findings in human VOR adaptation do not match the modulatory effect of online anodal cerebellar tDCS in humans on reaching movement adaptation (Galea *et al.*, 2011; Hardwick and Celnik,

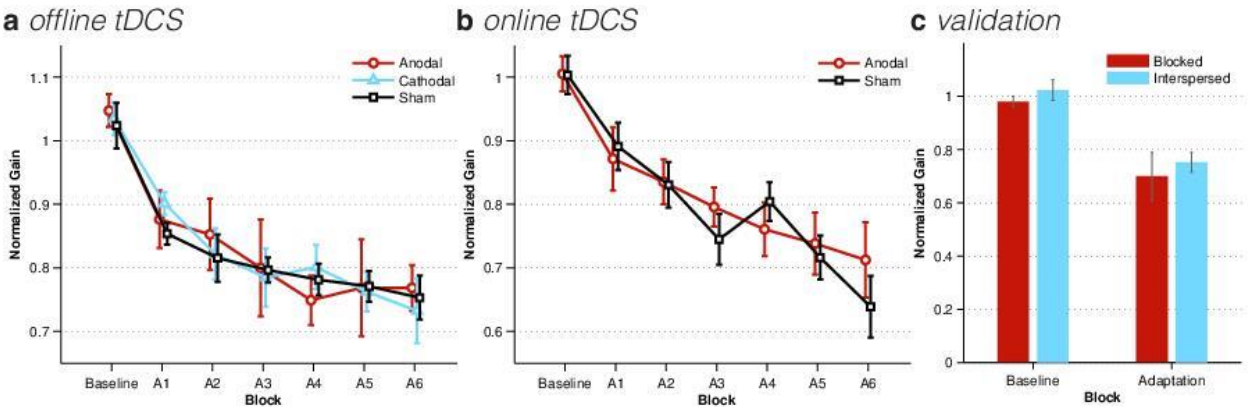

Figure 2: tDCS has no modulatory role in human VOR gain down adaptation

Trial-to-trial changes in mean VOR gain during VOR-decrease training. The VOR was tested pre- and post-training by measuring the eye movement response to the vestibular stimulus. **a)** tDCS was applied for 15 mins between baseline and block A1. **b)** tDCS was applied for entire session from A1 to A6.
Each point represents mean of the group. Error bars represent SEM.

2014; Herzfeld *et al.*, 2014) and locomotion adaptation (Jayaram *et al.*, 2012), Figure 2b. We believe that this relates to the fact that flocculonodular lobe which is responsible for VOR adaptation, sits deep within the human cerebellum near the brainstem (Voogd and Barmack, 2006). Even with maximum stimulation strength (2 mA) on the active electrode, we could not reach the effective field intensity which was used in reaching and locomotion adaptation studies (Galea *et al.*, 2011; Hardwick and Celnik, 2014; Herzfeld *et al.*, 2014; Jayaram *et al.*, 2012; Zuchowski *et al.*, 2014). This supports the idea that before using tDCS to augment a region specific task one needs to assess the critical distance between the region and the active electrode. Finally, we have shown how important it is to define a task before predicting the effectiveness of tDCS. VOR adaptation in human utilizes an extensive repertoire of gaze-holding and gaze-directing eye

movements to stabilize images of interest on the retina (Leigh and Zee, 2006), compared to the relatively simple situation in non-foveated animals like the mouse. Retinal slips can be compensated by catch-up saccades which could decrease the retinal error driving VOR adaptation (Melvill *et al.*, 1988). In addition, adaptation of the VOR is more gradual in humans and monkeys than in mice, possibly because of the strong significance of vision in foveated animals. This suggests that the role of the Flocculus during acute VOR adaptation is more complex and involves multiple mechanisms in the human. In conclusion, one needs to evaluate the location of interested brain region and the nature of a task before using tDCS to modify a motor action.

We must agree that animal and human stimulation methods in our study differs in term of stimulation procedure. First and most importantly, in the animal study, the cerebellum was stimulated directly after craniotomy without current having to cross the skull. Thus, the lack of behavioral modulation might be due to an insufficient field strength achieved with the standard stimulation configuration used in the human study. Second, the placement of the reference electrode – for animals it was on the belly and for humans it was on the ipsilateral buccinator muscle. Therefore, the current trajectory is also different. Finally, the thickness of hair may introduce variability in the current spread in human study.

6.2 Interaction between tDCS and inherent homeostatic nature of the network

In general, anodal and cathodal stimulation are accepted as excitatory and inhibitory to the network, respectively. What we have found that the polarity dependent effects of tDCS should not be generalized at all. Rather, we should consider inter-subject variability as well as cross species variabilities - such as skull thickness, structural and anatomical differences and electrode attachments methods – to predict the effects of tDCS. Most importantly, we need to understand that all the parameters which may influence the outcomes of tDCS, alter neuronal plasticity mechanisms which are a combination of synaptic and intrinsic plasticity of neurons. In the coming paragraphs, we will argue how synaptic plasticity and intrinsic plasticity is regulated in a homeostatic fashion which has immense strength to alter tDCS outcomes and what role our study plays to support this. We will discuss our results thoroughly to demonstrate why we should consider homeostasis as a critical mechanism to understand the mechanism of tDCS.

Synaptic plasticity provides machinery for learning and memory (Shouval *et al.*, 2002). In response to a change in presynaptic activity, synapses of a post-synaptic neuron can dynamically express LTP or LTD. For example, a synapse expressing LTP could be adjoined by synapses whose strengths are weakened by homeostatic mechanisms; such changes could be visible as an enlarged spine with a larger postsynaptic density (PSD) carrying more glutamate receptors that are surrounded by thinner spines. A study in the rat cerebellum provides evidence that this could be the case (Lee *et al.*, 2013). Motor learning promotes the incidence of multiple-synapse boutons on pairs of spines originating from the same dendrite rather than from different dendritic segments, such that the potency of synapses in eliciting dendritic excitation is locally enhanced. Upon motor learning, local homeostatic compensatory changes at the neighboring synapses could effectively balance local dendritic activity by redistributing the weight of select inputs to help maintain excitability while allowing for local synaptic strengthening.

Interestingly, synaptic plasticity can be complemented by the intrinsic plasticity of neurons (Hanse *et al.*, 2008). A study in rat visual cortex demonstrates that the induction and direction of synaptic plasticity depend on the excitability of the post-synaptic neuron at the time of stimulation (Artola *et al.*, 1990). The threshold for induction of LTP and LTD is flexibly adjusted to the level of post-synaptic excitability by homeostatic mechanisms (Turrigiano and Nelson, 2004).

The homeostatic regulation of synaptic and intrinsic plasticity maintains the functionality of a network. Studies show that the homeostatic mechanism regulates over expression of LTP or LTD to keep the dynamic range of neuronal activity within the physiological limit (Abraham 2008; Hulme *et al.*, 2013). This idea gets additional support from an experiment on a rat skilled reaching task (Rioult-Pedotti, 2000). Motor skill learning leads to LTP at M1. When rats have been trained for 5 days on a skilled reaching task, the trained M1 expressed less LTP and more LTD as opposed to the untrained M1 of control rats. This finding shows that the ability to induce LTP and LTD is homeostatically adjusted by previous learning experience, rendering the induction of LTP more difficult after intensive training. Probably, this homeostatic mechanism is a crucial factor in inducing variability in the polarity dependent effects of tDCS.

Local homeostatic mechanisms regulate the polarity specific effects of tDCS on the local micro-circuit. We demonstrate that both anodal and cathodal stimuli can cause either increase or decrease the multi-unit activity (MUA) in the C57BL/6 (wild type) mice long after the cessation of stimulation. Our explanation for this is that depending on the state of the neurons at a specific micro-circuit the firing rate was increased or decreased. For example, if the stimulated micro-circuit (neurons) is already towards higher active state then anodal stimulation causes lower in firing rate as per homeostatic mechanisms. On the other hand, lower active micro-circuits (neurons) transition to a higher activity state by anodal stimulation. In contrast, cathodal stimulation augments the shifting of lower state neurons to go the higher active state. This means that anodal can augment or hinder the activity state of a network based on the pre-stimulation activity level. We have to keep in mind that the higher active state does not only mean the basal firing rate but also intrinsic and extrinsic plasticity levels of neurons. Strikingly, our notion gets support from several studies. Siebner *et al.*, (2004) showed that the homeostatic mechanism can alter excitatory effects of anodal tDCS. One Hz repeated trans-cranial magnetic stimulation (rTMS) on M1 does not change cortico-motor excitability while a facilitatory anodal stimulation 15 mins prior to the subsequent 1Hz rTMS test session exerts an LTD-like effect, causing a reduction in cortico-motor excitability. Conversely, inhibitory priming with cathodal stimulation prior to 1Hz rTMS test session produces an increase in cortico-motor excitability. This polarity dependent priming effects of tDCS can be disrupted when the homeostatic mechanism of neurons is impaired due to neurological conditions (kang *et al.*, 2011; Quartarone *et al.*, 2005). Furthermore, cathodal tDCS applied before an orientation discrimination task execution induces an improvement of performance instead of hindering it (Pirulli *et al.*, 2014). Altogether, we think that the polarity dependent effects of tDCS directly linked to the homoeostatic mechanism of network.

Homeostasis regulates the polarity specific effects of tDCS

Furthermore, our results show that tDCS dependent modulation of the neuronal activity remains unaltered for a longer time period. This strengthens the idea that the homeostatic mechanism regulates the effects of tDCS. We think that the network state didn't change – no difference in the firing rate from early to late phase – because of two reasons, (i) after the stimulation the animal was not performing any goal directed learning task and (ii) there was no application of the second session of stimulation that could have modulate the neuronal activity to another direction.

The anodal and cathodal stimulation have similar early vs late effects on the firing rate. The strongest reason for this is that the animals were awake but not doing any sensory dependent learning task. In contrast, the reason for observing differential effects of anodal and cathodal stimulation on behaving mice (VOR gain down adaptation) is that animals were doing adaptation task following tDCS. When the animal is not performing any adaptation task the micro-circuit may be more sensitive towards local homeostasis rather behavior directed shift in the global homeostasis. The homeostatic synaptic strength changes can be rapid and local, and both global and local homeostatic mechanisms might operate in parallel in a nested manner (Pozo and Goda, 2010; Turrigiano *et al.*, 2008). We could have disentangled this problem by doing re-stimulation of the network while recording from the same region with a time delay from the first stimulation in an awake but non-behaving animal. However, we need a series of future experiments as we don't know the time-window to induce homeostasis in cerebellar network as well as how it is altered at the micro-circuit level how it is altered. Presently, we have only measured change in firing rate in our experiments. To understand this correctly one should use slice as well as *in vivo* patching techniques to examine the extrinsic and intrinsic plasticity of neurons as well as effects of tDCS on them.

Plausibly, the homeostatic mechanisms of the cerebellar circuit played a role in changing the firing rate while stimulation was applied and remained unchanged throughout the experimental time frame. We think that a second session of sensory or current stimulation is required to activate the mechanism of homeostatic plasticity. Our notion further gets support from a study in which two identical 5 min sessions of tDCS were paired as priming and test tDCS sessions which were separated by 0, 3 or 30 min (Fricke *et al.*, 2011). When priming and test tDCS were given without a break, the tDCS effect was simply prolonged. This is exactly what we saw in our experiment. On the other hand, if the two tDCS sessions were separated by 30 min, there was no priming effect on the plasticity-inducing effects of the test tDCS. Only when the test tDCS started 3 min after the end of priming tDCS, did the two tDCS protocols interact in a homeostatic fashion. These would be the next layer of experiments we should conduct on cerebellar tDCS.

Finally, our finding differs from the studies where anodal stimulation increases and cathodal stimulation decreases the neuronal activity in an isolated turtle cerebellum (Chan and Nicholson, 1986; Chan *et al.*, 1988). The major reasons of this difference could be due to the fact that they

have used – (i) isolated the cerebellum (causing reduction of inputs from other brain structures) (ii) flattened the cerebellum (leading to disruption of the lobular architecture) and (iii) no neuronal activity analysis of local neurons (MUA). In order to understand local homeostatic mechanism, MUA analysis is important.

Strikingly, the neuronal network of GluR2Δ7 mice responded to the anodal and cathodal stimulation alike to the wild type mice despite the fact that GluR2Δ7 mice do not have LTD at the PF-PC pathway. We think that only LTD mutation at the PF-PC synapses does not lead to the entire disruption of the network homeostatic mechanism. The network can still adjust its activity based on the spared homeostatic mechanisms. The results of disruption of homeostatic mechanism can be seen in L7-PP2B mice, where potentiation of the PC is genetically deleted (Schonewille *et al.*, 2010). One of the main reasons for the acute anodal effects may be due to the genetic ablation of the both synaptic and intrinsic potentiation which left the PCs with no homeostatic mechanism. Plausibly, acute reduction in MUA is inhibitory neuron dependent and as soon as that inhibition gone we observe a tremendous increase in MUA. As our group size in the mutant mice is small, we need to perform further experiments in order to establish the fact well.

Severe mutation disrupts homeostasis

Now the question comes how does cathodal stimulation evoke similar effects in L7-PP2B neuronal network compared to the control one. We think cathodal stimulation tends to drive PC homeostatic plasticity through other pathways. The serine/threonine phosphatases PP1, PP2A, and PP2B are involved in PC LTP induction (Belmeguenai and Hansel, 2005). Deletion of PP2B pathway leads to severe impairment of LTP and motor learning ability (Schonewille *et al.*, 2010). However, the exact role of PP2A is less clear. We can only speculate that cathodal stimulation may have involved one of these pathways to modulate neuronal activity in a opposite direction to the anodal effects. Future studies are required to prove this. We have to remember that this restoration may not be sufficient to handle several functional aspects of the network. Probably, that is the reason for not seeing a cathodal effect during VOR gain down adaptation task.

The surprising spatial specificity of tDCS

Our human experiment has highlighted the spatial specificity of tDCS. No stimulation effect on human VOR gain down adaptation is plausibly a result of differences in the stimulation method and anatomical location

of the Flocculus. The most likely reason for not finding a modulatory effect of tDCS on human VOR adaptation is that the electric field strength in the Flocculus is insufficient to affect neuronal firing. At the same time, it is proved that tDCS has not involved any other distal brain regions to modulate VOR gain. Because, we know that tDCS on the left parietal cortex alone resulted in bilateral albeit asymmetrical reduction in VOR slow phase velocities (Arshad *et al.*, 2014). If tDCS is a global stimulation, it would have engaged parietal cortex to alter VOR adaptation in our experiment. Interestingly, we see no effects of cerebellar tDCS on VOR adaptation. This indicates that tDCS has region specific effects and because of this we do not see an involvement of global homeostasis mechanism during cerebellar stimulation. In order to explore the polarity dependent homeostatic mechanism in human brain, one needs to assess electroencephalogram (EEG) data at various stages of adaptation.

6.3 Why nature does not permit us to learn with maximal capabilities?

In daily life we are continuously adapting to a different situation or learning new skills. Along with learning something new, we erase weakly associated memories. It is proposed that a selected minority (say "10 percent") of neurons can effectively deal with most situations (Buzsaki and Mizuseki, 2014). For example, only selective number of neurons (roughly 15%) of the lateral amygdala got engaged during fear memory formation and deletions of them caused memory loss (Han *et al.*, 2009). This process is important to keep an equilibrium state between learning and extinction. The extinction is important to keep a free space for learning new skills according to the environmental needs. For instance, when learning occurs in an overactive manner then delearning takes longer time (Knox *et al.*, 2012). Now think of a situation where we always learn every bit of information at our maximal limit, then it is easier to saturate the information storing capacity. It will be difficult to cope up with learning new skill or adapt to a specific condition in this continuously changing world. To make sure it does not happen, nature has kept a space (a buffer region) before it hits the ceiling; such that, when a situation arrives it can push the system further up (for example to enhance a specific skill we can train more). We think tDCS is actuating or suppressing a function by using that space.

6.4 Optimal control model of CEM and tDCS

Optimal control models are the dominant paradigm in current studies of motor control. Theories of motor control are primarily based on one of two main architectures. One theory suggests that the motor system relies on generating an ideal "desired movement" or "desired trajectory" that serves as a basis for subsequent control. An "inverse model" translates desired movement into motor commands (Jodan and Rumelhart, 1992). An alternative architecture suggests that the system operates in a "full feedback" mode: generating motor commands in response to the best guess regarding the current situation as opposed to using a pre-defined plan (Todorov and Jordan, 2002). Frens and Donchin (2009) used this architecture in their analysis of the CEM, which they called the state-predicting feedback control, SPFC, framework.

We have studied mouse CEM in a large variety of conditions (in terms of frequencies and amplitudes). Here, we have implemented the SPFC framework in a detailed computational model which can, with a single set of parameters, mimic the behavior of optokinetic response (OKR) and VOR. With the same set of parameters, the model also reproduces visuo-vestibular ocular reflex (vVOR), suppressed VOR (sVOR) and non-periodic Sum-of-Sine (SoS)-stimuli. Furthermore it successfully predicts the effects of lesions, and it is capable of showing adaptive behavior, similar to VOR learning. The SPFC model simulation is also able to correctly reproduce the non-linearity and superposition violations that are observed in physiological data.

The model responded accurately to SoS-stimuli, similar to those previously used by Sibindi et al. 2016, in press. Strikingly, two non-linearities in the results of Sibindi were reproduced: The first one is that when confronted with a stimulus that consists of two non-harmonic optokinetic sinusoids, the amplitude of the lower frequency is suppressed, independent of the absolute value of the constituent frequencies. This then also results in changes in the amplitudes in vVOR and sVOR conditions. The second one is that the lag of the response to especially the lower frequency is larger, resulting in a delayed overall response. This can be seen for both VOR, OKR and its combinations.

We think tDCS may play a crucial role in unraveling the role of Flocculus during SoS stimuli prediction. The VOR that works well in high velocities, operates in a partially open-loop fashion with feedback used to drive only the forward model of the eye without modifying processing of

the vestibular state itself. Interestingly, we have showed that the anodal stimulation can reduce VOR gain. The OKR loop that works well at low frequencies, on the other hand, incorporates forward models of the eye, the visual input, and also the VOR system. In our experiment, we see OKR responds well in higher frequencies during SoS stimuli. We think anodal tDCS may alter this state by activating PCs. The model replicates lesion studies but does not discuss what happens if the Flocculus is in hyper-active state or in a state where its sensitivity has been increased. tDCS will allow us to do such experiments and the framework provided by the model will in future be useful in delineating the functions effected by tDCS.

6.5 Future direction

tDCS has the potential to emerge as a promising and popular noninvasive brain stimulation therapy. However, many questions remain to be answered before it is accepted as a routine clinical therapeutic tool. For example, additional investigations are required to establish the optimal parameters of current intensity, duration, and electron montage for stimulation, which determine the efficacy of stimulation. Various outcome variables have been assessed across different studies, and this makes it difficult to pool study results for meta-analysis or to calculate effect size. In general, tDCS is safe and tolerable for use in healthy subjects or subjects with brain lesion. The neurophysiology underlying the neuroplasticity induced by tDCS is not well understood, and combination with cellular electrophysiology (extra- and intra-cellular recordings) and neuroimaging (i.e., diffusion tensor imaging or resting state functional magnetic resonance imaging) may provide novel insights with respect to changes in functional brain connectivity modulated by tDCS. There is an urgent need to do more animal experiments and theoretical developments, to replicate the promising preliminary results, and then to move into multicenter, randomized, sham controlled clinical trials to determine whether tDCS can be applied in clinical practice to benefit patients.

References:

Abraham, W.C. (2008) Metaplasticity: tuning synapses and networks for plasticity. *Nat. Rev. Neurosci.* 9, 387

Arshad, Q. *et al.* (2014) Left cathodal trans-cranial direct current stimulation of the parietal cortex leads to an asymmetrical modulation of the vestibular-ocular reflex. *Brain Stimul* 7, 85–91

Artola, A. *et al.* (1990) Different voltage-dependent thresholds for inducing long-term depression and long-term potentiation in slices of rat visual cortex. *Nature* 347, 69–72

Belmeguenai, A. and Hansel, C. (2005) A role for protein phosphatases 1, 2A, and 2B in cerebellar long-term potentiation. *J. Neurosci.* 25, 10768–10772

Buzsáki, G. and Mizuseki, K. (2014) The log-dynamic brain: how skewed distributions affect network operations. *Nat. Rev. Neurosci.* 15, 264–278

Chan, C.Y. and Nicholson, C. (1986) Modulation by applied electric fields of Purkinje and stellate cell activity in the isolated turtle cerebellum. *J. Physiol. (Lond.)* 371, 89–114

Chan, C.Y. *et al.* (1988) Effects of electric fields on transmembrane potential and excitability of turtle cerebellar Purkinje cells in vitro. *J. Physiol. (Lond.)* 402, 751–771

Ferrucci, R. *et al.* (2008) Cerebellar transcranial direct current stimulation impairs the practice-dependent proficiency increase in working memory. *J Cogn Neurosci* 20, 1687–1697

Ferrucci, R. *et al.* (2015) Cerebellar tDCS: how to do it. *Cerebellum* 14, 27–30

Frens, M.A. and Donchin, O. (2009) Forward models and state estimation in compensatory eye movements. *Front Cell Neurosci* 3, 13

Galea, J.M. *et al.* (2009) Modulation of cerebellar excitability by polarity-specific noninvasive direct current stimulation. *J. Neurosci.* 29, 9115–9122

Galea, J.M. *et al.* (2011) Dissociating the roles of the cerebellum and motor cortex during adaptive learning: the motor cortex retains what the cerebellum learns. *Cereb. Cortex* 21, 1761–1770

Han, J.H. *et al.* (2009) Selective erasure of a fear memory. *Science* 323, 1492–1496

Hanse, E. (2008) Associating synaptic and intrinsic plasticity. *J Physiol* 586, 691–692

Hardwick, R.M. and Celnik, P.A. (2014) Cerebellar direct current stimulation enhances motor learning in older adults. *Neurobiol. Aging* 35, 2217–2221

Herzfeld, D.J. *et al.* (2014) Contributions of the cerebellum and the motor cortex to acquisition and retention of motor memories. *Neuroimage* 98, 147–158

Hulme, S.R. *et al.* (2013) Emerging roles of metaplasticity in behaviour and disease. *Trends Neurosci.* 36, 353–362

Jayaram, G. *et al.* (2012) Modulating locomotor adaptation with cerebellar stimulation. *J Neurophysiol* 107, 2950–2957

Jordan, M.I. and Rumelhart, D.E. (1992) Forward Models: Supervised Learning with a Distal Teacher. *Cognitive Science* 16, 307–354

Kang, J.S. *et al.* (2011) Deficient homeostatic regulation of practice-dependent plasticity in writer's cramp. *Cereb. Cortex* 21, 1203–1212

Knox, D. *et al.* (2012) Unconditioned freezing is enhanced in an appetitive context: implications for the contextual dependency of unconditioned fear. *Neurobiol Learn Mem* 97, 386–392

Lee, K.J. *et al.* (2013) Motor skill training induces coordinated strengthening and weakening between neighboring synapses. *J. Neurosci.* 33, 9794–9799

Leigh, RJ. and Zee, DS. (2006) The neurology of eye movements. Oxford: *Oxford University Press*

Melvill Jones, G. *et al.* (1988) Changing patterns of eye-head coordination during 6 h of optically reversed vision. *Exp Brain Res* 69, 531–544

Pirulli, C. *et al.* (2014) Is neural hyperpolarization by cathodal stimulation always detrimental at the behavioral level? *Front Behav Neurosci* 8, 226

Pope, P.A. and Miall, R.C. (2012) Task-specific facilitation of cognition by cathodal transcranial direct current stimulation of the cerebellum. *Brain Stimul* 5, 84–94

Pozo, K. and Goda, Y. (2010) Unraveling mechanisms of homeostatic synaptic plasticity. *Neuron* 66, 337–351

Quartarone, A. *et al.* (2005) Homeostatic-like plasticity of the primary motor hand area is impaired in focal hand dystonia. *Brain* 128, 1943–1950

Rioult-Pedotti, M.S. *et al.* (2000) Learning-induced LTP in neocortex. *Science* 290, 533–536

Schonewille, M. *et al.* (2010) Purkinje cell-specific knockout of the protein phosphatase PP2B impairs potentiation and cerebellar motor learning. *Neuron* 67, 618–628

Shah, B. *et al.* (2013) Polarity independent effects of cerebellar tDCS on short term ankle visuomotor learning. *Brain Stimul* 6, 966–968

Shouval, H.Z. *et al.* (2002) A unified model of NMDA receptor-dependent bidirectional synaptic plasticity. *Proc. Natl. Acad. Sci. U.S.A.* 99, 10831–10836

Siebner, H.R. *et al.* (2004) Preconditioning of low-frequency repetitive transcranial magnetic stimulation with transcranial direct current stimulation: evidence for homeostatic plasticity in the human motor cortex. *J. Neurosci.* 24, 3379–3385
Todorov, E. and Jordan, M.I. (2002) Optimal feedback control as a theory of motor coordination. *Nat. Neurosci.* 5, 1226–1235
Turrigiano, G.G. and Nelson, S.B. (2004) Homeostatic plasticity in the developing nervous system. *Nat. Rev. Neurosci.* 5, 97–107
Turrigiano, G.G. (2008) The self-tuning neuron: synaptic scaling of excitatory synapses. *Cell* 135, 422–435
Zuchowski, M.L. *et al.* (2014) Acquisition of conditioned eyeblink responses is modulated by cerebellar tDCS. *Brain Stimul* 7, 525–531

Keywords
transcranial direct current stimulation (DCS), Eye movements, Cerebellum, Plasticity, Neuromodulation, Long-term potentiation, Long-term depression, Vestibulo-ocular reflex

Appendix

Summary

Samenvatting

Curriculum Vitae

PhD Portfolio

Acknowledgements

Summary

The thesis explores the mechanistic pathways of transcranial direct current stimulation (tDCS) in modulating a cerebellar dependent adaptation task. tDCS is a noninvasive, safe brain stimulation technique that modulates neuronal excitability and shows promise in the treatment of several neurological and psychiatric disorders. The modulatory role of tDCS opens a new door for its therapeutic usage in cerebellar patients. In order to optimize tDCS as an intervention to alleviate symptoms of cerebellar disorders, we need to understand the pathways through which tDCS modulates cerebellar learning. Hence, this thesis uses behavioral paradigms in various experimental models (such as mice with different genetic backgrounds and healthy human subjects), electrophysiological and computational techniques to dissect out the pathways involved in tDCS dependent modulation of cerebellar adaptation.

We have developed an animal model of cerebellar tDCS as a primary step towards unraveling the mechanistic pathways of tDCS in cerebellar adaptation. In **Chapter 2**, we used a simple gain down vestibulo-ocular reflex (VOR) adaptation task to probe the effects of DCS in wildtype and L7PP2B mice that lack synaptic and intrinsic long-term potentiation of the Purkinje cell (PC). Our findings suggest that the facilitation of gain down adaptation following anodal stimulation has a robust link to this potentiation mechanism. One of the reasons to use these mutant mice is that they fail to learn almost every cerebellar dependent learning task. If DCS can augment learning in these mice, the potential use of tDCS in motor rehabilitation therapy can be increased.

The role of tDCS in rehabilitation therapy can be further optimized if we study its efficacy in human brain. Therefore, we have done a similar VOR adaptation study in humans in **Chapter 3**. Surprisingly, we found no effects of tDCS on VOR adaptation in humans. The reasons for the differences in the results of the mouse and human studies are hard to determine. Perhaps, they are the result of difference in the effects of tDCS on the flocculus in the two paradigms. Perhaps it is the result of differences in the visual processing circuitry between species. We tend to believe that our results are in the line with evidence showing that tDCS is likely to affect superficial brain regions and not deeper structures. This adds valuable information towards optimizing tDCS in various cerebellar diseases.

We have demonstrated a stark difference between our animal and human experiments. Interestingly, researchers demonstrate that anodal stimulation of human cerebellum facilitates learning in locomotor, force field adaptation and eye-blink conditioning tasks while cathodal stimulation hinders leaning in

all of these tasks. The literature shows that tDCS has more complicated, polarity dependent effects on the neuronal network than was originally imagined. In **Chapter 4**, we present recording of neuronal multi-unit activity (MUA) from a population of neurons from epochs before (pre-DCS) and after (post-DCS, 30 mins after the cessation of stimuli) tDCS sessions. MUA was recorded from neurons in the cerebellar cortex while DCS was applied at the cortical surface directly above the recording. Our study demonstrates three major effects of DCS on cerebellar neuronal activity. First, DCS has polarity independent effects on neuronal activity in the control mice. Second, despite genetic deletion of long-term depression (LTD) at PF-PC synapses, both anodal and cathodal effects on neuronal activity is alike to the effects in the wild type mice. Third, our preliminary data suggests when PC long-term potentiation (LTP) is genetically ablated, anodal induced early vs late phase neuronal activity shows negative correlation, whereas the cathodal effects on the early vs late phase post-stimulation neuronal activity remains positively correlated. Hence, these results demonstrate that the effect of anodal stimulation may be dependent on the robustness of the potentiation mechanism of PC. It is important to replicate our findings in humans with cerebellar disorders so that a clear linkage can be made between cerebellar disorder and disrupted synaptic mechanisms. Meanwhile, other available mutant mice models may help unravel the mechanistic pathways of tDCS in the cerebellar network. At the least, we will be able to gather knowledge about how mouse and human brains respond differentially to the stimulation.

Finally, we have implemented a detailed computational model (based on previous theoretical work in our lab) which can, with a single set of parameters, mimic the behavior of a wide range of compensatory eye movement (CEM) behaviors, including adaptation of the VOR in **Chapter 5**. In that model, it was proposed that CEM are generated by a state-predicting feedback control (SPFC) framework where specific functional roles can be ascribed to specific nuclei in the CEM circuitry. The model shows that floccular damage leads to mal-adaptation of VOR. Hence, this supports the findings from animal study that the gain down adaptation of VOR can be altered when floccular activity is modulated by applying tDCS.

Ultimately, the experiments presented in this thesis have gathered multilevel information of tDCS on cerebellar network and helped to integrate cross species knowledge in order to utilize this technique optimally in the field of motor rehabilitation.

Samenvatting

Deze thesis onderzoekt de mechanische grondslag van transcraniële gelijk stroom stimulatie (tDCS) door het modelleren van cerebellair afhankelijke adaptatie taken. tDCS is een non-invasieve, veilige stimulatietechniek die neurale exciteerbaarheid kan modelleren en is veelbelovend in de behandeling van verscheidene neurologische en psychiatrische aandoeningen. De modulerende rol van tDCS opent een nieuwe deur voor therapeutische doeleinden voor cerebellaire patiënten. Om tDCS als een interventie te optimaliseren, met als doel symptomen van cerebellaire aandoeningen te verlichten, is het van belang dat de grondslag van het modulerende effect op cerebellair leren te begrijpen. Derhalve worden in deze thesis gedragsparadigma's gebruikt in verschillende experimentele modellen (zoals muizen met verschillende genetische achtergronden en gezonde proefpersonen), elektrofysiologische en computatie-technieken, om onderscheid te maken in de kenmerken die ten grondslag liggen aan tDCS afhankelijk moduleren van cerebellaire adaptatie.

We hebben een dierenmodel van cerebellaire tDCS ontwikkeld in een eerste stap naar het ontrafelen van de mechanische grondslagen van tDCS in cerebellaire adaptatie. In **Hoofdstuk 2** hebben we gebruik gemaakt van simpele *'gain down'* vestibulo-oculair reflex (VOR) adaptatietaak om het effect van tDCS te onderzoeken in een wild-type en L7PP2B muizen die geen synaptische en intrinsieke lange termijn potentiering van Purkinje cell (PC) bevatten. Onze resultaten suggereren dat facilitatie van *'gain down'* adaptatie als gevolg van anodale stimulatie een robuuste link heeft met dit potentieringmechanisme. Een van de redenen om deze muismutanten te gebruiken is omdat zij niet in staat zijn cerebellair afhankelijke taken te leren. Als tDCS leren kan verbeteren in deze muizen, dan kan het eventuele gebruik van tDCS in revalidatietherapieën worden vergroot.

De rol van tDCS in revalidatietherapieën kan verder worden geoptimaliseerd als we de doeltreffendheid ervan in het menselijk brein onderzoeken. Daartoe hebben we een gelijksoortig VOR adaptatiestudie in mensen gedaan in **Hoofdstuk 3**. Tot onze verrassing vonden we geen effecten van tDCS op VOR adaptatie in mensen. De reden voor de verschillende resultaten van de muis- en mensstudie zijn moeilijk te bepalen. Wellicht zijn de resultaten verschillend in deze twee paradigma's door de effecten van tDCS op de flocculus. Mogelijkerwijs is het een gevolg van verschillende visuele verwerkingscircuits tussen de twee soorten. We zijn geneigd om te geloven dat onze resultaten overeen komen met bewijs dat laat zien dat tDCS, naar alle waarschijnlijkheid, oppervlakkige hersengebieden beïnvloed en niet de diepere gebieden. Deze informatie is erg waardevol voor de optimalisatie van tDCS in verscheidene cerebellaire ziektes.

Wij hebben een sterk verschil aangetoond tussen onze dier- en mensexperimenten. Andere onderzoekers tonen echter aan dat anodale stimulatie van het menselijk cerebellum het leren in locomotor, force field adaptie en oogknipreflex taken faciliteert, terwijl cathodale stimulatie het leren bemoeilijkt in al deze taken. De literatuur laat zien dat tDCS gecompliceerde, polariteit afhankelijke effecten heeft op het neuronale netwerk, meer dan voorheen was voorzien. In **Hoofdstuk 4** laten wij data zien van neuronale multi-unit activiteit (MUA) van een populatie neuronen van periodes voor (pre-tDCS) en na (post-tDCS, 30 min na de beëindiging van de stimulatie) tDCS sessies. MUA werd gemeten van neuronen in de cerebellaire cortex terwijl tDCS werd toegepast op de corticale oppervlakte direct boven de meeting. Onze studie laat drie grote effecten van tDCS zien op neuronale activiteit. Ten eerste, tDCS heeft polariteit onafhankelijke effecten op de controle muizen. Ten tweede, ondanks de genetische eliminatie van lange-termijn depressie (LTD) bij de PF-PC synapsen, zijn zowel anodale als cathodale effecten op neurale activiteit hetzelfde als de effecten in de wild-type muis. Ten derde, onze data laat zien dat wanneer de PC lange-termijn potentiering (LTP) genetisch is weggehaald, anodaal geïnduceerde vroege vs late fase neuronale activiteit een negatieve correlatie laat zien, terwijl de cathodale effecten op vroege vs late fase post-stimulatie neuronale activiteit een positieve correlatie laat zien. Derhalve, laten deze resultaten zien dat het effect van anodale stimulatie afhankelijk is van de robuustheid van het potentiering mechanismen van de PC. Het is van belang om onze resultaten te repliceren in mensen met een cerebellaire aandoening, zodat er een duidelijke link gemaakt kan worden tussen cerebellaire aandoeningen en aangedane synaptische mechanismen. Tegelijkertijd kunnen andere beschikbare muismutant modellen helpen om mechanische grondslagen van tDCS op het cerebellaire netwerk te doorgronden. Zodoende kunnen we informatie verzamelen over de verschillende effecten van de stimulatie op muis en mens.

Ten slotte hebben we een gedetailleerd computer model gebruikt (gebasseerd op eerder werk gedaan in deze groep), welk met een enkele set aan parameters het gedrag kan imiteren van een scala aan compenserende oog bewegingen, hiertoe behoren adaptatie van de vestibulaire oog reflex beschreven in **hoofdstuk 5**. In dit model wordt de hypothese geponeerd dat de compenserende oog bewegingen bewerkstelligd worden aan de hand van een status-voorspellende terugkoppelings controle raamwerk. In dit raamwerk kunnen specifieke functionele rollen toegedicht worden aan specifieke nuclei. Het model laat tevens zien dat schade aan de flocculus kan leiden tot maladaptatie in de VOR. Dit ondersteunt de resultaten van de diermodellen in welk de afname adaptatie van de VOR beïnvloed kan worden wanneer tDCS gericht wordt op de flocculus.

Tenslotte, de experimenten in deze thesis hebben op meerdere niveaus informatie verzameld, betreffende het effect van tDCS op het cerebellaire netwerk en voorziet in het integreren van kennis tussen soorten om deze techniek optimaal te gebruiken in het domein van motorrehabilitatie.

CURRICULUM VITAE

Personal Information

Name: Suman Das
Date of Birth: 6 August 1984
Place of Birth: Kolkata, India
Email ID: dasuman.84@gmail.com

Education

2010 – 2015 **Joint PhD in Neuroscience**
Department of Neuroscience, Erasmus MC, The Netherlands,
promotor: Prof.dr. M.A. Frens
Department of Bio-medical Engg, Ben-Gurion University of the Negev, Israel, promotor: Prof.dr. O. Donchin

2008 – 2010 **M.Phil. Neuroscience – Department of Neuroscience**
National Centre for Biological Sciences, Bangalore, India

2006 – 2008 **M.Sc. Human Physiology – Department of Physiology**
All India Institute of Medical Sciences, New Delhi, India.

2003 – 2006 **B.Sc. Physiology – Department of Physiology**
Presidency College, Kolkata, India

Fellowships and Awards

2010 **C7 Marie Curie ESR Fellow (Early Stage Researcher)**
C7 - Cerebellar-cortical control: Cells, circuits, computation, and clinic

2009 **Dr. BK Anand** best Post-graduate award, AIIMS, India

2008 **Junior Research Fellowship** from NCBS, TIFR, India.

Research Experience

2010 – 2011 **Ph.D. (Candidate) Bio-medical Engineering, Donchin Lab**
Ben-Gurion University of the Negev, Beer-Sheva, Israel
Project: The mechanistic pathway of transcranial direct current stimulation (tDCS) in cerebellar adaptation

2011 – 2014 **Ph.D. (Candidate) Neuroscience, Frens Lab**
Erasmus MC, Rotterdam, The Netherlands
Project: The mechanistic pathway of transcranial direct current stimulation (tDCS) in cerebellar adaptation

2008 – 2010 **M.Phil. Student, Synaptic Plasticity in the Amygdala, Shona Lab**
National Centre for Biological Sciences, Bangalore, India
Project: Temporal effect of acute stress in fear generalization

2006 – 2008 **M.Sc Student, Pain Lab**
All India Institute of Medical Sciences, New Delhi, India
Project: Effects of chronic exposure to magnetic field on recovery from spinal cord injury: An electrophysiological and behavioral study in rat

LIST OF RESEARCH PUBLICATIONS

Impairment of long-term plasticity of cerebellar Purkinje cells eliminates the effect of anodal direct current stimulation on vestibulo-ocular reflex habituation: **Das S**, Spoor M, Sibindi TM, Holland P, Schonewille M, DeZeeuw CI, Frens MA, Donchin O. *Front Neurosci*; 11:444. eCollection (2017).

Impact of Transcranial Direct Current Stimulation (tDCS) on Neuronal Functions: **Das S**, Holland P, Frens MA, Donchin O. *Front Neurosci*;10:550. eCollection (2016).

Exposure to ELF-magnetic field promotes restoration of sensori-motor functions in adult rats with hemisection of thoracic spinal cord: **Das S**, Jain S, Avelev VD, Mathur R. *Electromagn Biol Med* Sep;31(3):180-94 (2012).

A neuroanatomically grounded optimal control model of the compensatory eye movement system: Holland P, Sibindi TM, Ginzburg M, **Das S**, Arkenstein K, Donchin O, Frens MA (*under review*)

Effects of anodal direct current stimulation on multiunit activity is sensitive to the long-term potentiation at parallel-fiber Purkinje cell synapses: **Das S**, Spoor M, Sibindi TM, Holland P, Schonewille M, DeZeeuw CI, Frens MA, Donchin O (*In preparation*)

Cerebellar tDCS does not modulate VOR adaptation in human: van der Vliet R, Louwen S, Donchin O, **Das S**, Frens MA, Holland P, Selles R, van der Geest JN (*In preparation*)

PhD Portfolio

General courses

Year		Course Name
2011	:	Computational Neuroscience *(BGU, Israel)*
2011	:	Methods in Neural Prosthetics *(BGU, Israel)*
2011	:	Animal Handling *(BGU, Israel)*
2012	:	Linear Control systems in the Oculomotor System *(Erasmus MC, The Netherlands)*

Presentation of research work in the conferences

Year		Name of the conference
2014	:	The 10th Computational Motor Control Workshop and ABC Robotics Annual Conference *(Beersheba , Israel)*
2013	:	Society for Neuroscience *(San Diego, USA)*
2013	:	NYC Neuromodulation 2013 *(New York, USA)*
2013	:	C7 Marie Curie ITN Workshop (EU FP7) *(Ma'ale Hachamisha, Israel)*
2013	:	9th BGU Computational Motor Control Workshop, *(Beersheba , Israel)*
2013	:	11th Dutch Endo-Neuro-Psycho Meeting (ENP 2013) *(Lunteren, The Netherlands)*
2012	:	C7 Marie Curie ITN Workshop (EU FP7) *(Amsterdam, The Netherlands)*
2011	:	7th BGU Computational Motor Control Workshop, *(Ein Gedi, Israel)*
2011	:	C7 Marie Curie ITN Workshop (EU FP7) *(Tubingen, Germany)*
2011	:	Marie Curie Researchers Symposium "SCIENCE – Passion, Mission, Responsibilities" (Warsaw, Poland)
2011	:	C7 Marie Curie ITN Workshop (EU FP7) *(Antwerp, Belgium)*

Teaching experience

2012 - 2013	Teaching assistant – Systems Physiology for ErasmusMC medical students

Acknowledgement

I am deeply indebted to my supervisor *Prof. Dr. Opher Donchin* whose stimulating suggestions, encouragement and magnanimous affection helped me enormously to accomplish this research and writing of this thesis. I still remember my initial days in Israel and how you made it easier (starting from the airport lounge where I met you for the first time) to settle down in a new country. Your first question of the day "how is your family?" always makes me happy. Don't know how it used to happen but every time I would be missing my family, you would call me over for a dinner and make me feel at home. I really appreciate the way you entertain my scientific view. You always say directly what is good in me and what is not – this has helped me a lot to grow as a person. *Prof. Dr. Maarten A Frens* It will be my privilege to express sincere thanks, deepest sense of gratitude for showering me with cool guidance, abundant benevolence and perpetual inspiration during the course of my study. Your humorous words on any critical situation gave me a take home message – *becoming a good person is far more important than becoming a crazy scientist*. The greatest gain from this journey of PhD is to have both Opher and you as my advisors. When I was struggling with data analysis Peter arrived like a savior disguised as a Post-Doctoral fellow. Not only you have helped with the analysis but your invaluable inputs during thesis writing have taught me a lot about scientific writing. When everyone would give up or even deny reading my scientific pages, you would step up and help me through. I owe my special thanks to you.

Here comes my Zimbabwean-Canadian-British-Dutch Captain *Taf*. You have provided the dry dock to this ship after arriving or before leaving Rotterdam port. Thanks for "*almost Baptising*" me. I enjoyed the Easter celebration – No mention about the parties which expanded from one continent to another, as they should stay as our secret. *Pascal* ever smiling, descent but crazy-cool Dutch captain and my one and only Lab ball-game partner. Man!!! you are a genius, so many times you brought an appropriate example that made scientific learning fun – specially the one time you ended up getting that teleost fish from the trenches of the sea-world on to our discussion table. Philosophical discussion with you is a treasure for me. *Mel* ever cool and always in a good mood personality - I think you have an Indian connection. I won't forget the dinner with your family in the USA. Your idea of cycling through the Tulip garden after having 'Dutch-cookies' was hilarious. It feels amazing that to meet you I have to go to India now. *Erik* a decent guy who is never angry and always smiling. It is great to have you as a friend. My wife still remembers and misses the tamarind candies you had got for her (the timing was so appropriate). Thank you so much. *Claire* the Hockey-Queen! I really need to learn few dance steps from you. I should learn from you how to balance nicely between a top career in sports and love for neuroscience. Greater part is that whenever I need a help you are always there. I will never forget in my life. *Jos*, a fantastic guy who was always skeptic about tDCS which in turn actually helped me to critically evaluate my work. *Cindy* Oh boy! Parties should always happen in your style - No debate on that. You taught me how loud-music helps in histology and I will remember this. *Mario* your love for art and science inspire me. Our discussions on art used to be so intense that we hardly talked about science. I think we should have interacted more to understand the scientific quest that we have common in us – it is great to have you as a friend. *Lieke* Never knew cats can give me hard time. Your fast and friendly process to procure life-saving drugs is an example – I will never forget how you helped me. *Martijn* I must thank you for your guidance in the electrophysiological analysis and

precious discussion during manuscript preparation. Your suggestions enrooted my writing towards the good understanding. *Elize* You are like my mom. Any problem in histology you were there to get me through with a big smile. *Annette* thank you for assisting me with all the bureaucratic work at Erasmus MC. Looking forward to party once again. The people from mechanical workshop: I offer my most sincere thanks to all of you for fixing any laboratory problem at any time. Even after 5pm on Friday which has indeed been a great assistance in completion of this dissertation.

Shlomi I have been fortunate to have you as a lab-mate. I will never forget how you went out in the middle of a sand-storm to find an accommodation for me. You gave me the opportunity to attend an Israeli wedding for the first time. Man! That was fun. Thanks for everything. *Ronit* your hard work and dedication while taking care of a family was an inspiration. It is great to have you as my senior colleague. *Raz* My bro! You are awesome - my sincere thanks to you. Any crazy Israeli problem, you were there for me – even in the middle of the night. I must say without you I could not finish this PhD – starting from my learning Matlab programming to abstract translation for submission. Looking forward for future collaboration with you. *Yulia* thanks for making the office so lively. We started as office-mates but soon after my wife arrived we became like relatives. Deepti and I had a great time with you. *Luai* You introduced me to some great restaurants with delicious food. You are the one who made me write his name in three different Indian languages. My special thanks to you. *Guy, Tamar* I express my sincere gratitude to you for making my stay wonderful. *Dorit* Thank you for assisting me with all the bureaucratic work of BGU. *Prof. Giora* I am very thankful for the support and encouragement. Whenever we met in the hall-way, you would always ask about my family. Thank you so much. *Late Prof. Amir* was a true inspiration and will always be. After I reached Israel he was the first person who was eager to have collaboration. I learnt a lot from his course not just about the subject but also about the art of teaching. My sincere gratitude to him.

Any amount of gratitude shall be less for my family, on whose constant encouragement and love I have relied throughout my time at the Academy. Their unflinching courage and conviction will always inspire me. I would not have been able to work wholeheartedly during the times when Deepti and kids were in India had it not been for my in-laws. Papa and Bhai, scientific discussions about the clinical application of my work always motivated me. Mummy along with the new member of the family Suruchi loved and took unconditional care of my daughters which kept my mind at peace while they were away.

Thanks Baba for letting me do what I loved to do rather than forcing me into what the society considered the best. Maa, you are my first love, you protected me but never kept me away from the reality. I am who I am because of the strong values you instilled in me. Deepti, you rock! Because of your support and dedication, I could excel in my path. Thank you Bhai, I could sit far away from home as I know you are there who take great cares of our parents.

Finally, I would like to express my gratitude to my little, sweet mice without whose active co-operation this thesis would never have been completed.

(Suman Das)